UNIVERSIDADE DE LISBOA
FACULDADE DE CIÊNCIAS
DEPARTAMENTO DE FÍSICA

Towards the Clinical Implementation of Deformable Image Registration in Gynecological Radiotherapy

Carolina da Silva Fernandes

Mestrado em Engenharia Biomédica e Biofísica

Dissertação orientada por:
Dra. Sandra Correia Vieira
Prof. Dra. Brígida da Costa Ferreira

2025

Para a Avó João, onde ela estiver.

“WE CANNOT SOLVE OUR PROBLEMS WITH THE
SAME THINKING WE USED WHEN WE CREATED THEM”
Albert Einstein

Agradecimentos

Esta dissertação é o culminar de 10 meses de muito trabalho, que por sua vez refletem 5 anos de muita aprendizagem. Foi um caminho exigente, mas também profundamente enriquecedor, que só foi possível graças ao apoio de várias pessoas, a quem aqui quero expressar a minha mais sincera gratidão. Porém, antes de as enumerar, não posso deixar de dirigir um agradecimento especial ao leitor que aqui se dispõe a iniciar a sua leitura.

Quero começar por agradecer à professora Brígida Ferreira, por toda a orientação ao longo desta dissertação. Mas acima de tudo por ter estado sempre presente no meu percurso académico ao longo destes 5 anos, um grande obrigada por me ter incentivado a chegar tão longe a nível académico e nunca me ter deixado desistir. Agradeço também aos professores Nuno Matela, Jorge Sampaio, Alexandre Andrade e Hugo Ferreira, por todo o conhecimento transmitido ao longo deste percurso, pela partilha de experiências e pela inspiração académica que marcaram de forma decisiva a minha formação.

Quero expressar um especial agradecimento ao Departamento de Radioterapia da Fundação Champalimaud e a toda a equipa que me recebeu de braços abertos e me acolheu de forma tão calorosa. Mas em especial à doutora Sandra Vieira, por todo o conhecimento transmitido ao longo destes 10 meses, e por me ter orientado sempre com muita paciência e carinho. Um obrigada ainda ao Joep Stroom por se demonstrar sempre disponível para me ajudar em tudo o que precisei. Maria, Gui, obrigada por todo o amor diário e por terem me ouvido a colapsar sempre que as minhas fusões não corriam como o esperado, sem vocês os meus dias de estágio não teriam sido os mesmos!

Aos meus pilares: mãe, pai, mano, obrigada por todo o amor incondicional, sem vocês nunca teria chegado onde cheguei. Ao meu Avô Balocas e aos meus avós que me acompanham lá de cima obrigada cheio de amor, porque sem o vosso exemplo e carinho não teria chegado até aqui. Joca, Joana, Ritinha, Margarida e Miguel obrigada por toda a paciência e amor.

Às minhas melhores amigas, Márcia, Sofi e Guigas, obrigada por me acolherem nas vossas vidas, nas vossas casas, e me ouvirem nos piores momentos. A vossa presença tornou os momentos mais duros muito mais leves, e é com enorme orgulho que vos chamo de família.

Aos meus melhores amigos, Pedro, Carapinha, Abreu, Miguel, Manel, Costa, Passinhas, Clara, obrigada por todas as quintas-feiras, que me fizeram espairecer a cabeça e me trouxeram leveza à minha semana. Obrigada por estarem sempre presentes, amo-vos.

Andreia, Sara, Maria, Mariana, Bianca obrigada por moldarem a pessoa que sou hoje e nunca me terei deixado percorrer este percurso sozinha.

Aos meus amigos da FCUL, Germano, Miguel e Parracho, um grande obrigado, sem vocês o curso não se faria sozinho! E um obrigada especial aos meus padrinhos Mariana e Gui, por terem estado sempre presentes.

E por fim, às minhas pequenas Elsa, Inês e Laura, por me fazerem sentir sempre especial.

Resumo

A radioterapia constitui, atualmente, um dos pilares mais relevantes no tratamento oncológico, sendo aplicada em aproximadamente entre 50% a 60% dos doentes com diagnóstico de cancro com o intuito curativo ou paliativo [1]. A sua eficácia baseia-se na capacidade de administrar doses elevadas de radiação sobre o volume tumoral, garantindo simultaneamente a preservação dos órgãos e tecidos adjacentes. Apesar do avanço tecnológico significativo observado ao longo das últimas décadas com a introdução de técnicas de modulação da intensidade (IMRT), técnica que utiliza colimadores multilâminas para modelar a distribuição espacial da fluência do feixe, permitindo uma conformação altamente precisa da dose ao tumor; radioterapia guiada por imagem (IGRT), que recorre à aquisição de imagens no acelerador imediatamente antes ou durante o tratamento para corrigir o posicionamento e compensar variações anatómicas diárias; e mais recentemente a utilização de algoritmos de registo deformável (DIR), a prática clínica continua a enfrentar desafios no que diz respeito ao equilíbrio entre eficácia e segurança.

Entre os múltiplos cenários clínicos que ilustram esta complexidade, esta dissertação irá focar-se em dois aspetos que merecem particular destaque. O primeiro corresponde às situações em que, durante um curso de radioterapia, ocorrem alterações anatómicas significativas, como variações no enchimento vesical e retal, perda de peso do doente ou até regressão tumoral volumétrica, que comprometem a validade do plano inicial. Nesses casos, o replaneamento torna-se essencial, permitindo replanear a distribuição de dose e assegurar o cumprimento dos objetivos clínicos. O segundo cenário refere-se à re-irradiação, situação em que, após um tratamento completo e a ocorrência de uma recidiva tumoral, o doente necessita de um novo curso de radioterapia. Esta prática, embora cada vez mais frequente devido ao aumento da sobrevivência oncológica, levanta sérias preocupações relacionadas com a dose cumulativa recebida pelos tecidos normais, que já foram previamente irradiados.

O trabalho desta dissertação teve como objetivo central avaliar, de forma integrada, o impacto clínico e dosimétrico do replaneamento e da re-irradiação. Visando explorar metodologias de cálculo da dose cumulativa, a aplicação do DIR e a utilização de conversões para dose equivalente em frações de 2 Gy (EQD2), que corresponde à conversão da dose administrada segundo diferentes esquemas de fracionamento para uma dose biologicamente equivalente se o tratamento tivesse sido realizado com frações de 2 Gy, utilizando o modelo linear-quadrático; de modo a permitir a comparação com limites clínicos de referência estabelecidos em protocolos internacionais, como os QUANTEC e as recomendações da RTOG. Ao abordar simultaneamente estas duas realidades clínicas, pretendeu-se contribuir para uma visão global sobre a importância de metodologias avançadas na prática da radioterapia, reforçando a necessidade de integrar ferramentas de avaliação dinâmica da dose na rotina hospitalar.

Para atingir estes objetivos, foram analisados dois grupos distintos de doentes tratados no mesmo centro. O primeiro grupo, composto por dezassete doentes, correspondeu a casos de replaneamento, e estes doentes possuíam esquemas de fracionamento de 23 ou 25 frações. O segundo grupo, constituído por sete doentes, incluiu situações de re-irradiação, em que um segundo tratamento foi realizado após recidiva tumoral. O esquema de fracionamento dos tratamentos de re-irradiação variava entre 1, 3 ou 5 frações.

Nos casos de replaneamento, o procedimento metodológico envolveu a aquisição de uma nova tomografia (CTreplan) a meio do tratamento, motivada por alterações anatómicas relevantes. Através do software Velocity®, a CTreplan foi deformada, obtendo-se assim a Dose Deformed. Este processo permitiu comparar a dose originalmente planeada (Dose Plan) com a dose efetiva fornecida caso se

prosseguisse com o plano inicial, sem ajustamentos. A análise focou-se sobretudo nos órgãos em risco da região pélvica, nomeadamente a bexiga, o reto, o sigmoide e o intestino delgado.

Os resultados mostraram que, na maioria dos doentes, a Dose Deformed apresentava valores superiores à Dose Plan, o que reforça a relevância do replaneamento. Este aumento era particularmente evidente para a bexiga e o reto, órgãos cujas dimensões e posição sofrem variações anatómicas significativas ao longo do tratamento. Para além disso, observou-se que a Dose Plan apresentava desvios padrão elevados, revelando heterogeneidade entre doentes, enquanto a Dose Deformed mostrava menor dispersão. Este fenómeno pode estar relacionado com o facto de a deformação tender a reduzir a variabilidade interindividual ao adaptar o plano inicial à anatomia do momento. Assim, concluiu-se que o replaneamento não é apenas uma opção desejável, mas em muitos casos uma necessidade clínica para garantir a eficácia terapêutica.

No grupo de re-irradiação, o procedimento metodológico envolveu maior complexidade. Cada doente realizou uma nova tomografia (CTreirr) antes do segundo curso de tratamento, na qual foram novamente delineados os volumes alvo e os órgãos em risco. A partir da aplicação do DIR, a CTplan do primeiro tratamento foi deformada para a anatomia da CTreirr, permitindo mapear a dose previamente administrada sobre a nova anatomia. Esta etapa foi essencial para a obtenção da Dose Deformed, que traduz a dose histórica transferida para a configuração anatómica atual.

Posteriormente, foram comparadas as doses resultantes do primeiro tratamento (Dose Plan), da deformação (Dose Deformed) e do novo plano de re-irradiação (Dose Reirr). Nos casos em que os dois cursos de tratamento apresentaram esquemas de fracionamento iguais, foi possível somar-se diretamente as doses dos dois planos de tratamento. No entanto, nos casos em que os dois cursos de tratamento apresentavam fracionamentos diferentes, foi realizada a conversão das doses para EQD2 através do modelo linear-quadrático, o que foi indispensável para viabilizar a comparação direta entre valores e para avaliar a dose cumulativa. Seguidamente, a dose EQD2 total foi reconvertida para o esquema de fracionamento do segundo tratamento, de forma a facilitar a interpretação clínica pelos radio-oncologistas.

Os resultados desta dissertação revelaram uma tendência geral para que os valores da Dose Deformed fossem inferiores aos da Dose Plan para a maioria dos órgãos avaliados, nomeadamente esta diferença foi mais evidente para a bexiga, o reto e o sigmoide. A interpretação deste resultado passa, em primeiro lugar, pelas alterações anatómicas ocorridas entre os dois tratamentos, que podem ter deslocado estruturas críticas parcialmente para fora do campo de radiação do primeiro plano, reduzindo assim a dose acumulada observada após a deformação. Em segundo lugar, é necessário considerar potenciais limitações metodológicas, visto que em alguns casos, a ausência de estruturas delineadas nas CT deformadas resultou em subestimações artificiais da Dose Deformed, devido à exclusão de voxels do cálculo.

Ainda assim, ao analisar as doses cumulativas, que correspondem à soma da Dose Deformed, do primeiro tratamento sobre a anatomia do segundo tratamento, com a Dose Plan, observou-se que em alguns doentes os valores atingiam ou ultrapassavam limites clínicos de dose de tolerância estabelecidos para os órgãos em risco. Este resultado evidencia que, embora a Dose Deformed isolada seja frequentemente inferior à Dose Plan, o risco de toxicidade em cenários de re-irradiação não pode ser negligenciado, sendo essencial uma avaliação rigorosa caso a caso.

Um aspeto adicional considerado foi o tempo decorrido entre o primeiro e o segundo tratamento. Quando esse intervalo ultrapassava seis meses, foi introduzido um fator de recuperação tecidular equivalente a 25% da dose acumulada, de acordo com recomendações da literatura. Esta correção permitiu uma estimativa mais realista da tolerância dos tecidos normais, ainda que se reconheça a necessidade de mais investigação para validar estes modelos de recuperação.

De forma global, este trabalho demonstrou que tanto os casos de replaneamento como de re-irradiação são práticas fundamentais na oncologia moderna, cada uma respondendo a desafios distintos.

O replaneamento mostrou ser uma ferramenta indispensável para corrigir desvios anatómicos que, de outra forma, poderiam comprometer a eficácia do tratamento ou aumentar a toxicidade. A re-irradiação, por sua vez, confirmou a sua relevância clínica como opção terapêutica viável em casos de recidiva, mas evidenciou igualmente os riscos associados, nomeadamente a proximidade aos limites de dose cumulativa.

Este trabalho pretende, portanto, contribuir para uma prática de radioterapia mais informada, personalizada e segura, em que a avaliação contínua da dose e da anatomia do doente permite melhorar não só a eficácia do tratamento, mas também a sua sustentabilidade clínica a longo prazo.

Palavras-chave: Replaneamento; re-irradiação; dose cumulativa; registo deformável; EQD2

Abstract

Radiotherapy (RT) plays a central role in cancer treatment, requiring a balance between tumor control and the preservation of healthy tissues. However, anatomical changes may occur during the course of treatment, potentially compromising the dose distribution initially planned. Furthermore, tumor recurrence after a first irradiation course introduces additional challenges, making strategies such as replanning and re-irradiation necessary.

The aim of this dissertation is to evaluate the dosimetric implications of these two approaches, with particular emphasis on the detailed and systematic analysis of cumulative dose delivered to organs at risk (OARs) and its relationship with tolerance limits established in widely recognized clinical reference protocols. A total of 17 patients who underwent replanning during their initial treatment course and 7 patients who underwent re-irradiation were included.

In both contexts, deformable image registration (DIR) was applied to transfer the initial treatment plan dose to the anatomy represented in subsequent imaging, thereby allowing a robust and clinically meaningful comparison between the Dose Plan and the Dose Deformed. These deformations were performed in Velocity® software, which allowed me to apply DIR to both replanning and reirradiation cases. For re-irradiation cases, doses from both treatment courses were summed, with conversion to EQD2 applied to ensure comparability between different fractionation schemes, followed by reconversion into a clinical reference framework.

The results highlighted distinct trends: in replanning, Dose Deformed was frequently higher than Dose Plan, underscoring the necessity of plan adjustment to safeguard OARs. In contrast, in re-irradiation, lower mean Dose Deformed values were observed relative to Dose Plan, a finding associated with substantial anatomical changes occurring between treatments. Cumulative analysis also found cases in which tolerance limits were reached or exceeded, highlighting the need of careful dosimetric evaluation. It can be therefore concluded that such combined methodological approaches, including DIR conversion and EQD2 conversion, form an essential strategy for clinical decision-making and strongly support the need for both replanning and re-irradiation to be implemented as fundamental strategies for effective therapeutic personalization.

Keywords: Replanning; re-irradiation; cumulative dose; deformable registration; EQD2

Acronyms

4D-CT Four-Dimensional Computed Tomography

CBCT Cone-Beam Computed Tomography

CT Computed Tomography

CTplan Planning Computed Tomography

CTreirr Computed Tomography acquired for planning the reirradiation

CTreplan Replanning Computed Tomography

CTV Clinical Target Volume

CTV HR High-Risk Clinical Target Volume

CTV IR Intermediate-Risk Clinical Target Volume

CTV LR Low-Risk Clinical Target Volume

DIR Deformable Image Registration

DVF Deformation Vector Field

DVH Dose-Volume Histogram

EBRT External Beam Radiation Therapy

EDMP Extended Deformable Multipass

EQD2 Equivalent Dose in 2 Gy Per Fraction

GTV Gross Tumor Volume

IGRT Image-Guided Radiotherapy

IMRT Intensity Modulation Radiation Therapy

LINAC Linear Accelerators

$m_{conformality}$ Weighted Average of Dice Score

MLC Multileaf Collimator

MRI Magnetic Resonance Imaging

PET Positron Emission Tomography

PTV Planning Target Volume

PTV HR High-Risk Planning Target Volume

PTV IR Intermediate-Risk Planning Target Volume

PTV LR Low-Risk Planning Target Volume

QA Quality Assurance

RIR Rigid Registration

ROI Region of Interest

RT Radiotherapy

SBRT Stereotactic Body Radiotherapy

SDG Sustainable Development Goal

SGD Structure Guided Deformable

SPECT Single-Photon Emission Computed Tomography

SRS Stereotactic Radiosurgery

VMAT Volumetric Modulated Arc Therapy

Table of Contents

List of Figures

List of Tables

1 Introduction

1.1 Context and Motivation

We live in an era marked by extraordinary scientific and technological progress, yet also by profound inequalities in access to healthcare. Acknowledging this reality, the United Nations established, in 2015, the 2030 Agenda for Sustainable Development, composed of 17 Sustainable Development Goals (SDGs), as illustrated in Figure 1.1. These goals represent global commitments aimed at eradicating poverty, protecting the environment, and ensuring prosperity and well-being for all, leaving no one behind.

Figure 1.1: United nation's sustainable development goals [2].

Health becomes one of the main focuses of the 2030 Agenda, reflected in SDG 3, "Ensure healthy lives and promote well-being for all at all ages", creating an international foundation towards equity and quality in health care for professionals across medicine, science, and biomedical engineering. At the interdisciplinary point of treatment in oncology, one of our major obstacles is accessibility, especially in resource weak settings and in technologically-advanced nations. Cervical cancer, for example, remains one of the leading causes of cancer-related mortality among women in regions with limited access to screening and specialized care. Despite more advanced technologies, therapeutic effectiveness is still predicated on individual's adaptation of therapeutic programs to anatomical and physiological alterations over time, in developed countries. It is in this setting, that adaptive RT has presented a new direction, adapting the treatment plan in response to anatomical changes seen throughout the health care course, thereby enhancing the precision and effectiveness.

While adapted plans have been successfully produced, RT departments are faced with ongoing challenges, including the absence of resources to assess cumulative dose and general quality assurance (QA) tools for the clinical workflow. This dissertation presents its research framework within this innovative paradigm. It proposes that DIR algorithms will be analyzed, validated, and utilized with the

Velocity® software concerning adaptive replanning in the treatment of patients with gynecological malignancies. This technique can be used to adapt the geometry defined in the planning CT to the patient's current anatomy, ensuring a better match that results in reduced toxicity to adjacent organs and more accurate dose delivery. The promotion of good healthcare practices, in line with SDG-3, contributes to safety, personalization, and impact. It also increases efficiency in the use of resources by reducing unnecessary repetitive imaging, thereby enabling more informed clinical decision-making.

In practice, however, repeat imaging is sometimes considered unnecessary for patient safety. It is important that all testing, follow up and treatment performed are clinically justified. In this aspect, the present research supports SDG 12, "Ensure sustainable consumption and production patterns", with encouraging better uses of science-based resources, without putting at risk the safety and quality of patient care. Finally, the integration with digital media and registration algorithms can help achieve SDG 9, 'Build resilient infrastructure, promote inclusive and sustainable industrialization and foster innovation.' The collaboration between biomedical engineers and radiation oncologists in this research area not only holds great scientific significance for future studies but also demonstrates the potential of science when placed at the service of people. In summary, this work not only aims to further technical understanding on deformable image registration and its application in adaptive RT, but also reinforces an ethical commitment to help build a system that is fairer, more efficient and sustainable. This aligns in many cases with the SDGs.

1.2 Objectives

This thesis aims to evaluate the clinical applicability and dosimetric implications of adaptive RT and re-irradiation, with a particular focus on the assessment of cumulative dose and its relationship with established clinical dose constraints. The goal is thus to guide the optimization of therapeutic approaches which balance tumor management with healthy tissue maintenance so that a more personalized and sustainable oncological strategy will be developed.

In addition to this main objective, the following secondary objectives are defined:

1. Review the state of the art in adaptive RT and re-irradiation, with emphasis on methodologies for cumulative dose calculation, dose deformation, and tissue recovery models.

2. Collect and process clinical imaging and dose data from patients undergoing adaptive treatments or re-irradiation.

3. Implement dose summation techniques, including the application of EQD2 conversions and normalization to reference fractionation schemes, to enable direct comparison with clinical reference limits.

4. Analyze the impact of anatomical changes between different treatment courses on the distribution of deformed doses, identifying patterns that may justify adaptive interventions.

5. Assess the potential clinical benefit of adaptive planning in both replanning and re-irradiation scenarios, taking into account the QUANTEC and RTOG guidelines.

1.3 Structure

This dissertation is organized into 6 chapters, following the structure outlined in Figure 1.2.

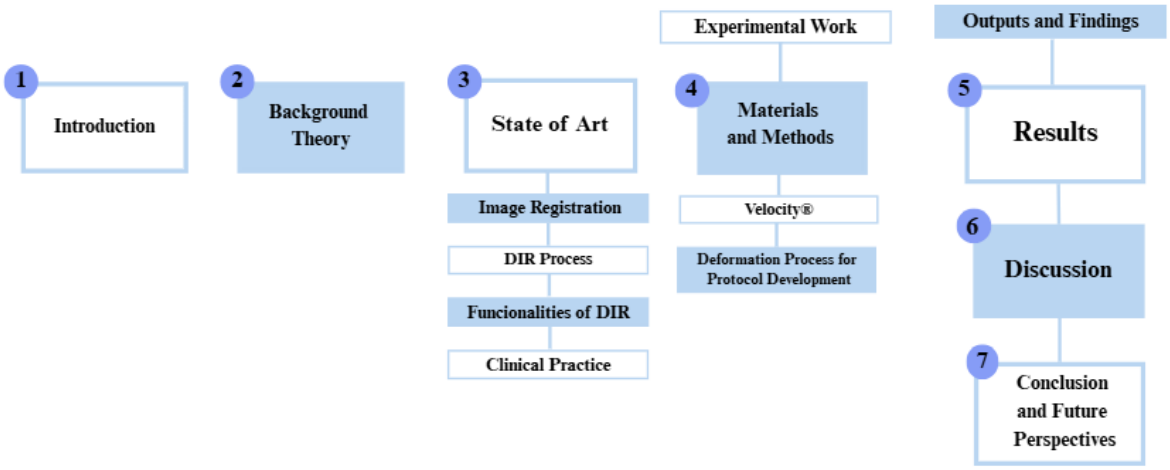

Figure 1.2: Structure of the dissertation.

In brief, the structure of this dissertation is as follows:

1. Introduction: Presents the motivation underlying this work, contextualizing the research problems, objectives, and research questions, as well as the overall organization of the manuscript.

2. Background Theory: Describes the theoretical foundations required for the development and understanding of this dissertation, including fundamental concepts in adaptive RT and re-irradiation.

3. State of the Art: Reviews the current knowledge on the topic, addressing subjects such as *Image Registration*, the Deformable Image Registration (DIR) process, its functionalities, and its applications in clinical practice.

4. Materials and Methods: Details the methodology employed, including the description of the *Velocity*® software and the deformation process applied for protocol development.

5. Results: Presents the findings obtained from the application of the described methodology, highlighting the main outputs of the experimental work.

6. Discussion: Provides a critical interpretation of the results, analyzing their clinical and scientific relevance, as well as their limitations and implications.

7. Conclusions and Future Perspectives: Summarizes the most relevant outcomes of the work, while also presenting final considerations and potential future research directions in this field.

2 Background Theory

2.1 Cancer

Tumor, or neoplasm, are new abnormal tissue growth which arises due to an uncontrolled cell division of the human body. This occurs as a result of mutations in genes governing the cell cycle, including genes, the products of which (proto-oncogenes) normally act to promote regulated cell growth and other genes, the products of which (tumor suppressor genes) normally function to limit proliferation. As a result, mutations in these genes lead to the disruption of cell cycle control. This disequilibrium allows for the continued expansion of cells leading to neoplastic growth or tumors, Figure 2.1 [3].

These masses are considered to be either benign, those that do not penetrate the surrounding tissue, or malignant, those which have the ability to invade surrounding structures and disseminat through the bloodstream or lymphatics. It is precisely by this invasive and metastatic ability that cancer is distinguished from normal cells, which is cancer cases less controllable and more likely to have a bad prognosis.

When an abnormality is found in an imaging study, e.g. computed tomography (CT), X-ray, positron emission tomography (PET), or magnetic resonance imaging (MRI), a biopsy is taken. This requires searching for and removing a small portion of the tumor, which is then tested in the laboratory to diagnose cancer and establish the type and nature of the tumor. The results are subsequently used to plan the most effective course of therapy [4].

2.2 Main Therapies for Cancer

Surgery is one of the key components of cancer therapy and continues to be the most effective way of controlling solid tumors, especially if diagnosed early. The goal of surgical oncology is to ensure complete extirpation of the tumor and adjacent healthy tissues in an attempt to minimize the risk of local recurrence. For this, the resection margins are strictly defined, on the basis of the histology of the tumor, the site of the tumor in the organ and the degree of tissue and lymphatic invasion [5].

When surgery is not curative or is not possible, for example, in the case of distant metastases, infiltration of vital structures, or other problems that contraindicate surgery [11], chemotherapy is frequently used as primary therapy or as an adjunct to other treatments. Chemotherapy uses cytotoxic drugs to kill or prevent the replication of cancer cells by exploiting the fact that these cells replicate at a faster rate than normal cells. This approach can be used in a number of clinical settings. In some instances, patients receive neoadjuvant chemotherapy to reduce the tumor mass before surgical removal of the tumor. On the other hand, adjuvant chemotherapy could also be recommended following surgery to bind up any remaining tumor cells and to prevent relapse. In the setting of advanced disease, chemoimmunotherapy contributes to palliation, prolongation of life, and improvement in quality of life, even if cure is not expected.

However, chemotherapy is not without side effects since the agents have a tendency to attack some of the normal, more rapidly dividing, cells as well. Thus, treatment can be related to side effects of vomiting, nausea, alopecia, asthenia and hematological (anemia, neutropenia) changes that need close follow-up and, in some cases, modulation of the treatment regimen [6], [7].

2.2.1 Radiotherapy

RT uses ionizing radiation to kill or slow the growth of tumor cells and is one of major components of the standard of care in cancer treatment, along with surgery and chemotherapy. Its main mode of action is to produce DNA damage in cancer cells, resulting in its inability to replicate. Radiation delivery technology has evolved in the last few decades allowing dose delivery with increased accuracy, focused on the target volume and sparing of healthy tissues [8], [9].

There are a variety of clinical settings in which RT is delivered currently – before surgery (neoadjuvant), with the intent to decrease volume of the tumor and facilitate surgical excision, adjuvant, with the aim of eliminating any residual malignant cells; curatively (definitive) with or without the use of chemotherapy, where complete eradication of the tumor is pursued in cases where a surgical approach may not be ideal or feasible; and palliatively, to manage symptoms such as pain and compression of vital structures in advanced disease [8], [9].

2.3 Types of Radiotherapy

2.3.1 External Beam Radiation Therapy

In external beam radiation therapy (EBRT), radiation beams are generated by devices external to the body and directed towards the target volume, usually produced by linear accelerators (LINACs) [10].

These devices, shown in Figure 2.1, are electron accelerators that use non-conservative radiofrequency fields, typically in the range of 10^3 MHz to 10^4 MHz, to accelerate electrons along a waveguide before converting them into high-energy radiation suitable for treatment [10].

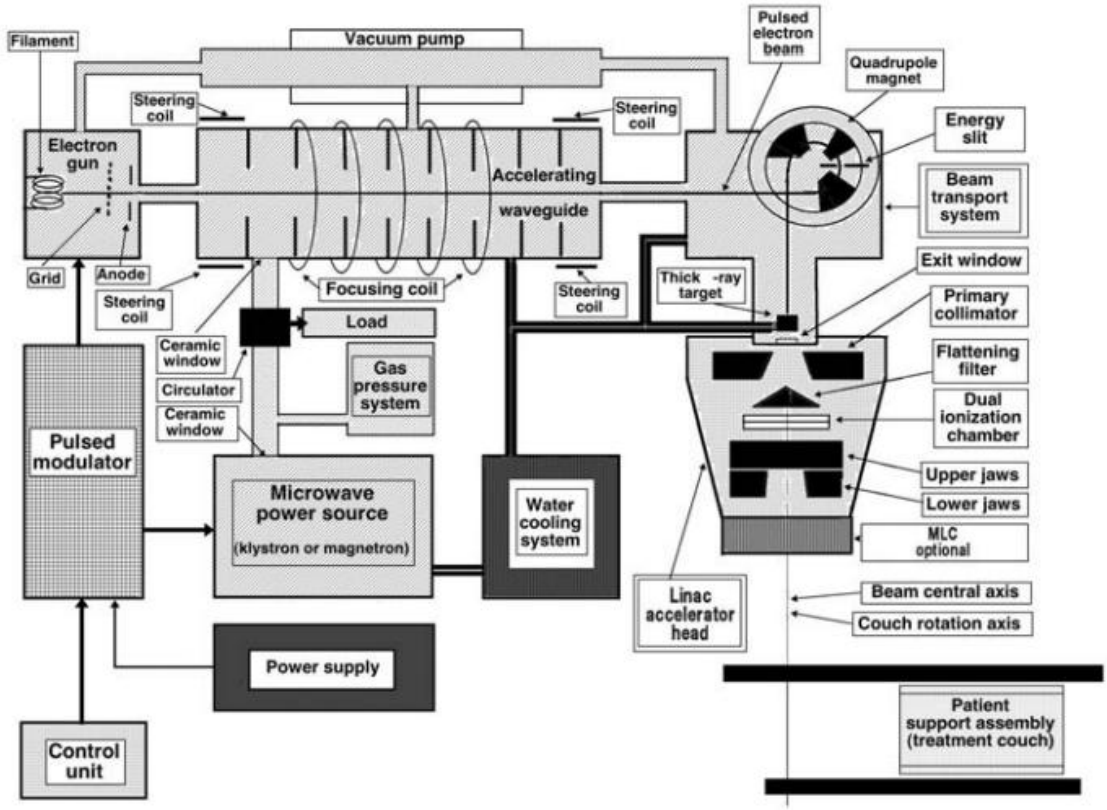

Figure 2.1: General view of a medical LINAC [10].

The main assembly of a linac is surrounded by a rotating gantry head which orbits the patient and provides radiation from multiple angles. The systems that produce the high power microwave energy, such as magnetrons and klystrons, that provide radiofrequency energy, are located at the bottom of the gantry. This energy is delivered to the accelerating waveguide, which is held under vacuum within the gantry system [10], [11].

The electron acceleration is performed in the waveguide. Second, a thermionic emission electron source comprises a heated cathode which thermionically emits electrons brought to the anode, to the wave guide. But the radiofrequency fields keep "shove" electrons inside this linear structure increasing step-by-step their kinetic energy up to those of clinical interest used in external beam radiotherapy. In the latest LINACs the electron gun as well as the X-ray target are integrated into the waveguide assembly making the component more compact and efficient [10], [11].

When the electrons achieve the desired energy, they impinge on a metallic target to generate MV X-rays or can exit the machine as an electron beam in the treatment mode of choice. The generated beam is subsequently conformed with collimators, and recently multileaf collimators (MLC), which can be shaped to the target volume during treatment or the segment shape defined for the delivery of IMRT beams [10].

To further increase precision image-guided systems were incorporated into linac as is the case of Cone Beam Computed Tomography (CBCT). CBCT is a volumetric imaging modality that allows three-dimensional images of the patient's anatomy to be obtained on the treatment couch prior to the delivery of radiation (Figure 2.2). These images are acquired by rotating a low-energy X-ray source and detection system around the patient in orthogonal orientation to the therapy beam. The generated volume may be used to ensure correct positioning of the patient and examine anatomical changes to verify the position of the target and Organ at Risk (OAR) in reference to the planned geometry. This is particularly important in the anatomical sites showing tremendous variability from fraction to fraction such as the pelvic region, and provide better accuracy in delivering radiation therapy and protection for the surrounding normal tissues [12].

Figure 2.2: Overview of a modern external beam radiography device. (Figure extracted and modified from [13]).

Presently, there is an increasing use of sophisticated techniques like IMRT, volumetric modulated arc therapy (VMAT), and stereotactic body radiotherapy (SBRT) or stereotactic radiosurgery (SRS). The techniques selected will depend on the tumor's characteristics, multidisciplinary team experience, and clinical protocols. Meanwhile, the number of fractions and dose per fraction (of both conventional and hypofractionated regimes) is led by clinical evidence and protocols of therapeutic effect and tolerance. Control during therapy is a way to maintain a constant parameter and to daily adapt to the real patient. IGRT, e.g., allows a daily verification of patient positioning with techniques like CBCT.

2.3.2 Brachytherapy

Brachytherapy, also known as internal RT, is a type of oncological treatment that consists of placing radioactive sources close to the tumor region or even inside the tumor.

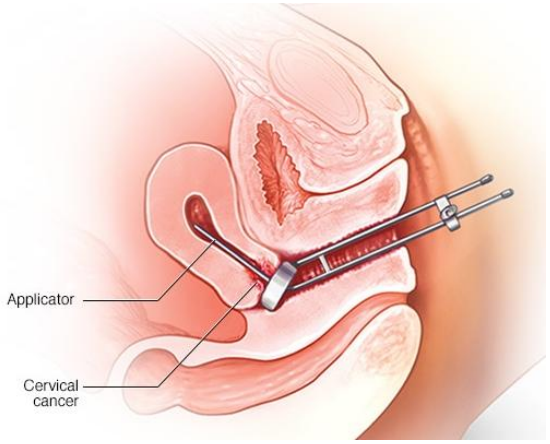

Figure 2.3: Example of Uterus Intracavitary Brachytherapy.

The tumor or the cavity which contains the tumor tissue is responsible for whether the intracavitary or interstitial brachytherapy method is applied. In the intracavitary method, the radioactive source is placed inside body cavities, as in cervical or endometrial or vaginal cancer (Figure 2.3). In interstitial brachytherapy the sources are placed directly, within the liver parenchyma, or in a tumoral mass, as it occurs in prostate cancer [14], [15].

Gynecological brachytherapy is an extensively applied therapy method in oncology; it is especially effective in the treatment of cervical cancer, endometrial cancer, and other malignancies in the gynecological area. The standard procedure, as established by the EMBRACE II protocol, consists of a first phase of EBRT that is administered to the pelvis. In this phase, 23 or 25 fractions are delivered, for a total prescription dose of 46 to 50 Gy. Aiming to irradiate the primary tumor and the related lymphatic chains, obtaining a locoregional control of the disease. This is then followed by a boost phase, which is usually performed with brachytherapy. This boost delivery is currently done in four fractions and is designed as a dose intensification to the high-risk target volume (PTV HR) to optimize local control while at the same time minimizing normal tissue toxicity (i.e., bladder, rectum, and small bowel [16]).

In the clinical routine at Champalimaud Foundation, this protocol was modified and the brachytherapy phase is replaced. The boost is administered by high-precision EBRT (SBRT) after the first 23 or 25 EBRT fractions. This strategy enables the delivery of two to four further fractions in a very conformal way, taking advantage of image-guided radiation therapy and intensity-modulated

radiation beams to deliver dose accurately. The decision for 2 or 4 fractions is based on the anatomical site, size of tumor, and clinical response.

The use of SBRT as a substitute for brachytherapy has become more important, particularly in instances where the delivery of brachytherapy is technically difficult, contraindicated, or not accepted by the patient. This non-interventional approach preserves the clinical aim of the localized dose intensification and provides a less invasive, more convenient, and more technically reproducible method that does not require anesthesia.

2.4 Individual Treatment Plan

2.4.1 Initial Assessment, Planning and Tumor Definition

The first step in preparing an individual RT treatment is a multidisciplinary approach to the patient involving clinical and physical and imaging examinations. At this point, one has to collect information about tumor location, extent of tumor, and (possible) metastases or involvement of neighboring organs. Diagnostic imaging techniques, including CT, MRI, and PET, can define accurate anatomical outlines and useful data for treatment planning [17].

During this planning session, the radiation oncologist specifies the regions to be irradiated and delineates the gross tumor volume (GTV), which represents the tumor as clinically observed—whether palpable (if applicable), visibly apparent, or identified through imaging. Additionally, the clinical target volume (CTV) is defined to encompass the GTV along with areas that may harbor microscopic disease not visible on imaging. To account for patient positioning variations and internal organ motion throughout the course of treatment, the planning target volume (PTV) is introduced, which includes the CTV plus appropriate safety margins, resulting in a comprehensive target volume referred to as the PTV [17], as illustrated in Figure 2.4.

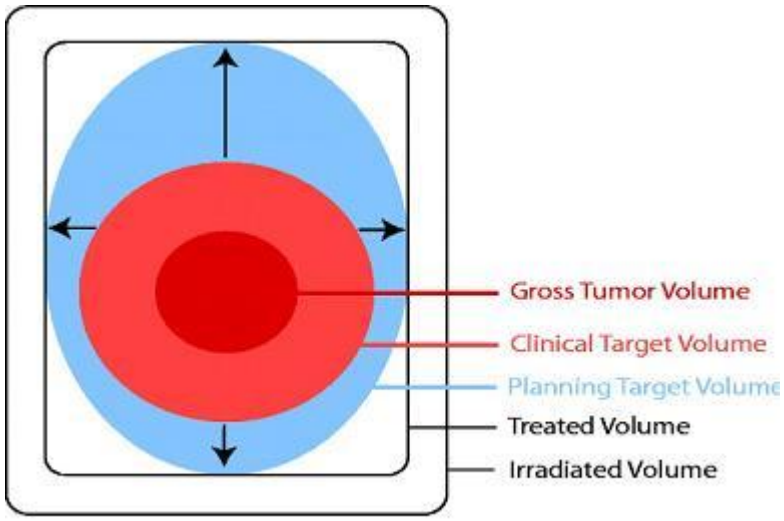

Figure 2.4: Volume concepts used in RT planning [18].

During planning, the anatomical and physiological configuration of a patient is considered, their comorbidities, the natural variations of an organ shape and filling, and variations in weight or positioning. The accuracy at this stage is optimized with individualized immobilization systems, such as vacuum cushions, thermoplastic masks, and others. These systems contribute to keeping the patient's anatomy stable and reproducible throughout the entire treatment. Additional imaging, for example

CBCT, can be performed prior to each treatment fraction for adequate positioning and to identify possible deviations. When substantial discrepancies are discovered, repositioning or reevaluation of the original plan may be considered.

2.4.1.1 Definition of Tumors in Gynecology

In RT of gynecological tumors, the delineation of the target plays a very important role in the individualization of treatments, allowing a more accurate distribution of dose, as well as the application of margins adjusted to the anatomical mobility of the structures involved. This process starts with the Clinical Target Volume (CTV) that encompasses tissue containing disease clinically or radiologically apparent, and at-risk for microscopic disease representation. For the EMBRACE II protocol, three CTV subvolumes are defined according to the expected risk of tumor spread: the high-risk clinical target volume (CTV HR), the intermediate-risk clinical target volume (CTV IR), and the low-risk clinical target volume (CTV LR) displayed in Figure 2.5 [16]

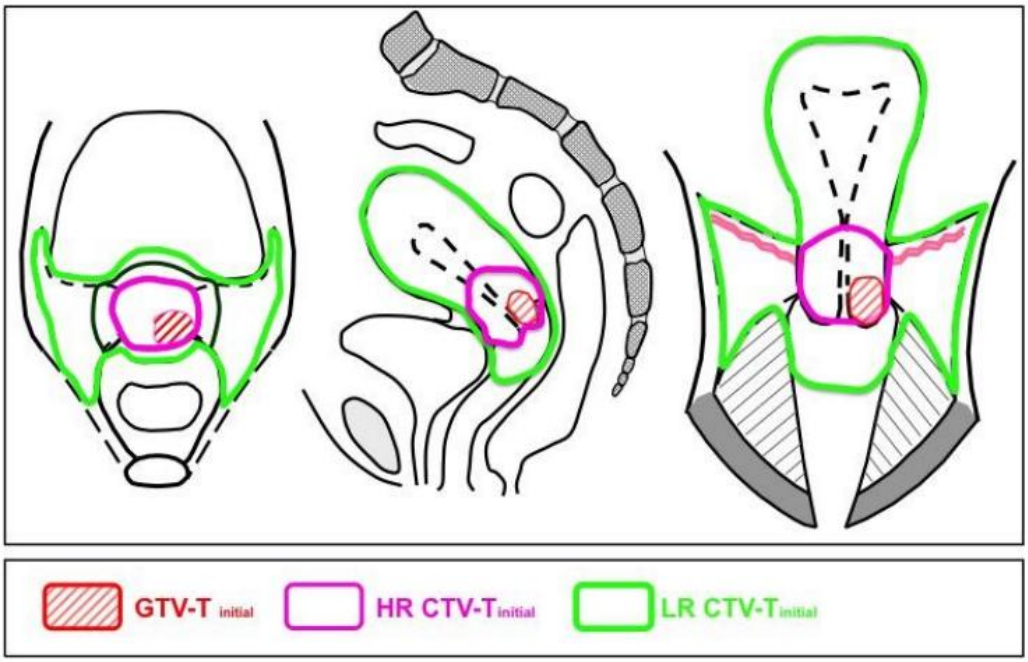

Figure 2.5: Schematic diagram for cervical cancer, with initial GTV-T, initial CTV HR (cervix) and initial CTV LR (margins for whole parametria, whole uterine corpus, upper third of vagina, utero-bladder and cervix-rectum space) for EBRT: coronal, transversal and sagittal view [16]

The CTV HR should consist of the GTV at diagnosis within and outside the cervix and the entire cervix. This volume represents area with the highest tumor burden and highest likelihood of local recurrence and is thus the primary target for dose escalation (boost) [16]

The CTV LR is a concentric volume about the CTV HR that extends beyond this volume by about 20 mm toward the vagina, the whole uterus, and up to 5 mm anteriorly and posteriorly at the level of the cervical os toward the bladder and rectum, respectively. This volume comprises areas of less likely direct tumor involvement, yet of potential clinical significance with respect to the risk of micro dissemination [16].

The CTV IR, when contoured, is an intermediate risk area and defines a zone in between HR and LR volumes for which dose can be adapted according to patient's anatomy and biology.

Although these clinical volumes are critically important, successful RT planning must also address internal organ motion and positional uncertainties. The Planning Target Volumes (PTVs) are determined by adding a guideline expansion to the CTVs. While the PTVs are not explicitly defined in the EMBRACE II protocol, treatment is derived this way from HR, IR and LR CTVs, with margins adapted to the mobility characteristics of each anatomical structure.

For example the left and right CTV HR borders, and in particular the margins that extend to the parametria, are relatively stable whereas the anterior and posterior borders, which are next to the bladder and rectum are less certain, and hence we would require margining. The uterine corpus involved in the CTV LR forms one of the most mobile regions within the pelvic anatomy, requiring larger safety margins to guarantee that it is adequately included over the course of fractionated therapy.

The anatomically accurate 3D description of the CTVs and the associated matching of PTVs stand as the very first essential stage to be met in order to guarantee that RT of any gynecological patient is not only effective, but also safe, since the anatomy complexity, together with its day-to-day variability, require the highest dose-planning accuracy.

2.4.2 Identification of Organs at Risk

There is great significance in the dosimetry of OARs, and the delineation of the OARs will form the basis for the protection of healthy organs during RT. For this purpose, imaging with sufficient resolution is used that allows for accurate anatomical representation of the structures. In turn, every OAR is delineated according to different protocols (for example, those by QUANTEC[19]or RTOG [20]) depending on its functional role and radiosensitivity. The area meant to be shielded in the optimization of treatment plans is decided with this step quantitatively, with volumes as indicators of the limits of the dose distribution[21].

Immediately following delineation, specific dose limits both for PTV and OAR, derived from clinical data and international guidelines, are integrated into the planning algorithm. In doing so, the dose calculation software generates and analyzes the dose-volume histogram (DVH) for each OAR, to evaluate if the defined tolerances or objectives set by the user are met. This control, combined with intensity-modulated techniques (IMRT, VMAT) and potential adaptations, tries to minimize the likelihood of complications, while maintaining a focus on tumor control with maximum possible safety [21].

2.4.2.1 Delineation of Organs at Risk in Gynecological Radiotherapy

The definition of the exact contours of OARs is a crucial step in RT planning, especially in the context of gynecological malignancies, where the planning target volumes (PTVs) are in close relationship with numerous pelvic structures. In modern RT, particularly in advanced techniques as Intensity-Modulated Radiation Therapy (IMRT) or Stereotactic Body Radiation Therapy (SBRT), the preservation of these OARs constitutes one of the most important aims, given the potentiality of high-dose conformity and escalation.

In the framework of this study, four OARs were assessed: the bladder, the rectum, the sigmoid colon and the small bowel. The anatomy of these structures was delineated according to internationally recognized anatomical guidance [16] which make the data to be analyzed comparable to different clinical cases.

The entire bladder, wall and content, is outlined from the apex to the bladder neck. The bladder is a hollow organ with multidirectional volume variations during emptying and filling and can

dramatically change shape and position during treatment. Such variations could influence the dose to the bladder itself and to neighboring target volumes and could support the importance of a daily imaging guidance or adaptive techniques [16].

The rectum is outlined from anorectal sphincter to the recto-sigmoid junction. Even though a relatively definitive tubular form exists within the pelvic canal, the rectum can suffer from positional changes associated with abdominal distension and fecal load. Because of its position posterior to the cervix, it tends to be in a high-dose region and as such needs to be accurately contoured and tracked [16]

The sigmoid colon is defined as an individual organ from the rectosigmoid junction to the left iliac fossa. Its complex mobile loop arrangement and its variable location among the imaging slices are the reasons that make its delineation very difficult. A methodical approach is necessary to segment this radiosensitive organ in its entirety and with precision [16].

The small bowel is delineated by the outside border of all visible bowel loops on the scanning series and the surrounding mesentery. Thus, this technique allows visualization of not only the bowel walls but also the entire volume of these loops in the vicinity of the pelvis and lower abdomen. On account of its high radiosensitivity and high mobility, the small intestine is considered one of the most important organs in plan optimization decisions and is frequently the dose limiting organ in treatment planning [16].

In Figure 2.6 the bladder is contoured in orange, the small bowel in yellow, the rectum in green, and the sigmoid colon in pink.

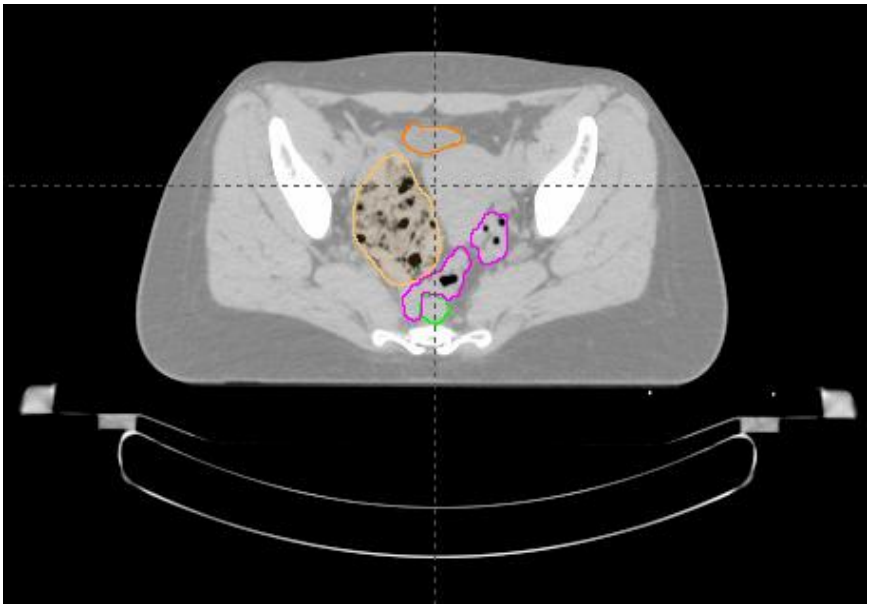

Figure 2.6: Axial CT image of a patient with a gynecological tumor, in which several anatomically relevant structures for RT planning are delineated.

2.4.3 Patient Workflow in the Radiotherapy Department of the Champalimaud Foundation

The treatment pathway of an individual patient, as it arrives at the Radiotherapy Department of the Champalimaud Foundation, is an organized series of steps designed to guarantee safety, efficacy, and personalization of the treatment.

Preoperatively, the patient has a consultation with the radiation oncologist based upon a clinical examination and a discussion on the treatment options. Following confirmation of indication for RT,

the procedure continues with the acquisition of a planning CT scan that serves for anatomical contouring and for computing the dose distribution to be administered.

The radiation oncologist delineates the patient anatomy during the planning CT; including the critical organs and the target volumes. This is essential for optimally planning the dose distribution such that therapy is maximized and toxicity to surrounding healthy tissues is minimized.

Once contouring is done, treatment plan is made by the dosimetry team based on dedicated software (Eclipse^{RM}) that calculates the dose distribution to be the best possible. The radiation delivery then follows clinical protocols and dose constraints, according to clinical protocols and dose constraints, which are based on national and international (QUANTEC [19] and RTOG [20]) or following protocols approved by the Champalimaud Foundation ethical committee.

After planning is completed, a treatment plan is approved. This plan specifies the number of fractions, the dose per fraction and the irradiation technique. Prior to patient irradiation, a CBCT is performed before each treatment session on the LINAC. This image facilitates real-time confirmation of whether or not the patient's current anatomy matches that depicted in the planning CT.

The performance of CBCT is a basic precondition for accurate treatment in high biological complexity with strong anatomical variety (e.g., pelvis). Thus, if there are any major anatomical changes, e.g., organ shift, volume change, or gas presence, the radiation oncologist may interrupt the treatment and initiate a new planning process, to ensure patient safety and guarantee that the therapeutic objectives are achieved.

3 State of Art

3.1 Image Registration

When analyzing medical images, the correspondence between significant features and their spatial locations allows for the comparison of specific anatomical structures within the images. This relationship provides the ability to transfer information that can be used as prior knowledge for tasks such as the segmentation of anatomical structures, treatment planning, and the monitoring of changes over time that may occur due to factors like weight loss, edema, internal organ movements, or tumor regression [22].

In the field of medical imaging and computer vision, the task of computing and aligning correspondences between different images is called image registration. Given two images, image registration algorithms employ methods such as image intensities or structural features present in the images to achieve a transformation that best aligns the correspondences between them. This process is crucial for integrating information from different modalities or temporal instances, ensuring that clinical decisions are based on the most accurate and comprehensive information possible[22].

Image registration is thus described as a method for finding the spatial correspondence between two or multiple sets of images. If two image sets are available—a fixed image, $F(x)$, and a moving image,$M(x')$—image registration seeks to find the best transformation, $T(x')$, that minimizes the difference between $F(x)$ and $M\big(T(x')\big)$. The transformation can be described as the sum of the local position vector in the moving image, x', and the displacement vector, $u(x')$[23]. Thus, an ideal image registration between two sets of images can be expressed as:

$$F(x) = M\big(T(x')\big) = M\big(x' + u(x')\big), \tag{3.1}$$

Image registration can be categorized into two categories, rigid registration (RIR) and non-rigid registration, which is also known as DIR.

RIR corresponds to an image alignment process in which all pixels move or rotate uniformly so that the spatial relationship between pixels remains unchanged after the transformation.

Such registration is particularly valuable when no anatomical transformation is anticipated, such as in the case of images taken across very small-time intervals, or the imaging of a rigid anatomy. One example is brain images from (CT, or MRI) studies: registering them using RIR is suitable, since the brain does not undergo substantial deformation between scans. Likewise, in the combining of bone images or in the correction of small patient movements between scans, the rigid body involution return aligns images by correcting displacements or rotations, but without considering local deformations or morphological changes in the shape of anatomical structures. It is worth noting that even in clinical cases where some degree of deformation may occur — such as with CBCT images acquired prior to treatment — RIR is still routinely used. In these situations, the radiation oncologist manually adjusts the alignment so that the tumor or organ of interest in the CBCT matches the planning CT as closely as possible.

Although DIR yields a greater number of degrees-of-freedom than rigid image registration and theoretically can compensate for anatomic changes such as weight loss, treatment response (i.e., tumor regression), or organ deformation, DIR is not widely applied in daily clinical practice. As the majority of centers continue to use RIR for daily image guidance, the development and validation of DIR strategies – as addressed in this work – becomes especially pertinent for future clinical translation.

DIR can control the local deformation between two image sets; this is because the relationship between pixels is not kept constant, and therefore it can take into account nonlinear and local

deformations. This allows for each section of the image to be modified independently for a perfect match of altered anatomical structures. Therefore, DIR would be a great help in adjusting the planning and administration of RT to the anatomical modifications of the patient, to increase the accuracy of the application of the radiation dose and, consequently, the possible therapeutic efficacy.

3.2 Deformable Image Registration Process

The DIR process encompasses three main components: the objective function, the transformation model, and the optimization model.

This process generally begins with a preliminary alignment of the moving image $M(x')$ with the fixed image $F(x)$, using a RIR or an affine transformation to correct global differences in position and orientation between the images. After this initial alignment, DIR algorithms are applied to locally adjust the moving image to the fixed one, taking into consideration the specific deformations of the anatomical structures.

3.2.1 Objective functions

The similarity between the two images is evaluated through an objective function that calculates a similarity index. This function is crucial for guiding the registration process and can be categorized into three types. In the context of DIR, the three main types of objective functions used are intensity-based functions, anatomy-based feature functions, and hybrid functions that utilize both techniques [23].

Intensity-based objective functions use the pixel intensities of the images to assess similarity, assuming that after correct alignment, the corresponding regions in both images will exhibit similar intensities. Some examples of strategies used to achieve a good similarity index are the sum of squared differences, the correlation coefficient, and mutual information.

Anatomy feature-based objective functions rely on the correspondence of elements extracted from the images, such as points of interest, contours, or specific anatomical structures, and evaluate similarity based on the geometric correspondence of these features between the two images. This approach is particularly useful when intensities are not directly comparable or when dealing with different imaging modalities or poor image quality.

Regarding hybrid functions, these combine elements of intensity-based and feature-based functions, seeking to leverage the advantages of both approaches and increasing the robustness and accuracy of the registration[23].

3.2.2 Registration

For registration, based on the chosen objective function, an iterative process begins in which a deformation vector field (DVF) is generated according to a transformation model (Figure 3.1). The transformation model mathematically defines how deformations are applied to the moving image and can involve techniques such as B-splines—the technique used by the software that will be utilized in this project. This technique corresponds to a biomechanical method that simulates the physical behavior of tissues or statistical models that use population data to predict deformations. The DVF is then used to deform the moving image, updating the objective function at each iteration. After this phase, an optimization algorithm is employed, whose function is to progressively adjust the parameters of the transformation model with the goal of maximizing the similarity index between the deformed image and the moving image. This iterative process continues until a satisfactory level of similarity is achieved or

the convergence criteria are met, thus ensuring precise alignment of the anatomical structures between the images. Figure 3.1 schematically illustrates the steps involved in this DIR process [23]

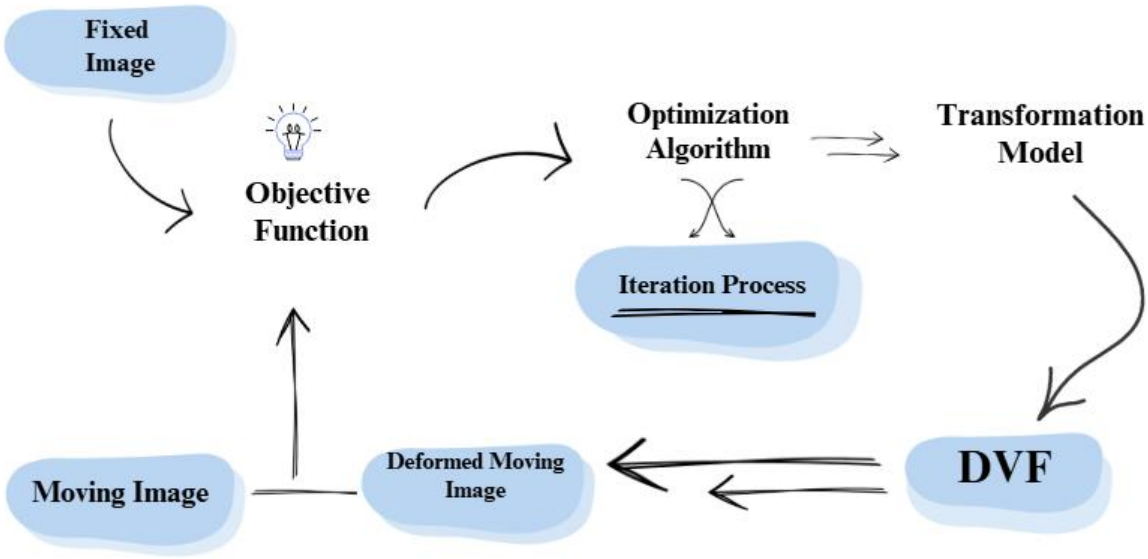

Figure 3.1: Flow chart of DIR process[23].

3.3 Functionalities of the deformable image registration

DIR has many uses in RT, particularly in the areas of automatic mathematical modeling, functional imaging, segmentation and dose accumulation.

3.3.1 Mathematical Modeling

DIR enables the creation of mathematical models that describe the organ and tissue evolution as a function of time. Through analysis of different groups of images of a patient, patterns of motion and deformation, formulating predictive models that may be introduced into therapy planning are learned. This is particularly relevant in the prediction of the evolution of anatomy throughout treatment, which allows modifications in treatment planning also to be accounted for. In addition, the mathematical modeling applied when using DIR helps to comprehend the bio-logical processes and mechanism that induce tissue responses to radiation, thereby contributing to the improvement of individualized treatments.

In a recent study, Fu et al. (2020) explored the application of DIR in modeling tumor motion in patients with lung cancer. The authors utilized four-dimensional computed tomography (4D-CT) images to develop mathematical models that capture the three-dimensional deformation of lung tumors throughout the respiratory cycle. Specifically, they implemented LungRegNet, an unsupervised deep learning network comprising two subnetworks: CoarseNet, which predicts large-scale pulmonary movements in coarse-resolution images, and FineNet, which captures local movements in fine-resolution images [24]. Another pertinent example concerning mathematical modeling is the study by Wang et al. (2021), who applied DIR to model prostate deformations during RT, aiming to enhance precision in delineating dominant intraprostatic lesions and in treatment planning. The authors utilized MRI acquired at different treatment stages to develop models representing positional and structural

variations of the prostate and adjacent organs, with the purpose of accurately registering the prostate on MRI and CBCT images for external beam RT. This method can assist in dominant intraprostatic lesions delineation on CBCT and in treatment planning [25].

3.3.2 Functional Imaging

The use of DIR in functional imaging enables the evaluation not only of organ anatomy but also of their physiological function. In fact, the study conducted by Guerrero et al. (2005) introduced a pioneering method to generate pulmonary ventilation images using 4D-CT data in combination with DIR algorithms by tracking the displacement of lung tissue between different phases of the respiratory cycle. The authors succeeded in creating ventilation maps that reflect regional lung function, providing functional information that can be incorporated into RT planning [26]. Subsequently, Yamamoto et al. (2011) conducted a validation study to assess the accuracy of ventilation images obtained through DIR. In this study, they compared ventilation images generated from 4D-CT data using DIR with those obtained via single-photon emission computed tomography (SPECT) lung perfusion scans, considered the clinical standard for evaluating pulmonary ventilation. The results demonstrated a significant correlation between the two methods, reinforcing the reliability of ventilation maps derived from 4D-CT and DIR in assessing lung function [27].

3.3.3 Automatic Segmentation

Automatic segmentation is a functionality of DIR that aims to optimize the process of delineating anatomical structures. Traditionally, segmentation is performed manually by radiation oncologists, which is a time-consuming process subject to inter- and intra-observer variability. DIR allows for the automation of this process by propagating contours previously defined on a reference image to other images acquired throughout the treatment. By doing this, increased reproducibility of the structures is obtained, time is saved and errors due to human subjectivity are reduced.

Cubero et al. (2022) investigated the application of DIR for automatic segmentation of head and neck organs, they introduced a technique that integrates DIR and deep convolutional neural network to improve the accuracy of segmentation. The results demonstrated superior performance in segmenting fifteen OARs, achieving a mean Dice coefficient of 0.8059 and a surface Dice similarity coefficient of 0.8874 [28]. Another relevant study is by Li D (2016), which examined the application of DIR for automatic pelvic organ segmentation in CT images. In that work, the authors proposed a method integrating DIR with a statistical shape model to automatically segment structures such as the prostate, bladder, and rectum. The results demonstrated significant improvements in segmentation accuracy: the mean Dice similarity coefficient achieved was 0.751 for the prostate, 0.783 for the bladder, and 0.573 for the rectum. Notably, compared with other segmentation methods, Li D's (2016) approach was found to be more accurate for both the prostate and bladder. Furthermore, the study indicates that the method is robust in the presence of anatomical variations and pathologies, reinforcing its applicability in complex clinical scenarios. However, despite these notable improvements, the authors acknowledge the limitation imposed by the size of the training dataset, suggesting that segmentation accuracy could be further optimized with a more comprehensive dataset [29].

3.3.4 Dose Accumulation

In an actual clinic, such as in the Champalimaud Foundation and other institutions, dose accumulation is typically conducted using the maximum dose point in each OARs. In each fraction, the

areas that received the highest dose are identified and then the maximum doses are accumulated throughout treatment. Although this estimate of the deposited dose may be conservative, it might not represent the actual spatial profile of the dose in the tissues, due to inter or intrafraction position changes of that particular OAR.

Dose accumulation is an important application of DIR in the RT scenario. The method provides a technique to map dose distributions from each fraction on to a common reference image accounting for anatomic deformations and displacements suffered in the course of the treatment. This method may be used to sum up the dose from different sessions to obtain a more realistic estimation of the accumulated dose in the target tissues and in the neighboring organs.

Veiga et al. (2016), investigated dose accumulation in patients with prostate cancer using DIR. They applied DIR to deform the planning CT (CTplan) images to match the CBCT images acquired during treatment. This allowed to account for daily anatomical changes and to calculate the actual accumulated dose received by the prostate and adjacent organs [30].

A comprehensive review of the clinical application of adaptive RT in cervical cancer was performed by Shelley et al (2021) [31]. In this approach, treatment planning is modified based on anatomical changes occurring during the course of treatment, such as variations in tumor volume and in the position or filling of adjacent organs at risk. The implementation of advanced imaging techniques and DIR in the present study also made it feasible to accumulate radiation dose more accurately, ensuring that the dose delivered to the target is maximized while minimizing exposure to organs at risk such as the bladder and rectum [31].

Razdevsek et al. (2022) carried out a study to evaluate the impact of DIR on dose accumulation in proton therapy for patients with tumors subject to movement. By applying DIR techniques, researchers aimed to precisely align images acquired at different phases of the treatment, taking into account anatomical changes and movements. This approach allowed for a summation of dose distributions administered throughout the treatment, providing an assessment of the actual dose received by both the target and surrounding healthy tissues. The findings of that study highlighted the importance of incorporating DIR into dose accumulation processes to ensure effective treatment planning and outcome assessment in proton RT [32].

3.4 Clinical practice

3.4.1 Treatment Replanning

Replanning in radiation therapy aims to maintain treatment effectiveness and patient safety. Adjustments to the treatment plan may become necessary due to the dynamic nature of both tumours and surrounding normal tissues, which can change in position, size, or shape, and due to patient-related factors such as weight loss. Regular reviews are essential to ensure the existing plan remains accurate and effective. With modern imaging technologies, as with CBCT, these anatomical changes can be monitored, making it possible to update the treatment plan when clinically indicated. It is a treatment strategy in which the radiation plan is adapted to the anatomic variations of the tumor and its volume between any two daily treatments.

Weight loss and changes in PTV, or organ movement due to filling of other structures, can alter the original planned dose distribution significantly, harming the treatment ratio. By adjusting the treatment plan according to the actual position of the target, retreatment plan can be applied to enhance the target coverage, and to avoid undesired exposure of organs [33].

3.4.1.1 Current Procedures

Currently, procedures for treatment replanning, the original RT plan is adjusted to coherently accommodate changes in the patient's anatomy or in the size and position of the tumor and this is usually achieved through periodic imaging studies such as CBCT that provides up-to-date anatomical information. Radiation oncologists evaluate these images to identify any significant deviations from the initial CT that may require modifications. In cases where significant anatomical changes are observed, replanning becomes necessary.

The replanning process involves generally acquiring a new planning CT scan, in which the target volumes and the OARs are redefined by the radiation oncologists. Based on this new image, a new treatment plan is developed for the remaining fractions that need to be delivered, (i.e., the total number of initially prescribed fractions by subtracting the fractions already administered). For example, if the original plan prescribed 25 fractions and replanning occurs after 10 fractions, the new plan will be calculated for the remaining 15 fractions [34].

In their study, Avgousti et al. (2021) demonstrated that adaptive replanning in RT significantly improves dose compliance to the tumor and reduces radiation exposure to adjacent healthy organs. Research has demonstrated that the use of advanced imaging technologies allows treatment plans to be adjusted. However, the authors also identified challenges, such as the increased time required for planning and the need for additional technological and human resources. These aspects highlight the complexity of effectively implementing adaptive replanning Furthermore, they emphasized the importance of standardized protocols to ensure consistency and quality in patient care [35].

3.4.1.2 Benefits Of DIR In Replanning

DIR enables the accurate registration of images in presence of anatomical deformations that naturally occur and allows structural changes to be correctly taken into account for replanning. This is crucial for online PTV and OARs adaptation, to make sure that the radiation delivered is well targeted at the tumor.

Moreover, DIR enables monitoring of treatment evolution by comparing CBCT images over time. Although not yet generally used clinically, this continuous monitoring capability would be crucial to quickly detect any anatomical variations that may affect treatment efficacy.

Another important factor is the assistance provided by DIR in the process of dose accumulation. Through the registration of various CT/CBCT image sets, DIR enables accurate calculation of the actual total dose delivered to both the tumor and surrounding normal tissues over the course of the different treatment fractions. "Higher order" dose calculation tools are needed to monitor these detailed dose comparisons to track that the cumulative doses do not exceed the prescribed tolerated limits in order to prevent toxicities and ensure safer patient treatment.

3.4.2 Re-Irradiation

Re-irradiation refers to the process of administering a second or more courses of RT to an area previously treated. This is often necessary in three scenarios: in cases of tumor recurrence (Re-irradiation Type 1), progression to regional tissues or lymph nodes near the original site, or distant metastases from the primary tumor (Re-irradiation Type 2) [36].

Reirradiation in the modern oncological setting has taken on an important role because of the recent advances in tumor treatment that have shown a clearly favorable impact on survival. As these patients live longer, the likelihood of having tumor recurrences also increases, and reirradiation becomes

an essential approach in the treatment of these lesions. Consequently, this method, apart from offering extra disease control, may help to enhance the quality of life of patients by reducing symptoms of relapse tumors.

Nevertheless, reirradiation in such a radiotherapy setting is a serious problem, with an increased risk of toxicities in tissues previously irradiated by the first dose, due to progressively increasing doses summing up to a total biologically effective dose that acts as a crucial risk factor in such cases. To reduce these risks, the application of new radiotherapy planning and treatment techniques is necessary, as they allow a more accurate estimation and delivery of the dose. The individualization of the re-treatment approach along with careful assessment of clinical status, is essential to be able to achieve the optimal benefit with an acceptable level of risk [36].

3.4.2.1 Current Reirradiation Procedures

Current reirradiation procedures in RT begin with the acquisition of a new CTplan scan, which allows healthcare professionals to identify changes in the patient's anatomy since the first treatment, including alterations in the size and position of the tumor and adjacent organs.

Regarding the biological dose, that is, the actual amount of radiation that the patient can effectively receive, the image fusion between the old and new planning CT may currently be used to identify the maximum dose levels received by the PTV and the OARs. These maximum dose points are compared with those from the previous treatment and with the established tolerance limits for each organ. This comparison aims to determine the additional amount of dose that can be administered without exceeding safe levels. In some cases, OAR recovery can also be included in this assessment.

In the context of current reirradiation procedures, Kang et al. (2023) explored the use of maximum dose points to guide planning in patients with pelvic recurrence of cervical cancer and emphasized the importance of carefully evaluating the additional dose administered to OARs to avoid toxicities [37]. Ren et al. (2022) also utilized this approach in their studies, but both research groups highlighted that relying exclusively on maximum dose points may not be sufficient [38].

Thus, it is evident that using maximum dose points presents significant limitations, as the total dose effectively received by the tissues may be underestimated. This is because maximum dose points represent only isolated values and do not reflect the complete dose distribution within the organ.

Additionally, between the two treatments or more, significant changes can occur in the position of organs, variations in tumor volume, among other physiological modifications that can significantly affect the distribution of the radiation dose. Therefore, using this methodology may not be the best approach to capture these changes, as it does not consider these alterations. Hence the need to use tools that enable the three-dimensional dose assessment, which are not available in most systems.

3.4.2.2 Dose Fusion through DIR

The fusion of doses based on DIR is a major step forward in re-irradiation treatments, since DIR permits to retrospectively incorporate previously received radiation doses into the patient’s current anatomical situation.

The effectiveness of DIR in re-irradiation is illustrated by Nobnop et al. (2017), who evaluated DIR methods in patients with nasopharyngeal cancer undergoing RT. Although the study’s focus lies outside the pelvic region, its findings demonstrate the utility of DIR in accurately quantifying the accumulated dose and detecting anatomical changes over the course of treatment, enabling more assertive adjustments to the therapeutic plan. Nevertheless, the study emphasizes the need to refine

methodologies and algorithms, as well as to establish standardized protocols, to ensure reproducibility and instill confidence in applying DIR to other anatomical regions [39].

Similarly, the analysis conducted by Vozzo et al. (2021) focuses specifically on the pelvic region, utilizing DIR to estimate the accumulated dose in organs at risk following external beam radiation therapy and high-dose-rate brachytherapy for prostate cancer. In this scenario, DIR facilitated a more accurate assessment of the dose distribution in adjacent tissues, thereby improving the understanding of the treatment's cumulative impact and enabling subsequent optimization of therapeutic plans. Still, the study highlights the importance of further clinical validation of DIR to firmly establish its routine application in pelvic re-irradiation and to ensure the highest level of safety and efficacy in patient care [40].

4 Materials and Methods

In this project, Eclipse^{RM} was used for visualization and selection of patient plans. Velocity® was used for DIR and dose calculations. Python was used for statistical analysis.

4.1 Velocity®

The Velocity® platform is a resource at the Champalimaud Foundation, that addressed the DIR workflow. Being innovative in medicine for the future and potentially deciding on treatment, the generated registrations should be (a) reliable, and (b) correctly validated. Figure 4.1 shows an image of the Velocity® main panel.

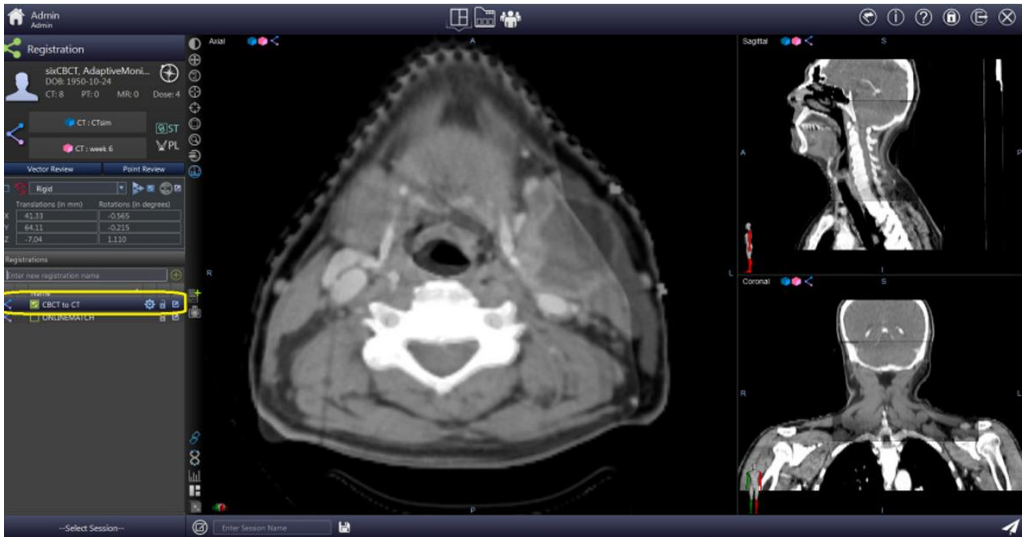

Figure 4.1: Image of the Velocity® main panel, where the primary image corresponds to a CT and the secondary image to a CBCT [41].

4.1.1 Deformation Process and DIR Algorithms Validation

Velocity® software initiates the registration process by automatically aligning the anatomical regions covered in each CT scan, repositioning the secondary CT scan to approximate the primary CT scan. In this work, we will consider the CTplan as the secondary CT and the replanning CT (CTreplan) as the primary CT.

However, it is essential to define a consistent region of interest (ROI) across patients to ensure data comparability. For this project, the selected ROI covered the entire CT scan volume of all included patients, so that the deformation was performed between all points of the image.

To evaluate the deformation process of DIR algorithms, two samples of patients were used. Firstly, the DIR deformation process for replanning cases was evaluated, and in this situation a sample of 17 gynecological patients was used. In the second part of the work, the provision of the objective functions of the DIR for re-irradiation cases was evaluated and for this case a sample of 7 gynecological patients was used.

For image registration, a rigid registration was first performed to optimize and validate the initial alignment, ensuring consistent anatomical overlap before applying deformable registration methods.

For deformable registrations, Velocity® allows the selection of the most appropriate objective function depending on the characteristics of the image set, which can be based either on pixel intensity

or on the anatomical properties of the delineated structures. In the context of this study, the aim was to assess the most suitable objective function for gynecological patients. Thus, priority was given to the extended deformable multipass (EDMP) and structure guided deformable (SGD) methods, which proved particularly suitable for the analysed cases. SGD was selected because it is the only structure-based objective function, and EDMP was selected because it is, among all the other grayscale-based functions, the function with the highest degrees of freedom.

4.1.1.1 Intensity Based vs Image of Structure

The EDMP technique is a deformable registration approach based on grayscale analysis, employing multiple deformation passes (six in total). In each pass, the algorithm evaluates discrepancies between the reference image and the image to be deformed, generating a deformation field that minimizes intensity differences. This refinement procedure provides an incremental improvement to aligning misalignment, and may be particularly useful for CT-to-CT registrations for which simpler registration methods are not sufficient.

In contrast, the SGD is of hybrid category which introduces the anatomical structure contour to guide the deformation. This method is especially useful in situations where there is strong anatomical difference between primary and secondary CT scans, e.g. large differences in bladder filling or other volumes, the situation where standard deformable registrations often fail.

To compare the two deformable registration functions, the Dice Similarity Score (DSC) was used, whose value can be calculated by expression (4.1), for each individual structure, this value can also be calculated directly in Velocity®. The two areas compared correspond to structures from the deformed CT and the replanning CT.

$$DSC = \frac{2 \cdot Area\ of\ overlap}{Sum\ of\ the\ two\ areas} \tag{4.1}$$

This coefficient assumes values between 0 (no overlap) and 1 (perfect overlap), and is widely used as an evaluation metric in image registration studies.

Dice values were obtained for the critical organs selected for analysis ($conf_{PTV}$, $conf_{Bladder}$, $conf_{Bowel\ Small}$, $conf_{Rectum}$ and $conf_{Sigmoid}$). Subsequently, a weighted average was calculated, with the intention of obtaining a standard measure for each objective function, considering the relative weight assigned to each organ, as defined in consultation with a radiation oncologist. The weighted average of dice score $(m_{conformality})$ was determined based on the following expression:

$$m_{conformality} = \frac{conf_{PTV} \cdot 0.500 + conf_{Bladder} \cdot 0.125 + conf_{SB} \cdot 0.125 + conf_{Rectum} \cdot 0.125 + conf_{Sigmoid} \cdot 0.125}{5} \tag{4.2}$$

Where “SB” is Small Bowel.

Statistical Hypotheses

To assess whether there is a significant difference in performance between the two algorithms, EDMP and SGD, in terms of $m_{conformality}$, the following hypotheses were formulated:

Replanning Cases:

- H_0 (null hypothesis): There is no statistically significant difference in $m_{conformality}$values between the EDMP and SGD algorithms.

- H_1 (alternative hypothesis): There is a statistically significant difference in $m_{conformality}$ values between the EDMP and SGD algorithms.

Reirradiation Cases:

- H_0 (null hypothesis): There is no statistically significant difference in $m_{conformality}$ values between the EDMP and SGD algorithms.
- H_1 (alternative hypothesis)**:** There is a statistically significant difference in $m_{conformality}$ values between the EDMP and SGD algorithms.

These hypotheses were tested using the Wilcoxon signed-rank test, due to the small sample size, the non-Gaussian distribution of the data, and the paired nature of the observations (each patient was evaluated with both algorithms).

4.1.2 Quality Assurance and Validation of DIR Processes in Velocity®

One of the most direct approaches to validate the quality of the deformable registration method is to analyze the deformation distortion map, i.e., the calculated DVF. This map gives a visual display of the spatial morphing of each voxel to an unique coordinate where it indicates the deformation vector field to warp the secondary image into the primary image. The vector field reveals not only the intensity of the deformations but also their direction, thus allowing for a deeper analysis of the registration accuracy, as shown in Figure 4.2.

However, in Velocity®, it is not possible to directly calculate the values of these DVFs, so the need arose to create a tool that would extract these values and allow their values to be verified.

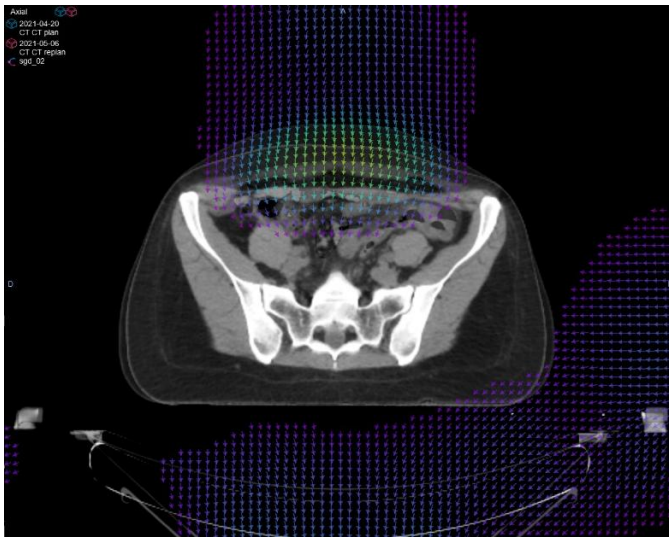

Figure 4.2: Axial CT image overlaid with the vector map resulting from deformable registration between two CT scans. The arrows indicate the direction and magnitude of the displacement vectors applied to the voxels, allowing the visualization of anatomical regions.

In this study, a script was developed to produce and represent the deformation map resulting from the Velocity® platform. The map was encoded as a .bdf extension and its was analyzed and interpreted using Python. By means of a custom-generated script, the displacement vectors in this file can be read and arranged in a three-dimensional grid corresponding to the CT volume (512 × 512 × 232 voxels).

The norm of each vector, representing the amount of deformation experienced for each voxel, can then be displayed graphically.

This script made it possible to prepare a three-dimensional geometric map of displacement vectors, which can be explored in the axial, coronal, or sagittal anatomical planes, thus rendering slice-by-slice the spatial distribution of deformations. The color scale in the images demonstrates the magnitudes of the deformation vector norm i.e., the size of the displacement in mm. The larger values correspond to places with more deformation, whereas the values near zero signify situations with small to no displacement.

The geometric field was additionally overlaid on the original CT image together with the same spatial grid to highlight the anatomical regions impacted by the larger deformation. This procedure was particularly useful in identifying high displacement regions that were clinically relevant anatomical regions (e.g., bladder, rectum, small bowel).

4.1.2.1 QA Validation – Laterality Test

To ensure the reliability of the Python script developed, a laterality test was implemented as part of the quality assurance process. This test consisted of applying a controlled deformation to a single region of the image, by defining a ROI restricted to one of the quadrants of an axial slice (Figure 4.3). The purpose of this assessment was to verify whether the script accurately identified that the deformation occurred exclusively within the defined region, without affecting other areas of the image.

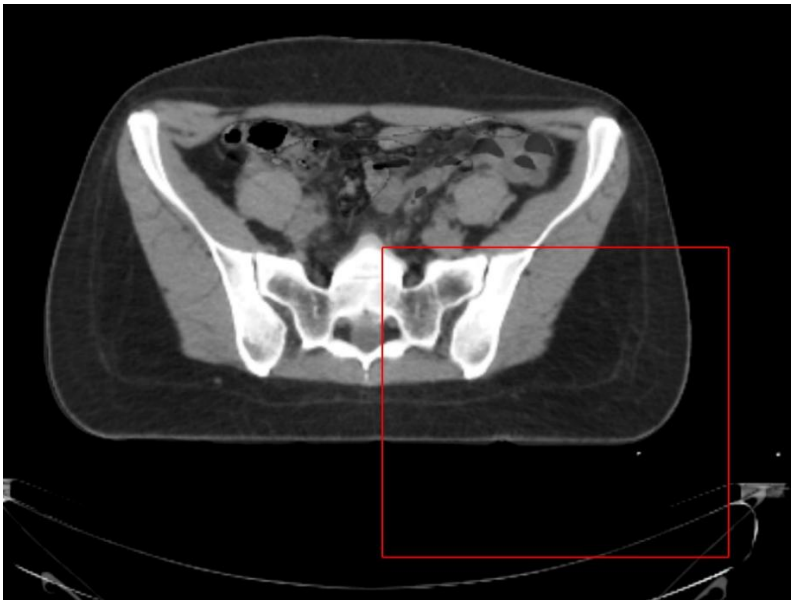

Figure 4.3: Axial CT image with the selected ROI used for the laterality test.

4.2 Deformation Process for Protocol Development

4.2.1 Patient Sample

The first patient sample examined in the present study included 17 patients with gynecological tumors who had all been replanned during the course of their RT treatment as documented in the institutional database.

Among these 17 patients, three patients were treated with a fractionation of 23 fractions, 46 Gy at 2 Gy per fraction. 14 patients were treated with 25 fractions, at total doses of 50 Gy or 55 Gy, with a fraction size of 2 Gy or 2.2 Gy, respectively.

The main objective was to determine which OARs are most vulnerable to major changes during the course of treatment. For this purpose, the following anatomical regions were analyzed: bladder, small intestine, rectum, and sigmoid colon.

This analysis enabled the assessment of each structure's susceptibility to anatomical deformation and associated dosimetric variation, thereby contributing to the definition of criteria that can guide the replanning process.

In the second part of the work, related to the re-irradiation group, a sample of seven gynecological patients was used with the fraction scheme listed in Table 4.1:

Table 4.1: Study sample of re-irradiation cases.

Patient	First Treatment	Second Treatment
1	3 fractions	5 fractions
2	1 fraction	3 fractions
3	5 fractions	5 fractions
4	5 fractions	1 fraction
5	5 fractions	1 fraction
6	5 fractions	5 fractions
7	3 fractions	5 fractions

4.2.2 Dose Deformation

4.2.2.1 In Replanning Cases

In this case study, the CTplan acquired at the beginning of the treatment was defined as the secondary CT, while the CTreplan was defined as the primary CT. The main objective of this subtask was to assess the dose distribution on the patient's updated anatomy, in other words, to understand how anatomical changes influence the dose that is effectively delivered.

Velocity® allows the deformation of the originally planned dose distribution (associated with the secondary CT) onto the anatomy of the secondary CTreplan. For this step, the EDMP registration algorithm was used because its registration is based solely on pixel intensity values and does not depend on any predefined anatomical contours, whereas other methods, such as the SGD, are used in conjunction with delineations of the anatomical structure.

The result of this process is a new dosimetric distribution, referred to as deformed dose, which corresponds to an estimation of the originally planned dose projected onto the anatomy of the day through deformable registration. Although it does not represent the actual dose delivered to the patient, it provides a useful approximation that enables the evaluation and accumulation of dose across different treatment sessions. This simulated dose makes it possible to more realistically evaluate the dose distribution over time and calculates the actual dose absorbed by each voxel at its new spatial position in the anatomy.

From this approach, three dose distributions became available for each patient:

- Dose Plan: the dose distribution initially planned on the anatomy of the planning CT;
- Dose Replan: the new dose calculated on the CT after replanning;

- Dose Deformed: the initial dose deformed onto the secondary CT anatomy, without recalculating the plan.

To analyze these dose distributions, a dosimetric evaluation protocol was created in Velocity®, based on the constraints defined by the QUANTEC [19] guidelines and RTOG [20]. This protocol enabled a systematic assessment of both the Dose Deformed and Dose Replan, allowing the identification of potential violations of established clinical limits. It also made it possible to determine whether the replanning was clinically justified.

It is useful to be aware, however, that the Dose Replan is simply a theoretical simulation in a real clinical setting and the decision to replan is made prior to its calculation. Hence, the analysis of practical decision-making consists exactly of a comparison of the original Dose Plan with the Dose Deformed.

4.2.2.2 In Re-irradiation Cases

In this case study, the CTplan was considered the primary CT, while the CT corresponding to the reirradiation (CTreirr) was considered the secondary CT. The main objective of this subtask was to assess the total dose actually received by the patient throughout her treatment course.

To achieve this, the Velocity® software was used to deform the anatomy of the primary CT onto that of the secondary CT, thereby generating a new CT image—referred to as the deformed CT, similarly to what is done in replanning cases. The derived deformation matrix is applied to the originally planned dose values projected onto the patient's updated anatomy, allowing for a more realistic estimation of the dose distribution effectively absorbed by each anatomical region over time.

From this approach, three dose distributions became available for each patient:

- Dose Plan: the dose initially planned on the anatomy of the primary CT;
- Dose Reirr: the new dose distribution calculated on the secondary CT after replanning;
- Dose Deformed: the initial planned dose deformed onto the anatomy of the secondary CT, without recalculating the plan.

As in the replanning cases, a dosimetric evaluation protocol was implemented in Velocity®, based on the dose limits defined by the QUANTEC[19] guidelines and the RTOG [20]. This protocol enabled a systematic analysis of the deformed dose.

Unlike replanning, in which treatments consisted of 23 or 25 fractions, reirradiation fractionations schedules use a different number of fraction, which can be 1, 3, 5, 23, or 25 fractions.

By applying DIR, it was possible to estimate the dose on the deformed CT, thus allowing the cumulative dose from both treatment regimens to be evaluated.

This summation is necessary to determine the total dose delivered to the patient and to assess whether the dose to the OARs remained within predetermined dose-toxicity limits. It also makes it possible to identify situations of underdosage in the target volume or overdose to the OARs, both of which could compromise the effectiveness and safety of the treatment. However, the direct summation of dose is acceptable only if the two treatments were administered with equal fractions. When the fractionation schemes differ, the correction for fractionation must be made and by converting the dose to an equivalent dose in 2 Gy per fraction (EQD2) (Equation 4.3), using the appropriate formula.

$$EQD2 = D \cdot \frac{d+\frac{\alpha}{\beta}}{2Gy+\frac{\alpha}{\beta}} \tag{4.3}$$

The EQD2 equation considers the total delivered dose (D), dose per fraction (d), and the ratio between the α/β constant of the linear-quadratic model that predicts the response of tissues to fractionation, where α/β = 10 Gy is usually administered for tumors and rapidly dividing tissues and α/β = 3 Gy is used for organs that are at risk and in slow proliferating process. In this study, for the OARs a α/β of 3 Gy was used.

This conversion is taken after which clinically informative dose assessment can be taken (Equation 4.4).

$$EQD2_{total} = EQD2_{DosePlan} + EQD2_{DoseDeformed} \tag{4.4}$$

Subsequently, the total EQD2 dose is converted into the fractionation adopted in the medical prescription, making it compatible with the clinical criteria in use (Equation 4.5).

$$D = \frac{-\frac{\alpha}{B} + \sqrt{\left(\frac{\alpha}{B}\right)^2 + \frac{4\left(2+\frac{\alpha}{B}\right)EQD2_{total}}{n}}}{\frac{2}{n}} \tag{4.5}$$

Where *n* is the number of fractions given in the treatment.

Following these procedures, it becomes possible to determine with greater precision the accumulated dose delivered to each OAR, thereby enabling robust conclusions regarding the adequacy of the treatment plan and the potential need for future reassessments.

4.2.3 Distortion Unit Analysis in Replanning Cases

A distortion unit analysis provided by the Velocity® software was also performed, with the aim of quantifying the degree of geometric displacement between the CTplan and CTreplan. Using the Navigator panel in Velocity®, it was possible to generate a patient-specific report, which graphically represents the relationship between the proportion of the volume affected and the magnitude of the distortion, expressed in millimetres. This report enables an objective evaluation of the spatial displacement of voxels resulting from the deformation applied to align the CTreplan anatomy with the CTplan. As in previous steps, CTplan was defined as the secondary image, and CTreplan as the primary image, with the deformable registration applied accordingly.

5 Results

5.1 Velocity® Validation

5.1.1 Evaluation of Deformable Image Registration Algorithms

5.1.1.1 Replanning Cases

As part of this study, the two main deformable image registration algorithms available in the Velocity® software were validated: EDMP and SGD. To compare the performance of both methods, the metric $m_{conformality}$ was used, calculated according to Equation (3), which quantifies the degree of volumetric overlap between the deformed structures from CT Deformed and the reference contours from CTreplan.

The analysis was carried out on a sample of 17 patients who underwent replanning. Both algorithms were applied to each patient in a paired manner. The resulting $m_{conformality}$ values are summarised in Figure 5.1.

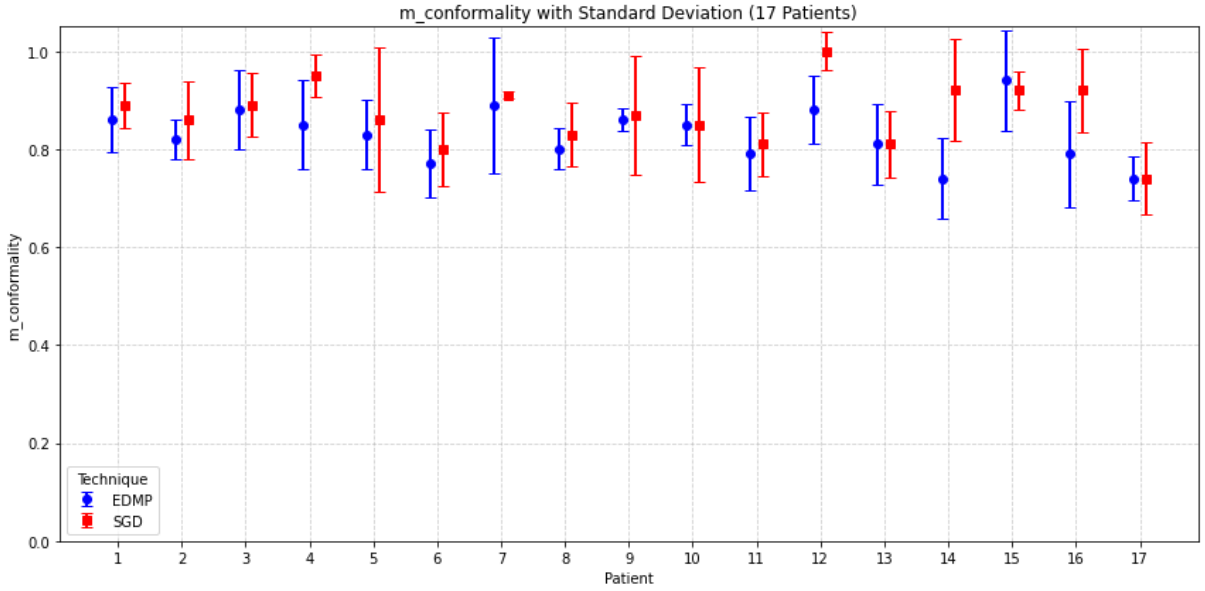

Figure 5.1: Comparison of $m_{conformality}$ for the two objective functions for 17 different patients.

Besides, to further explore the $m_{conformality}$ values of each patient, as shown in Figure 5.1, a boxplot of these values (Figure 5.2) was generated to visually and compare the performance of the two DIR algorithms, namely EDMP and SGD. This kind of graphic shows both the medians and spread of data as well as any outliers and the interquartile range. The visual analysis supports the statistical interpretation and shows that the values returned by the SGD algorithm are distributed around higher conformity levels, with the EDMP algorithm producing lower median and wider spread values, which indicate higher variability in performance. The error bars represent the variability of the values across patients, indicating the standard deviation relative to the mean. The error bars represent the standard deviation associated with the conformity values calculated for each organ.

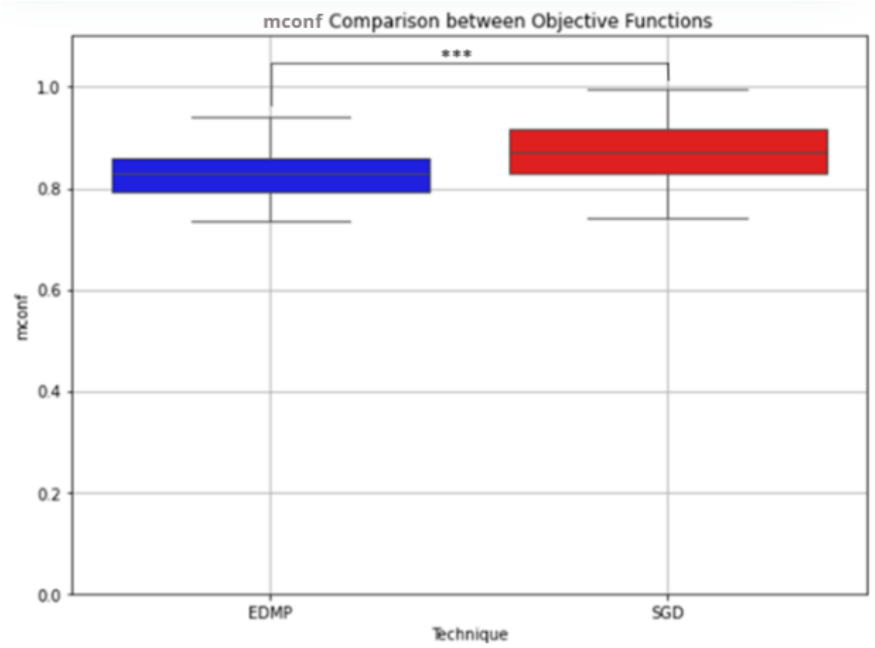

Figure 5.2: Graphical representation in boxplot of the comparison between the two objective functions EDMP and SGD. (*** significant at p<0.001)

A statistical comparison was also performed using the Wilcoxon signed-rank test. We chose this test due to the small sample size (n = 17), the non-Gaussian distribution of the data, and the fact that the observations were paired (each patient was examined with both algorithms).

The Wilcoxon test statistic was 8.0 and the p-value was 0.00038, demonstrating that the difference between these two algorithms is statistically significant at the 5% significance level. These findings lead us to reject the null hypothesis, meaning that the SGD method is clearly superior to the EDMP method.

5.1.1.2 Re-irradiation Cases

In this phase, the same methodology used for the replanning cases was applied, with the aim of evaluating which objective function, EDMP or SGD, performs better in re-irradiation scenarios. To this end, the $m_{conformality}$ value was assessed for each of the seven patients included in this group, and the results are presented in Figure 5.3.

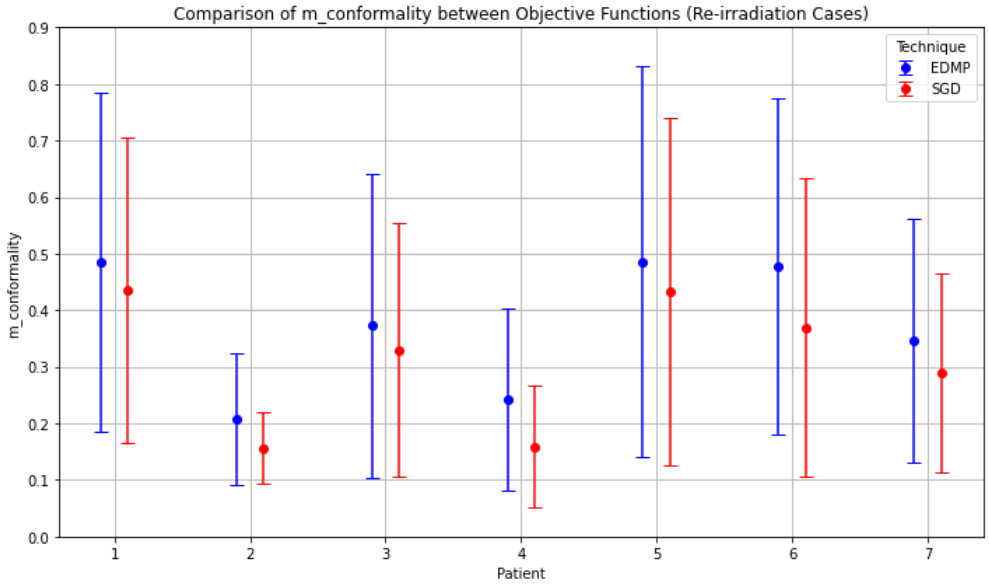

Figure 5.3: Comparison of $m_{conformality}$ for the two objective functions for 7 different patients.

In addition to the per-patient analysis, a boxplot diagram was constructed to provide a clearer visual representation of the distribution of conformity values for each objective function, including the median, spread, and potential outliers, as illustrated in Figure 5.4. The error bars represent the variability of the values across patients, indicating the standard deviation relative to the mean. The error bars represent the standard deviation of the $m_{conformality}$ values for each patient, reflecting the degree of variability in deformation across the considered structures in the re-irradiation cases.

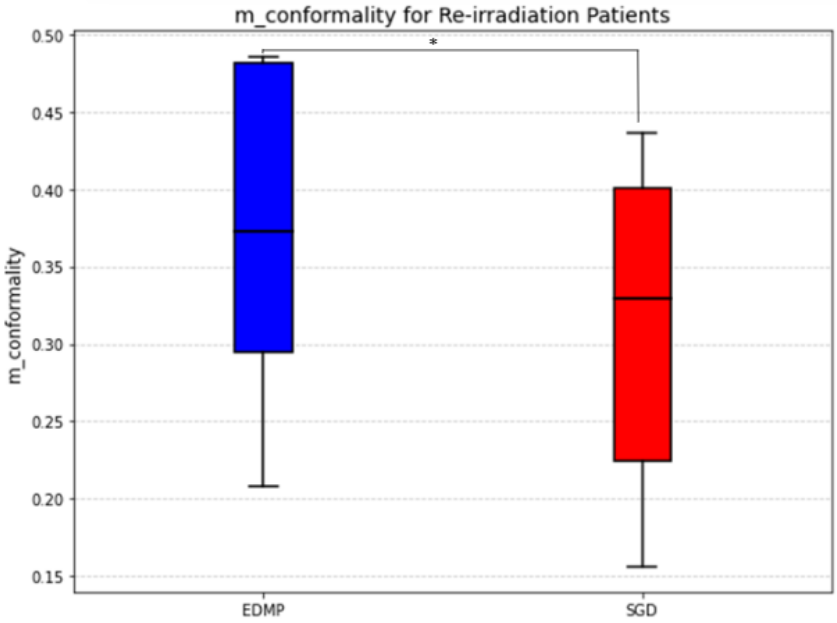

Figure 5.4: Graphical representation in boxplot of the comparison between the two objective functions EDMP and SGD. (* significant at $p<0.05$)

As in the previous cases, and considering the small sample size (n = 7), the Wilcoxon signed-rank test was applied to statistically compare the performance of the two algorithms. The test yielded a

test statistic of 0 and a *p-value* of 0.016. These results allowed for the rejection of the null hypothesis, indicating that the EDMP function produces significantly higher $m_{conformality}$ values than the SGD function in re-irradiation cases.

5.1.2 Velocity® QA and Validation Testing

To ensure the reliability of the deformation process generated by the Velocity® software, an analysis of the geometric map corresponding to the norms of the DVFs was carried out. From this volume, an axial slice - typically corresponding to the mid-plane - was selected and subsequently overlaid with the corresponding CT image. Only one CT slice was selected in order to optimize code compilation time, and to represent the slice viewed by the physician.

This overlay enabled a direct qualitative assessment of the spatial coherence between the anatomical image and the regions of greatest deformation, serving as a QA tool for deformable registrations. In clinical practice, radiation oncologists frequently rely on CBCT images acquired at the linear accelerator to identify anatomical changes that may justify the need for replanning. As such, by comparing these clinical observations with the areas of highest vector intensity displayed in the geometric map, it is possible to evaluate the quality of the deformation. When the regions of greatest intensity in the geometric map coincide with the areas identified in the CBCT as most altered, it can be concluded that the deformation was successfully performed. This correspondence is particularly important as it reinforces confidence that the deformation applied to the dose distribution will also be valid and clinically meaningful.

To validate the consistency of the geometric map, two complementary validation methods were employed: comparison with the Velocity® -provided vector review map and the execution of a laterality test.

The first method involved a visual comparison with the vector revision map available in the Velocity® platform, since this software does not provide any type of quantitative value for DVFs (Figure 5.6). Although this internal map does not provide an explicit quantitative scale for vector magnitudes, qualitative observation allows identification of regions with greater vector density or length, interpreted as areas of more pronounced deformation. Figure 5.5 presents the Velocity® vector map for a selected axial slice, while Figure 5.6 displays the corresponding geometric map generated from the data extracted using Python. Despite the differences in graphical representation and the lack of directly comparable scales in Velocity®, a global correspondence was observed between the regions of greatest deformation in both maps. This similarity suggests that data extraction and subsequent processing were performed correctly, supporting the validity of the developed approach.

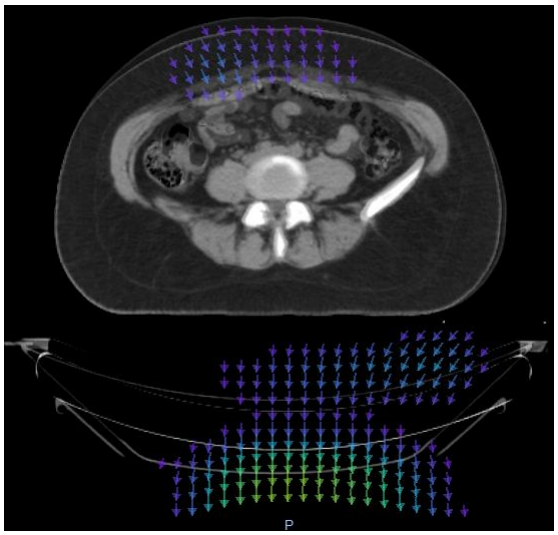

Figure 5.6: Axial CT image overlaid with the vector map resulting from deformable registration between two CT scans.

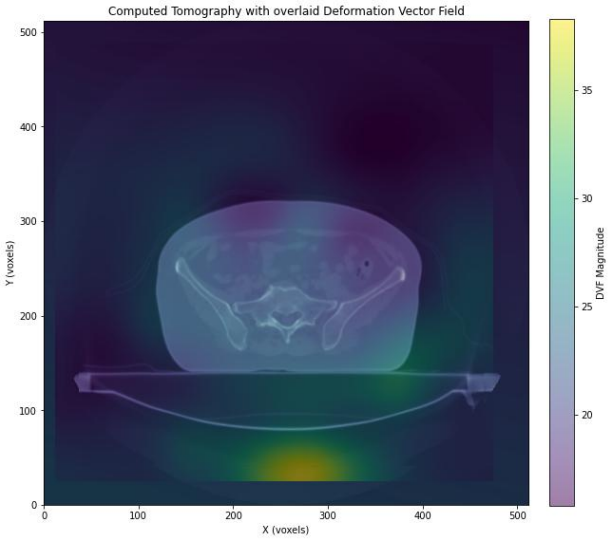

Figure 5.5: Axial slice of the planning CT overlaid with the magnitude of the DVF.

The second validation method consisted of a laterality test designed to determine whether the geometric map could accurately detect a deformation confined to a specific quadrant of the image. To this end, a deformation was restricted to the fourth quadrant of an axial slice by defining a localized ROI. The geometric map derived from this controlled deformation demonstrated, as shown in Figure 5.7, a markedly higher deformation intensity in the targeted region, while the remaining quadrants exhibited significantly lower values. The intensity in adjacent zones decreased proportionally with distance from the deformation center, validating not only the spatial localization capabilities of the tool but also its sensitivity to vector intensity gradients.

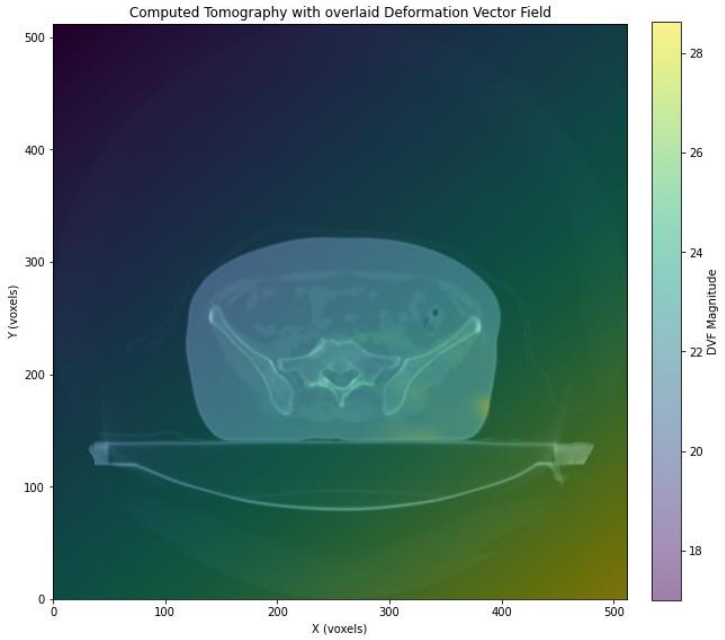

Figure 5.7: Axial slice of the planning CT overlaid with the magnitude of the DVF.

5.2 Replanning

5.2.1 Differences in Dose Deformation

The Dose Plan, Dose Replan, and Dose Deformed distributions, for the various constraints defined, were collected for analysis from 17 patients. To systematically organize and allow for meaningful comparison between different organs and patients, a normalization of the obtained values relative to their clinical reference limits was carried out. This normalization consisted of calculating the ratio between the measured dose value and the recommended dose limit, thereby providing a relative quantification of the severity of each potential clinical constraint violation.

For each organ, the maximum normalized value among all constraints, both volumetric and maximum dose constraints, was selected to graphically represent the most critical scenario per structure. In the case of the small bowel, normalized maximum dose values were also included, since this anatomical region is evaluated based on maximum explicit dose thresholds.

The results of this analysis are summarized in Table 5.1, where the most critical normalized values per organ are presented. The full dataset, including all constraints analyzed per patient, is available in Appendix A.

Table 5.1: Maximum normalized values associated with each anatomical structure, comparing planned and deformed doses, including maximum dose and dose-volume constraints where applicable.

Dose Plan Associated with each Structure	Dose-Volume Constraints	Maximum Normalized Value
Bladder Plan	V35Gy<=50% V40Gy<=35% V50Gy<=5%	2.18 ± 0.69
Bladder Deformed		2.96 ± 1.81
Bowel Small Plan	V15Gy<=120cc V30Gy<=200cc V35Gy<=150cc V45Gy<=20cc V45Gy<=195cc Dmax<=50Gy	5.87 ± 3.87
Bowel Small Deformed		12.90 ± 5.94
Bowel Small Plan Max		1.00 ± 0.02
Bowel Small Deformed Max		1.10 ± 0.11
Rectum Plan	V30Gy<=200cc V35Gy<=1500cc V45Gy<=20CC V50Gy<=50%	1.15 ± 0.53
Rectum Deformed		1.28 ± 0.58
Sigmoid Plan	V30Gy<=200cc V35Gy<=1500cc V45Gy<=20CC V50Gy<=50%	2.10 ± 1.96
Sigmoid Deformed		2.57 ± 1.92

To support data interpretation and visually highlight discrepancies between the initially planned dose and the deformed dose mapped onto the updated anatomy, a scatter plot was generated (Figure 5.8). In this figure, blue dots represent the normalized values for the Dose Plan, simulating a scenario where no fractions would have been delivered due to unfavorable anatomy observed at treatment, while red crosses represent the normalized values for the Dose Deformed, i.e., the originally planned

dose distribution mapped onto the updated anatomy via DIR. The error bars represent the standard deviation of the normalized dose values across the 17 pelvic patients, illustrating the variability in dose distribution for each organ. Larger error bars indicate greater inter-patient anatomical variability and deformation effects during treatment.

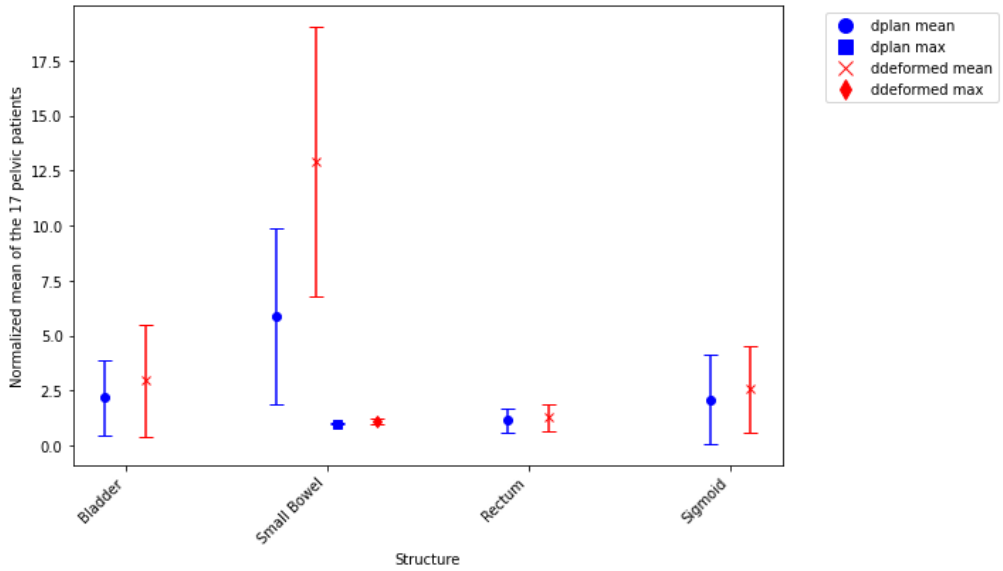

Figure 5.8: Average and standard deviations of the planned dose and deformed dose for 17 patients with gynecological pathology for the mean and maximum dose of each structure. Normalized values are presented for each anatomical structure, bladder, rectum, sigmoid colon, and small bowel.

The small bowel is shown as the primary organ prompting replanning throughout the treatment process, due to the large gap between planned dose and deformed dose. This result is consistent with clinical literature, as the small bowel combines a very narrow dosimetric tolerance with a high degree of anatomical variability, both of which make it particularly relevant in adaptive replanning. Due to its mobility and propensity to encroach into high-dose regions (for example the pelvic fields), even slight positional changes may result in considerably higher doses than they were originally designed. It accounts for the increase in clinical focus in this structure and permits replanning whenever drastic anatomical changes are registered in its posture or volume.

Apart from statistical examination of the dose values, a DVH was also created, showing the regression curves of the Replan Dose and the Deformed Dose (Figure 5.9). This graphic depiction enables for a clear visual correspondence of the two cases and to differentiate dose distributions for each of the volumes as well.

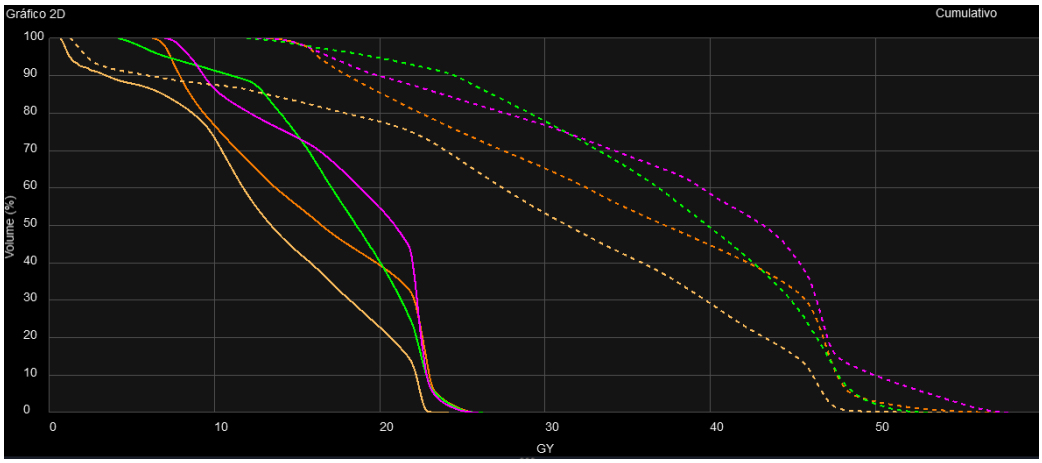

Figure 5.9: DVH comparing the Replan and Deformed dose curves, where the orange line represents the bladder, the yellow line represents the small bowel, the green line corresponds to the rectum and the pink line to the sigmoid colon. Continuous lines depict the replan dose, while dashed lines indicate the deformed dose.

A dedicated clinical replanning protocol was developed and implemented directly into the Velocity® platform, as shown in Figure 5.10. This protocol involved integrating dosimetric constraints based on the aforementioned guidelines directly into the software. It allows the radiation oncologist to perform dose deformation and immediately assess compliance with clinical limits for each structure, tailored to each patient's anatomy, in a unified environment.

Estrutura	Fonte de dados	Tipo	Nome do volume	Volume da estrutura (cc)	Valor mín.	Valor médio	Valor máx.	Nome da restrição	Texto da restrição
Bladder	Velocity	ORGAN	Dose Deformed	274.6	13.31	35.40	57.45	V 35 GY <= 50 %	54.48 % (149.6 cc)
								V 40 GY <= 35 %	44.74 % (122.8 cc)
								V 50 GY <= 5 %	2.94 % (8.1 cc)
Bowel Small	Velocity	ORGAN	Dose Deformed	588.5	1.22	29.74	54.45	V 15 GY <= 120 CC	83.19 % (489.6 cc)
								V 30 GY <= 200 CC	53.23 % (313.3 cc)
								V 35 GY <= 150 CC	41.82 % (246.1 cc)
								V 45 GY <= 20 CC	15.48 % (91.1 cc)
								V 45 GY <= 195 CC	15.48 % (91.1 cc)
								Dose máx. <= 50 GY	54.45 GY
Rectum	Velocity	ORGAN	Dose Deformed	55.6	11.90	37.82	53.32	V 30 GY <= 200 CC	77.83 % (43.2 cc)
								V 35 GY <= 150 CC	65.41 % (36.3 cc)
								V 45 GY <= 20 CC	29.35 % (16.3 cc)
								V 50 GY <= 50 %	2.30 % (1.3 cc)
Sigmoid	Velocity	ORGAN	Dose Deformed	55.3	12.54	38.92	58.27	V 30 GY <= 200 CC	76.80 % (42.5 cc)
								V 35 GY <= 150 CC	68.66 % (38.0 cc)
								V 45 GY <= 20 CC	42.32 % (23.4 cc)
								V 50 GY <= 50 %	9.92 % (5.5 cc)
Bladder	Velocity	ORGAN	Dose replan	274.6	6.19	16.21	26.05	V 35 GY <= 50 %	0.00 % (0.0 cc)
								V 40 GY <= 35 %	0.00 % (0.0 cc)
								V 50 GY <= 5 %	0.00 % (0.0 cc)
Bowel Small	Velocity	ORGAN	Dose replan	588.5	0.64	13.66	24.17	V 15 GY <= 120 CC	43.01 % (253.1 cc)
								V 30 GY <= 200 CC	0.00 % (0.0 cc)
								V 35 GY <= 150 CC	0.00 % (0.0 cc)
								V 45 GY <= 20 CC	0.00 % (0.0 cc)
								V 45 GY <= 195 CC	0.00 % (0.0 cc)
								Dose máx. <= 50 GY	24.17 GY
Rectum	Velocity	ORGAN	Dose replan	55.6	4.15	17.75	26.25	V 30 GY <= 200 CC	0.00 % (0.0 cc)
								V 35 GY <= 150 CC	0.00 % (0.0 cc)
								V 45 GY <= 20 CC	0.00 % (0.0 cc)
								V 50 GY <= 50 %	0.00 % (0.0 cc)
Sigmoid	Velocity	ORGAN	Dose replan	55.3	6.94	18.32	25.99	V 30 GY <= 200 CC	0.00 % (0.0 cc)
								V 35 GY <= 150 CC	0.00 % (0.0 cc)
								V 45 GY <= 20 CC	0.00 % (0.0 cc)
								V 50 GY <= 50 %	0.00 % (0.0 cc)

Figure 5.10: Protocol created in the Velocity® platform displaying the Replan and Deformed dose values in relation to the predefined dose constraints established by QUANTEC and RTOG guidelines (listed on the 8th column).

5.2.2 Differences Observed in Distortion Units

In addition, a comparison between deformation units of the deformable registration process with dose distributions was done to supplement the analysis of these differences. The Velocity® software automatically delivers values for every contoured anatomical structure of the deformation unit produced by the applied registration. Using this functional mechanism, the mean deformation unit was calculated for each organ, for the study sample of 17 patients, along with the corresponding standard deviation, in order to quantify the variability observed across cases.

These results are summarized in Table 5.2 and graphically displayed in Figure 5.11, which facilitates a clear depiction of the most vulnerable structures due to anatomical variation throughout the course of treatment.

Table 5.2: Mean values and standard deviations of distortion units per anatomical structure, calculated based on the deformation maps of 17 patients.

	Bladder	**Small Bowel**	**Rectum**	**Sigmoid**
Mean (mm)	9,55	16,08	6,93	9,98
Standard Deviation	3,45	4,16	2,69	3,08

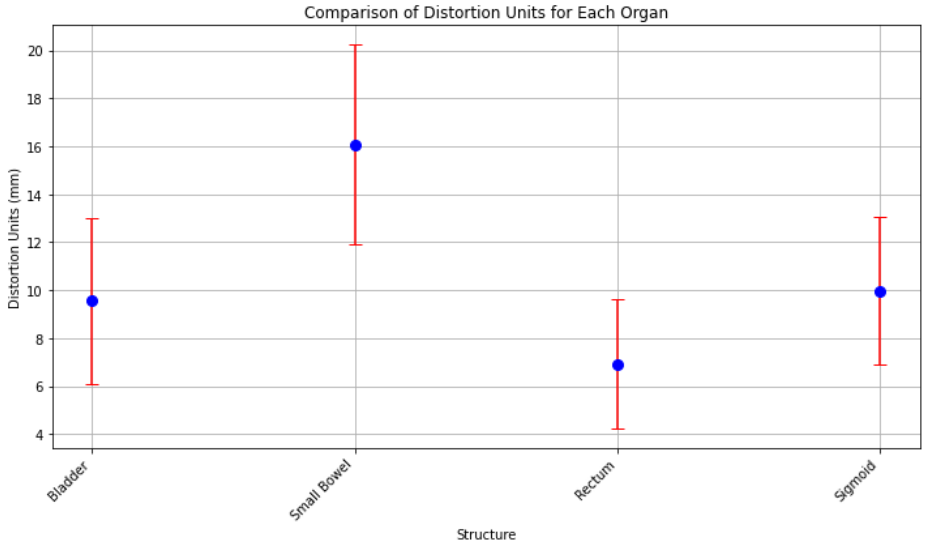

Figure 5.11: Mean distortion units for each anatomical structure, represented with standard deviation error bars, based on data from 17 patients.

Velocity® also permits you to create a graph showing the distribution of distortions throughout the volume of interest, as displayed in Figure 5.12, helping to identify anatomical regions which underwent the largest geometric changes. Such a visual representation is a powerful approach for qualitative and quantitative evaluation of deformation and an estimation of the quality of deformable registration.

This step was done for all 17 patients included in the study, and an individual analysis was performed for each organ evaluated. Through interpretation of the distortion graphs, it was possible to determine which anatomical structures presented the most deformations, providing information for determining the clinical situations in which replanning would be most necessary. This approach

therefore promotes improved surveillance of key anatomical regions throughout treatment and the implementation of more stringent criteria for adaptive replanning decisions.

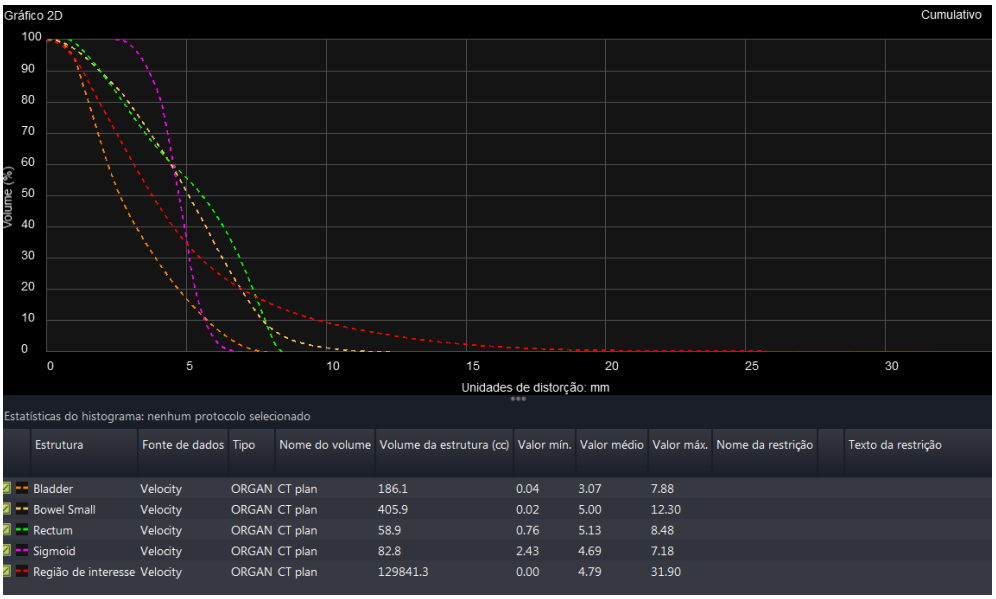

Figure 5.12: Distribution of distortions units (mm) throughout the volume of interest for the target volumes and the different OARs.

5.3 Re-irradiation

5.3.1 Differences Observed in Dose Deformation

To evaluate and analyze the data collected for the seven reirradiation patients, the same methodology was used as for the replanning cases. That is, the Plan Dose, Reirr Dose, and Deformed Dose data were collected, but this time, we obtained a broader fractionation plan, since these were cases of tumor recurrence. The fractionation plans used for the different patients and their associated constraints according to the QUANTEC and RTOG standards are tabulated in Table 5.3.

Table 5.3: Fractionation system used for the 7 reirradiation patients.

	Constraints			
OARs	**1 Fraction (1#)**	**3 Fractions (3#)**	**5 Fractions (5#)**	**25 Fractions (25#)**
Bladder	V18.4Gy<=0,035cc V11.4Gy<=15cc	V28.2Gy<=0.035cc V16.2Gy<=15cc	V38Gy<=0.035cc V18.3Gy<=15cc	V35Gy<50% V40Gy<35% V50Gy<5%
Small Bowel	V15.4Gy<=0,035cc V11.9Gy<=5cc	V25.2Gy<=0,035cc V17.7Gy<=5cc	V35Gy<=0.035cc V19.5Gy<=5cc	V15Gy<120cc V30Gy<200cc V35Gy<150cc V45Gy<20cc V45Gy<195cc Dmax<50Gy
Rectum	V18.4Gy<=0,035cc	V28.2Gy<=0.035cc	V38Gy<=0.035cc	V30Gy<200cc

	V14.3Gy<=20cc	V24Gy<=20cc	V25Gy<=20cc	V35Gy<150cc V45Gy<20cc V50Gy<50%
Sigmoid	V18.4Gy<=0,035cc	V28.2Gy<=0.035cc	V38Gy<=0.035cc	V30Gy<200cc
	V14.3Gy<=20cc	V24Gy<=20cc	V25Gy<=20cc	V35Gy<150cc V45Gy<20cc V50Gy<50%

After collecting the clinical data corresponding to the various defined constraints, the values obtained were normalized according to their clinical reference limits, as in the replanning cases. Table 5.4 shows, for each patient, the fractionation scheme used in each plan and the maximum normalized value obtained for that fractionation plan. The complete data set, including all constraints analyzed per patient, is available in Appendix B.

Table 5.4: Fractionation followed by each patient for each of the treatment plans, as well as the maximum normalized value, for the respective treatment plan. Where # represents the fraction nomenclature.

	Patients													
	1		**2**		**3**		**4**		**5**		**6**		**7**	
OARs	#	Max Val.	#	Max Val.	#	Max Val.	#	Max Val.	#	Max Val.	#	Max Val.	#	Max Val.
Bladder Plan	3#	0.97	1#	11.43	5#	0.68	5#	-	5#	-	5#	0.00	3#	-
Bladder Deformed	5#	0.20	25#	0.77	5#	0.00	1#	0.00	1#	-	5#	0.00	5#	-
Small Bowel Plan	3#	0.00	1#	0.00	5#	0.00	5#	0.00	5#	0.00	5#	-	3#	0.00
Small Bowel Deformed	5#	0.00	25#	0.00	5#	0.00	1#	0.00	1#	0.44	5#	0.00	5#	0.00
Rectum Plan	3#	0.09	1#	17.14	5#	0.00	5#	-	5#	-	5#	0.00	3#	-
Rectum Deformed	5#	0.08	25#	0.36	5#	0.00	1#	0.00	1#	0.00	5#	0.00	5#	0.00
Sigmoid Plan	3#	0.00	1#	4.29	5#	0.00	5#	0.00	5#	0.00	5#	-	3#	0.00
Sigmoid Deformed	5#	0.00	25#	0.06	5#	0.00	1#	-	1#	0.00	5#	-	5#	0.00

Subsequently, the doses from the two treatment plans (Dose Plan and Dose Deformed) were summed to assess whether the accumulated dose values fell within the dose limits previously established by [16]. To this end, the mean EQD2 values corresponding to the Dose Plan and the Dose Deformed

were first calculated. In cases where the interval between the two treatment plans exceeded six months, a tissue recovery period equivalent to 25% of the accumulated dose was considered.

Accordingly, for patients 1, 2, 4, 5, and 7, whose fractionation schemes differed between the two plans, the EQD2 means were calculated after applying the recovery correction. Conversely, for patients 3 and 6, who had identical fractionation schemes in both treatment plans, it was possible to directly sum the Dose Plan values (with the recovery already included) and the Dose Deformed values.

Subsequently, for the five patients with differing fractionation schemes, the total accumulated EQD2 value was converted to the reference clinical scheme in accordance with Equation 4.5. Following this conversion, the overall mean for the group of seven patients was calculated. All results are presented in Table 5.5.

Table 5.5: Mean EQD2 dose values for Dose Plan, Dose Deformed, and for conversion to the clinical reference scheme. Where S.D. is Standard Deviation.

	Mean Dose Plan			**Mean Dose Deformed**					
OARs	**EQD2 (Gy)**	**S.D. EQD2**	**EQD2 with recovery (Gy)**	**EQD2 (Gy)**	**S.D EQD2**	**Sum (Gy)**	**SD Sum**	**Reference Dose units (Gy)**	**Maximum Dose per OAR (Gy)**
Bladder	52.08	8.94	39.06	30.49	21.45	69.55	38.25	21.30	90.00
Bowel Small	14.33	14.75	10.75	36.94	18.44	47.69	21.14	23.79	60.00
Rectum	58.63	14.54	43.97	31.12	23.99	75.09	42.70	30.58	75.00
Sigmoid	20.27	13.28	15.20	23.43	15.64	38.63	27.17	22.63	75.00

To analyze the discrepancies between the Planned Dose and the Deformed Dose, a scatterplot was generated, shown in Figure 5.13. To create this graph, the maximum dose for each organ for the seven patients was used. Therefore, the blue dots represent the maximum normalized values for the Planned Dose in EQD2, simulating an ideal scenario in which the patient would have received only an initial treatment plan, while the red dots represent the Deformed Dose in EQD2, which corresponds to the dose the patient would have received if the plan for the first treatment had been applied to the anatomy of the second treatment, without deformation and without any replanning or clinical adjustments. It is important to note that the error bars were adjusted to avoid negative dose values.

Furthermore, Figure 5.13 also includes a third line corresponding to the total accumulated dose in EQD2. This line represents a cross that marks the maximum tolerance limit established for each organ according to clinical references [16]. This additional indication allows the results obtained to be

contextualized, clearly demonstrating whether the total dose exceeds or remains within the safety values defined for the organs at risk.

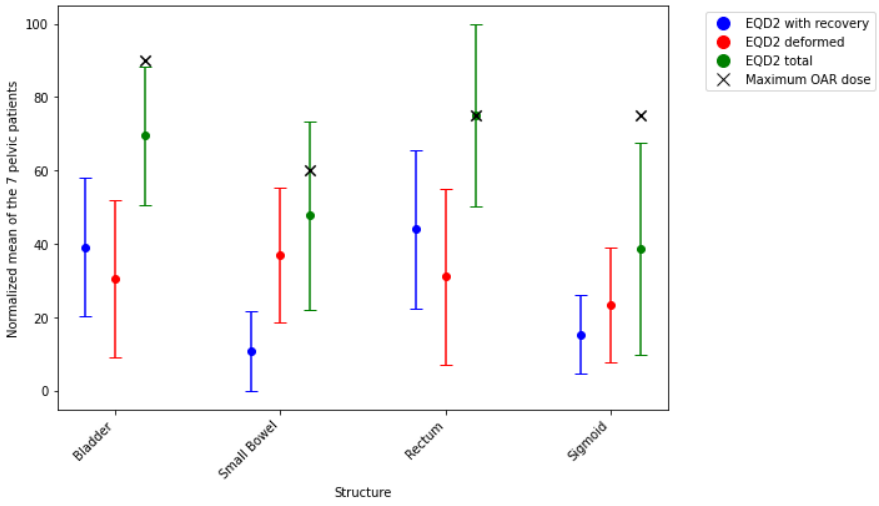

Figure 5.13: Comparison of normalized mean EQD2 values (with recovery, deformed, and total) for the seven re-irradiation patients, including error bars (standard deviation). The blue markers represent EQD2 with recovery, the red markers correspond to EQD2 deformed, and the green markers indicate the total EQD2 (sum). Black crosses denote the maximum dose constraints established for each organ at risk (OAR).

6 Discussion

6.1 Velocity® Validation

6.1.1 Evaluation of Deformable Image Registration Algorithms in Replanning Cases

The value of the two objective functions, EDMP and SGD, the respective DSC values were compared. The comparative analysis in Figure 5.1 demonstrates the $m_{conformality}$ based on the two approaches, the EDMP and SGD, for 17 patients. Overall, the SGD approach consistently achieved higher $m_{conformality}$ results than EDMP, indicating a better deformation overlap with reference contours. In addition, the error bars around each point illustrate that, SGD also exhibits in some cases less spread (even if higher average values) to show less dispersion and greater robustness and reproducibility. These findings further support the advantage of the SGD algorithm in a gynecology RT setting, as it appears on average to optimize the spatial correspondence between structures performing the best [42].

Figure 5.2 portrays a graphic representation of the statistical result. The median $m_{conformality}$ for the SGD function was higher than for the EDMP, meaning more overlap between the structures deformed and the reference contours. However, one interesting point is that the values of the SDG statistic scatter more in the extremes than in the middle, reflecting that there are cases which depart further from the mean. However, the overall distribution of SGD data was still above, still favoring their better average. The EDMP function instead showed more clustered values, but lower performance average, which seems less efficient in preserving anatomical correspondence between patients, especially for those concerning more clinically complex cases.

These findings are consistent with the theoretical characteristics of each algorithm [42], [43]. The SGD method is especially powerful when structural delineation is available due to the inclusion of anatomic contour information to guide the deformation. It is therefore well-suited for use in the clinics where large volumetric changes are anticipated due to, for example, tumor shrinkage in OARs such as the bladder or the rectum over the treatment course. SGD is thus strongly recommended for the purpose of adaptive replanning involving contours in gynecological cases.

However, it is important to highlight that SGD cannot always be applied. In cases where no delineated structures are available, such as during dose deformation processes, the EDMP algorithm becomes the preferred method. EDMP relies solely on grayscale intensity analysis, requiring no anatomical contours, which makes it particularly useful when estimating dose distribution in new anatomies without prior recontouring.

6.1.2 Evaluation of Deformable Image Registration Algorithms in Re-irradiation Cases

Upon analyzing Figure 5.3, it can be concluded that, for most patients, the $m_{conformality}$ values are higher when using the EDMP objective function is compared to SGD. However, the absolute values obtained are generally low. This is explained by the considerable time interval between the CT scans, as many of the older CTs had structures without delineated contours when imported into Velocity®. As the Dice Similarity Score calculation requires delineated contours for each structure, their absence resulted in a score of zero for those cases.

Therefore, the analysis was conducted only on the structures that were effectively delineated in Velocity® for each patient. As a result, none of the cases included all the structures of interest. This

limitation was deemed acceptable, given that the main goal of this evaluation was to determine which objective function performed better relatively, rather than to achieve the highest possible $m_{conformality}$ values.

When comparing the boxplots (Figure 5.4), it becomes evident that the EDMP function demonstrates better reproducibility in re-irradiation cases. This can be attributed to the fact that SGD relies on anatomical contours. In re-irradiation scenarios, where there is typically a longer time gap between treatments, anatomical changes are often more pronounced, for instance, significant variations in bladder volume or overall body shape. As a result, the contours no longer serve as a reliable reference for guiding deformable image registration, thereby reducing the effectiveness of structure-based methods such as SGD.

In Figures 6.1 and 6.2, where the SGD objective function was applied, clear discrepancies can be observed between the anatomy of the secondary CT and that of the resulting deformed CT. In particular, Figure 6.1 shows a marked discrepancy in the position and shape of the bladder, while Figure 6.2 reveals considerable misalignment of the body contour. These deviations highlight the limitations of the SGD function in situations involving substantial anatomical variation between scans, further supporting the superiority of EDMP in this specific context.

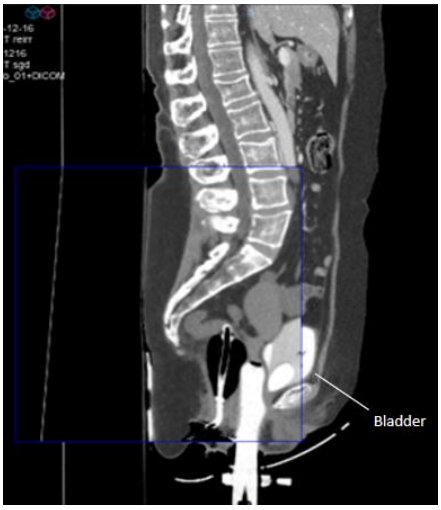

Figure 6.1: Sagittal CT image showing the delineation of the bladder.

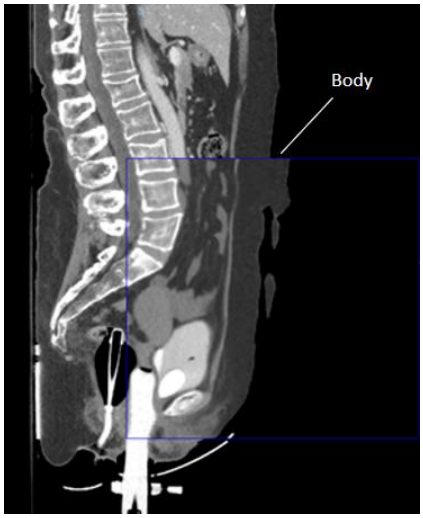

Figure 6.2: Sagittal CT image showing the delineation of the body.

6.1.3 Velocity® QA and Validation Testing

The results of the validation technique applied on the Velocity ® deformable registration algorithm need to be interpreted critically in perspective to the state of the art. There were various reports of techniques utilized in oncological DIR validation studies, and quantitative validation methods were most commonly used. These approaches include landmark-based target registration error estimates, comparison with known deformations on physical or digital phantoms, and utilization of global image similarity metrics, such as Mutual Information or Dice Similarity Coefficient.

For instance, Kadoya et al. (2015) tested the Velocity® algorithm on images from a thoracic phantom that sustained known deformations and stated mean errors of registration of less than 2 mm for most areas. This kind of methodology paves the way for exact, objective measurement of spatial alignment, since a ground truth is known. It however fails to account for the complexity of the anatomical variations present in actual clinical cases (particularly in a highly variable region such as the female pelvis) [44].

Similarly, Hardcastle et al. (2012) used clinical images where fiducial markers were implanted at some anatomical sites, and measured their positions after image registration. This approach allows one to directly measure registration error in individual patients, but relies on repeatable and accurate localization of the same anatomical landmarks in multiple images, which can be difficult to do, especially in soft-tissue structures such as the rectum, bladder or small bowel. Further, fiducial markers are applicable only in prospective or research settings for ethical and practical reasons [45]

Against such a context the approach proposed in the current study appears a feasible, straightforward and clinically applicable option. The first part of the method is a visual comparison between the geometric map resulting from norms of DVFs and the vector internal review map of Velocity® platform. While fundamentally qualitative, this technique allows for a quick check of the spatial correspondence of the applied deformation, by matching regions of highest vector intensity - expected to correspond to regions of greatest anatomical motion, in both visualizations. The reasonable extent of conformity of these high deformation regions, albeit differences in display scale and style, indicates both the reliability of the data obtained by Python as well as the soundness of the algorithm based on the cases studied. The second part of the validation was a laterality experiment in which an artificial, controlled, localized deformation was introduced in a single quarter of an axial slice. This test was designed to measure the information provided by the geometric map to local changes. The deformation region was positively associated with increased vector magnitude in the corresponding quadrant, with near-zero values in the other three quadrants. This finding validated the ability of the technique to identify localized anatomical changes and supported its role as a real-time verification tool in a clinical workflow, particularly regarding replanning.

Although this is not a quantitative approach (as TRE, or explicit millimetric error quantification), it offers large advantage to the same applied at clinical level. Its simplicity, the lack of requirement for extra equipment, markers, or controlled deformations, and the possibility of application to real clinical datasets makes it particularly suitable for everyday clinical practice, where rapid but confident clinical decisions often need to be made. Moreover, since the tool is visual and intuitive, radiation oncologists can interpret the output almost at a glance, allowing for a quick check of whether the registration looks reasonable and whether the transformation would be trustworthy to apply deformations to the anatomic or dose data.

6.2 Replanning

6.2.1 Differences Observed in Dose Deformation and in Distortion Units in Replanning Cases

When analyzing Figure 5.6, where the differences observed between the Dose Plan and the Dose Deformed are present, the small intestine clearly stands out as the main organ responsible for triggering replanning during treatment, due to the significant difference between the planned and deformed dose values. This finding is in line with previous clinical knowledge, given that the small bowel has a particularly restrictive dosimetric tolerance and high sensitivity to anatomical variations [46]. Given its mobility and tendency to invade high-dose regions (such as pelvic fields), even small positional changes can lead to substantially higher doses than originally planned. This explains the greater clinical attention given to this structure and justifies replanning whenever significant anatomical changes in its position or volume are observed. In addition to the small bowel, other organs, such as the rectum and bladder, presented some discrepancies between the planned and deformed doses, although to a lesser extent.

In Figure 5.9, the DVH is presented for the main target volumes and organs at risk, comparing two distinct situations: the replan dose (solid lines) and the deformed dose (dashed lines). The Replan dose corresponds to the new treatment plan calculated on the second CT, whereas the Deformed dose results

from the deformation of the initial plan to match the patient's actual anatomy at the time of evaluation. Examination of the graph shows that for most structures (especially organs at risk, e.g. the small bowel, rectum, and sigmoid colon), the dashed lines of the Dose Deformed are positioned to the right more than the solid lines of Dose Replan. This shows that in some areas, these organs received a higher dose than expected, thus potentially elevating hazardous reactions. This discrepancy between the curves indicates that the anatomy of the patient has changed during treatment (i.e., organ displacement or volume change of the tumor), impacting the accuracy of the initial treatment plan. In general, the deformed dose is greater than the replan dose for such cases which justifies the necessity of replanning to reconfigure the dose distribution according to the patient's new anatomy. The primary objective is to preserve therapeutic efficacy without harming normal tissues, in accordance with the constraints defined in the clinical protocol.

In addition, the implementation of the created protocol has significant clinical value, as it allows a faster and more informed decision-making process regarding the need for replanning. As illustrated in Figure 5.10, the asymmetric dose partition values are substantially higher than those in the nominal plan, for several organs. This discrepancy corresponds to the anatomical changes during treatment and indicates that, had there been no intervention, the voxels would have received a much higher dose than originally planned. In this sense, this protocol only further underscores the importance of dose deformation as an essential instrument in clinical decision-making, sparing patients from potential unnecessary toxicities and maintaining safe and effective RT administrations.

It's important to note that the Dose Replan and the Dose Deformed were combined in the same DVHs and protocol for clarification purposes, as it's not yet possible to create a protocol with two doses associated with different CTs. However, in a real-world scenario, the study will focus on the Dose Plan and the Dose Deformed. Therefore, protocols for each of these doses will need to be created individually and then compared. Otherwise, Velocity will need to introduce the possibility of an update that allows the comparison of two doses related to different CTs. For now, this study only aims to illustrate what a scenario comparing two doses in a protocol would look like.

Regarding the study of distortion units, analyzing the results presented in Table 5.2 and Figure 5.9, it is evident that the small bowel presents, by far, the highest mean distortion values, as well as a relatively large standard deviation. This pattern is consistent with the known high mobility of this structure and its tendency to occupy different anatomical regions between treatment fractions. Its variable positioning within the abdominal cavity makes deformable registration in this region more challenging, resulting in a greater degree of deformation required for image alignment.

After the small bowel, the bladder and sigmoid present moderately high mean distortion values. Both the bladder and the sigmoid are hollow structures with substantial volumetric variability, which justifies their high mean values and associated dispersion. On the other hand, the rectum presents the lowest mean distortion among all structures, indicating greater anatomical integrity during treatment. However, it should be considered that, despite being less variable in terms of position, the rectum can still present small volumetric variations that, even if subtle, can be clinically relevant.

In general, Figure 5.11 highlights the need to consider distortion units as an independent metric in the adaptive replanning procedure. Structures with greater susceptibility to anatomical variations, such as the small bowel and bladder, require more rigorous clinical monitoring, and their position and morphology should be carefully reassessed before proceeding with the originally planned treatment.

It is extremely important to highlight that this study does not focus on the PTVs, as the main objective is to evaluate and optimize the protection of organs at risk. This approach is justified by the fact that most clinical protocols already ensure adequate PTV coverage during the initial planning phase. Therefore, it becomes more relevant to assess the impact of anatomical changes on the dose received by healthy tissues, whose excessive exposure may lead to significant adverse effects.

6.3 Re-irradiation

6.3.1 Differences Observed in Dose Deformation in Re-irradiation Cases

The missing values in Tbale 5.4 is explained by the fact that, in patients 4, 5, and 7, the treatment plans were directed to the iliac region; therefore, the bladder and rectum were not in close proximity to the tumor and were consequently not delineated. Additionally, several null values can also be observed, which result from the maximum dose received by a given OAR not reaching the tolerance limits established for that structure. Table 5.4 was generated from the protocols implemented in the treatment planning system, and thus, from these protocols, it was possible to assess compliance or violation of the clinical dose constraints defined in international guidelines such as QUANTEC and RTOG.

Table 5.5 and Figure 5.13 further show that only the rectum exceeded the maximum dose constraint established by reference. This outcome is plausible, as the rectum is an anatomical structure located in close proximity to the target volume in pelvic tumors, making it particularly susceptible to cumulative dose exposure in successive treatments. Furthermore, variations in its morphology and position between treatments, such as intestinal distension or changes in its relative mobility, increase the likelihood of exceeding cumulative tolerance limits.

It is important to highlight some particularities associated with the results obtained in the context of re-irradiation. Firstly, significant anatomical changes between the two treatment courses play a decisive role. Over the interval between the first and the second course, phenomena such as tumor volume reduction, tissue retraction, or displacement of adjacent organs (e.g., a less full bladder or reduced bowel distension) may occur. These changes may cause critical structures, such as the rectum, bladder, or sigmoid, to partially shift out of the original radiation field, thereby altering the dose distribution when the initial plan is deformed to the anatomy of the second CT.

Another relevant aspect concerns contouring issues (segmentation bias). In some cases, not all structures were delineated in the deformed CT scans, particularly in patients whose treatment plans targeted exclusively the iliac region, which led to portions of the OARs not being included in the analysis. This may have resulted in underestimation or artificially lower dose values for certain structures. Consequently, it is reasonable to assume that the results would have shown greater reliability and accuracy if all relevant structures had been consistently delineated in every deformed image.

6.4 Workflow perspective at the clinic

6.4.1 For replanning cases

The rationale for incorporating DIR in a clinical setting has a very well-founded logic, the goal of which is to preserve the efficacy of RT treatment, and the safety of the patients, in accordance with pre-treatment planning. Figure 6.1 conceptually gives a direction of a clinical workflow view within a hospital setting.

This involves a clinical discussion by the radiation oncologist who assesses the patient's oncological circumstances as a whole and defines the treatment approach. This is in turn followed by the planning phase where dosimetrists delineate target volumes and organs at risk, and construct a treatment plan that fulfills the requirements for tumor coverage and dose sparing of normal tissues.

At the beginning of the treatment, one obtains cone beam computed tomography (CBCT) images on a daily basis before each session, in order to confirm that the patient's actual anatomy matches the one that was used in planning. This is necessary to ensure that radiation is delivered accurately.

When a significant discrepancy is observed in the acquired image, including relevant anatomical shifts, volume differences, and the presence of gas, the radiation oncologist may choose to pause treatment and perform a deformable registration. The intent of the DIR is to shift the planning image to the anatomy currently visible on the CBCT so that the delivered dose can be re-evaluated, and replanning considered if necessary. The deformed geometry is then validated using python script following DIR in Velocity® software.

After quality verification of the DIR process, the dedicated gynecological pathology protocol is locked on the DIR outcome. This protocol involves reevaluation of the organs at risk, and checking the conformity of the new dose distribution to look for any violations in the treatment plan. In this manner, deformable registration becomes part of the clinical loop, not only as an imaging technique, but as direct assistance in the personalization of the decision for therapy.

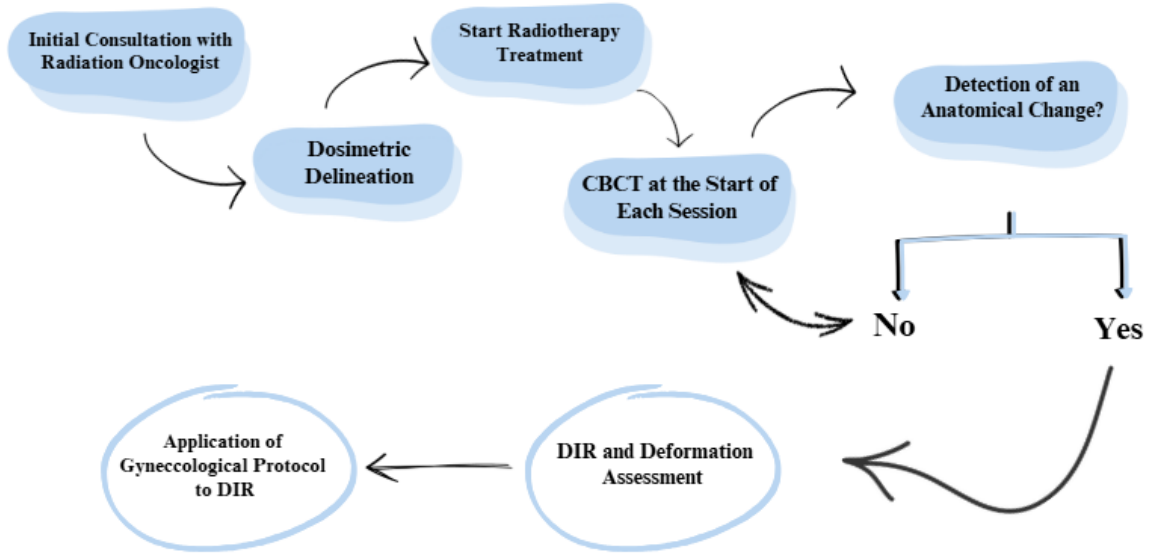

Figure 6.1: Flowchart of a workflow perspective at the clinic for replanning cases to be implemented in the clinic.

6.4.2 For re-irradiation cases

In case of recurrence a tumor is detected after the first treatment regimen, a fresh clinical evaluation is performed on the patient. This evaluation is performed by the radiation oncologist, and he/she assesses the whole oncological status of the patient, including the time period since the initial irradiation, the location of the recurrence, the therapies available and the dangers of toxicity associated with a dose previously administered to normal tissue. This evaluation may lead to a second process, i.e. re-irradiation.

If re-irradiation is also viable, a new planning phase of clinical execution is commenced. At this point a new computed tomography scan (CTreirr) is taken in which the target volumes and OARs are delineated again. Then a DIR process is carried out, in which the CTreirr has been deformed to match the planning CT (CTplan). This step is of crucial importance. It helps to transfer dosimetric information from the first treatment to the current anatomy, providing a comparative basis for evaluating cumulative dose. The CTdeformed is generated with the follow-up dosimetric evaluations protocol. The current protocol is designed to establish whether the dose limitations for OARs are exceeded when considering the sum of the deformed dose and planned dose of the second treatment.

The OAR values on the CTdeformed are evaluated and compared with established clinical thresholds. In case of significant violations, the radiation oncologist would then choose an adaptive replanning approach, which entails adjusting the parameters to ensure safety to patients.

In the next step using the enhanced functionality of the Velocity® software, the cumulative dose from each treatment is estimated. This is necessary to achieve a measurement of the combined dose delivered to the OARs and the target volume. The dose will be converted to EQD2 depending on the fractionation schemes with the linear-quadratic model.

After this step, the EQD2 is converted to standard clinical fractionation, so that results can be interpreted directly with the tolerance limits agreed upon for reference protocols like the QUANTEC and RTOG to see whether an OAR received underdosage or overdosage. The illustrated schematic is of a proposed clinical workflow for re-irradiation. This workflow is represented in Figure 6.2.

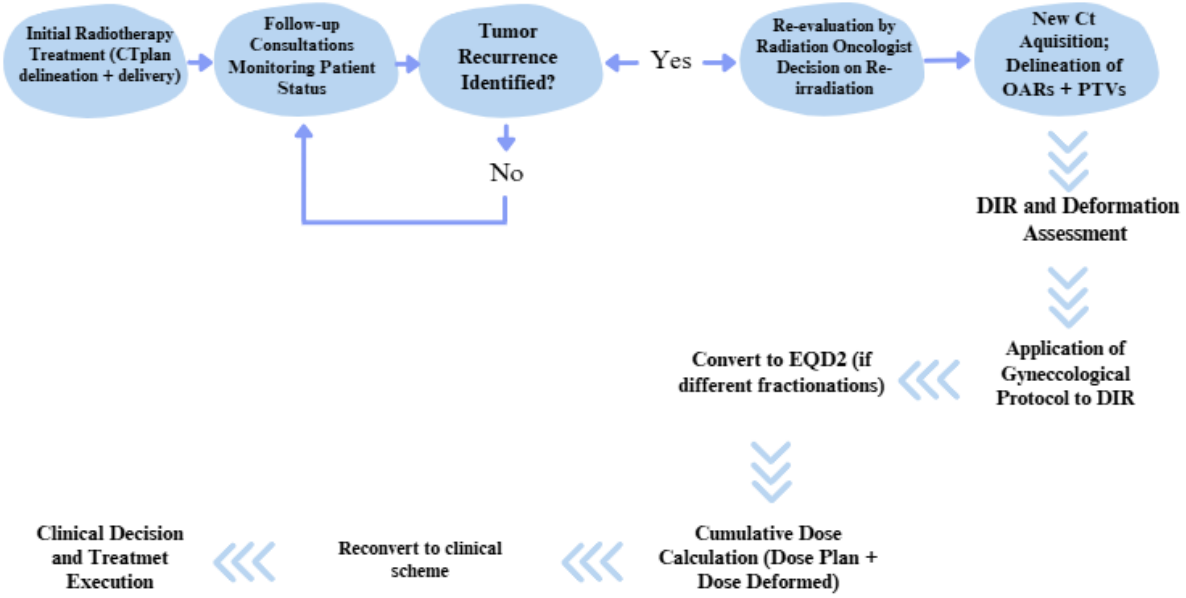

Figure 6.2: Flowchart of a workflow perspective at the clinic for re-irradiation cases to be implemented in the clinic.

7 Conclusion and Future Perspectives

This dissertation has been designed to detail the dosimetric implications of replanning and re-irradiation in RT, with specific emphasis on the comparison of cumulative dose received by the OARs against a range of clinical limits set by reference guidelines, e.g., including QUANTEC and RTOG. In-depth studies were done using multiple DIR based methodologies followed by a dose conversion to EQD2 approach that not only allowed us to perform a retrospective analysis on the data for included patients but also suggested a structured approach with the aim of clinical translation throughout this study to help improve safety and efficacy as a therapy.

In replanned cases with 17 patients, a comparison was performed between the Planned Dose (Dose Plan) and the Deformed Dose (Dose Deformed). In most of the organs under investigation, the data showed that the Dose Deformed increased relative to the values assigned to the Dose Plan because of the anatomical changes taken through the treatment, including bladder filling changes, intestines distention changes, weight loss or patient postures. These findings showed relevant distributions of dose that would lead to a risk for toxicity for many OARs, without replanning. Statistical analysis of this study also showed quite high standard deviations from the Dose Plan, indicative of heterogeneous treatment and emphasizing the necessity of adhering to the correct protocol with regard to clinical cases. These results suggest the relevance of replanning in RT, treatment efficacy, and the conservation of healthy tissues in a clinical scenario where anatomical variations in the course of treatment are unavoidable.

For the seven cases with the re-irradiation approach, we have introduced a different method of the evaluation as we sought to calculate the sum of the cumulative dose throughout a treatment course in presence of different dosing. For this reason a second CT (CTreirr) was deformed to the anatomy of the CT of the first plan (CTplan), the Dose Deformed was calculated and its sum with the Dose Plan with recovery obtained. The concept of tissue recovery with a 25% reduction of accumulated dose whenever the time between the two treatments exceeded six months became the cornerstone to find more realistic values. Dose conversion to EQD2 was used in patients who had different fractionation routines compared to the plans before normalization of doses to clinical reference schemes to be able to compare with the established limits.

Second, it is the consequence of the significant anatomical changes between the two treatment paths, that some of the OARs were partially displaced to the original radiation fields, reducing the absorbed dose. The sum of EQD2 showed some of the OAR exceeded the reference values in tissues as they were taken for tissue recovery, including rectal organs. As this highlights the fact that whilst re-irradiation may have clinical viability and risk mitigation in general, the risk of late toxicity is always elevated and should be kept in mind in each clinical decision. An interesting key point is that while planned doses analysis was presented, it also aimed to reflect on the limitations of the deformation process. For example, in case of re-irradiation if the first treatment plan was aiming for the left iliac bone, not all the structures in the contralateral side were delineated. Therefore the deformed dose was likely underrepresented as voxels were not accounted for in the patient. This contouring problem (segmentation bias) probably conditioned some of the results so stringent delineation requirements can be followed to guarantee the dosage calculations are more robust. All in all, the results of this thesis support some practical findings.

Firstly, in re-irradiation situations deformed doses may be lower in some cases, the cumulative EQD2 might reach or exceed tolerance limits, indicating need for dose summation methodologies and cumulative evaluation. Secondly, this study validated the significance of DIR as an indispensable method, not only for retrospective computation, but as a tool for future clinical workflows, thus leading to a more individualized approach backed by scientific evidence.

However, this work has several limitations including few patients were included in the re-irradiation arm, anatomical heterogeneity of studied cohort, and a challenge in delineating deformed CT. Thus, the methodology proposed here can be an important insight for future efforts: establishing standardized dose summation protocols at different organizations; prospective analysis of patient cases; and the deployment of automatic delineation algorithms to minimize contouring bias.

7.1 Future Work

Despite the advances achieved with the development of this dissertation, there are still several limitations and aspects that warrant further investigation in future work, to consolidate and expand the results obtained.

For the replanning cases, one of the main challenges identified relates to the use of images acquired during the course of treatment. In this study, the analysis was based on a secondary CT, however, to transpose this methodology into clinical practice, it will be necessary to ensure that the process is carried out using CBCT images, which represent the gold standard for daily monitoring. The integration of CBCT into the workflow, however, requires the development or adaptation of automatic methods for structure delineation in Velocity®, enabling the process to be accelerated, reducing inter-observer variability, and facilitating the creation of standardized protocols directly from these images.

Another point to be considered in future work is the development of joint protocols that simultaneously integrate the Dose Plan and the Dose Deformed. In the present study, these calculations were performed independently, which implies additional processing effort and increases the risk of inconsistencies. The implementation of an integrated protocol would allow for a more direct and robust assessment of the accumulated dose, with greater clinical applicability, while also making the process more efficient and less prone to error.

Finally, one goal that was stated for this study, but could not be achieved due to the problem with the Velocity® software lasting for about four months, is the analysis of image fusion with and without intraluminal devices.

This step is particularly relevant to the clinical assessment, since intraluminal devices may produce large artefacts within the image that affect both structure delineation and the accuracy of deformable registration. Systematically comparing the results of fusion in scenarios with and without intraluminal devices would clarify their impact on dose distribution and, consequently, improve the reliability of dosimetric calculations.

8 References

[1] G. P. Delaney and M. B. Barton, "Evidence-based Estimates of the Demand for Radiotherapy," *Clin Oncol*, vol. 27, no. 2, pp. 70–76, Feb. 2015, doi: 10.1016/j.clon.2014.10.005.

[2] D. of E. and S. A. United Nations, "Sustainable Development."

[3] W. C. Hahn and R. A. Weinberg, "Rules for Making Human Tumor Cells," *New England Journal of Medicine*, vol. 347, no. 20, pp. 1593–1603, Nov. 2002, doi: 10.1056/NEJMra021902.

[4] P. Roy and B. Saikia, "Cancer and cure: A critical analysis," *Indian J Cancer*, vol. 53, no. 3, p. 441, 2016, doi: 10.4103/0019-509X.200658.

[5] M. H. G. Katz, A. B. Francescatti, and K. K. Hunt, "Technical Standards for Cancer Surgery: Commission on Cancer Standards 5.3–5.8," *Ann Surg Oncol*, vol. 29, no. 11, pp. 6549–6558, Oct. 2022, doi: 10.1245/s10434-022-11375-w.

[6] I. M. Zraik and Y. Heß-Busch, "Management von Nebenwirkungen der Chemotherapie und deren Langzeitfolgen," *Urologe*, vol. 60, no. 7, pp. 862–871, Jul. 2021, doi: 10.1007/s00120-021-01569-7.

[7] C. E. Knezevic and W. Clarke, "Cancer Chemotherapy: The Case for Therapeutic Drug Monitoring," *Ther Drug Monit*, vol. 42, no. 1, pp. 6–19, Feb. 2020, doi: 10.1097/FTD.0000000000000701.

[8] C. Allen, S. Her, and D. A. Jaffray, "Radiotherapy for Cancer: Present and Future," *Adv Drug Deliv Rev*, vol. 109, pp. 1–2, Jan. 2017, doi: 10.1016/j.addr.2017.01.004.

[9] G. Minniti, C. Goldsmith, and M. Brada, "Radiotherapy," 2012, pp. 215–228. doi: 10.1016/B978-0-444-52138-5.00016-5.

[10] E. B. Podgorsak, "Radiation Oncology Physics: A Handbook for Teachers and Students."

[11] J. C. Slater, "The Design of Linear Accelerators," *Rev Mod Phys*, vol. 20, no. 3, pp. 473–518, Jul. 1948, doi: 10.1103/RevModPhys.20.473.

[12] P. Mayles, A. Nahum, and J. C. Rosenwald, Eds., *Handbook of Radiotherapy Physics*. CRC Press, 2007. doi: 10.1201/9781420012026.

[13] IPO Porto, "SERVIÇO DE RADIOTERAPIA." Accessed: Nov. 11, 2024. [Online]. Available: https://www.ipoporto.pt/dev/wp-content/uploads/2014/01/radioterapia_AF.pdf

[14] B. J. Monk, K. Tewari, R. A. Burger, M. T. Johnson, F. F. Montz, and M. L. Berman, "A Comparison of Intracavitary versus Interstitial Irradiation in the Treatment of Cervical Cancer," *Gynecol Oncol*, vol. 67, no. 3, pp. 241–247, Dec. 1997, doi: 10.1006/gyno.1997.4877.

[15] R. Baskar, K. A. Lee, R. Yeo, and K.-W. Yeoh, "Cancer and Radiation Therapy: Current Advances and Future Directions," *Int J Med Sci*, vol. 9, no. 3, pp. 193–199, 2012, doi: 10.7150/ijms.3635.

[16] Kari Tanderup, "Image guided intensity modulated external beam radiochemotherapy and MRI based adaptive brachytherapy in locally advanced cerrvical cancer EMBRACE-II."

[17] E. Glatstein, J. Rosenman, E. L. Chaney, S. Sailer, G. W. Sherouse, and J. E. Tepper, "Recent Advances in Radiotherapy Treatment Planning," *Cancer Invest*, vol. 9, no. 4, pp. 465–481, Jan. 1991, doi: 10.3109/07357909109084645.

[18] A. Al-Mamgani *et al.*, "The dosimetric and clinical advantages of the GTV-CTV-PTV margins reduction by 6 mm in head and neck squamous cell carcinoma: Significant acute and late toxicity reduction," *Radiotherapy and Oncology*, vol. 168, pp. 16–22, Mar. 2022, doi: 10.1016/j.radonc.2022.01.013.

[19] L. B. Marks *et al.*, "Use of Normal Tissue Complication Probability Models in the Clinic," *International Journal of Radiation Oncology*Biology*Physics*, vol. 76, no. 3, pp. S10–S19, Mar. 2010, doi: 10.1016/j.ijrobp.2009.07.1754.

[20] W. A. Hall *et al.*, "NRG Oncology Updated International Consensus Atlas on Pelvic Lymph Node Volumes for Intact and Postoperative Prostate Cancer," *International Journal of Radiation Oncology*Biology*Physics*, vol. 109, no. 1, pp. 174–185, Jan. 2021, doi: 10.1016/j.ijrobp.2020.08.034.

[21] S. Bisello *et al.*, "Dose–Volume Constraints fOr oRganS At risk In Radiotherapy (CORSAIR): An 'All-in-One' Multicenter–Multidisciplinary Practical Summary," *Current Oncology*, vol. 29, no. 10, pp. 7021–7050, Sep. 2022, doi: 10.3390/curroncol29100552.

[22] Min Chen, *Image Registration: Fundamentals and Recent Advances Based on Deep Learning*. 2023.

[23] S. Oh and S. Kim, "Deformable image registration in radiation therapy," *Radiat Oncol J*, vol. 35, no. 2, pp. 101–111, Jun. 2017, doi: 10.3857/roj.2017.00325.

[24] Y. Fu, Y. Lei, T. Wang, W. J. Curran, T. Liu, and X. Yang, "Deep learning in medical image registration: a review," *Phys Med Biol*, vol. 65, no. 20, p. 20TR01, Oct. 2020, doi: 10.1088/1361-6560/ab843e.

[25] H. Wang *et al.*, "Validation of an accelerated 'demons' algorithm for deformable image registration in radiation therapy," *Phys Med Biol*, vol. 50, no. 12, pp. 2887–2905, Jun. 2005, doi: 10.1088/0031-9155/50/12/011.

[26] T. Guerrero *et al.*, "Quantification of regional ventilation from treatment planning CT," *International Journal of Radiation Oncology*Biology*Physics*, vol. 62, no. 3, pp. 630–634, Jul. 2005, doi: 10.1016/j.ijrobp.2005.03.023.

[27] T. Yamamoto *et al.*, "Pulmonary Ventilation Imaging Based on 4-Dimensional Computed Tomography: Comparison With Pulmonary Function Tests and SPECT Ventilation Images," *International Journal of Radiation Oncology*Biology*Physics*, vol. 90, no. 2, pp. 414–422, Oct. 2014, doi: 10.1016/j.ijrobp.2014.06.006.

[28] L. Cubero, J. Castelli, A. Simon, R. de Crevoisier, O. Acosta, and J. Pascau, "Deep Learning-Based Segmentation of Head and Neck Organs-at-Risk with Clinical Partially Labeled Data," *Entropy*, vol. 24, no. 11, p. 1661, Nov. 2022, doi: 10.3390/e24111661.

[29] D. Li, P. Zang, X. Chai, Y. Cui, R. Li, and L. Xing, "Automatic multiorgan segmentation in CT images of the male pelvis using region-specific hierarchical appearance cluster models," *Med Phys*, vol. 43, no. 10, pp. 5426–5436, Oct. 2016, doi: 10.1118/1.4962468.

[30] C. Veiga *et al.*, "First Clinical Investigation of Cone Beam Computed Tomography and Deformable Registration for Adaptive Proton Therapy for Lung Cancer," *International Journal of Radiation Oncology*Biology*Physics*, vol. 95, no. 1, pp. 549–559, May 2016, doi: 10.1016/j.ijrobp.2016.01.055.

[31] C. E. Shelley, L. H. Barraclough, C. L. Nelder, S. J. Otter, and A. J. Stewart, "Adaptive Radiotherapy in the Management of Cervical Cancer: Review of Strategies and Clinical Implementation," *Clin Oncol*, vol. 33, no. 9, pp. 579–590, Sep. 2021, doi: 10.1016/j.clon.2021.06.007.

[32] G. Razdevsek, U. Simoncic, L. Snoj, and A. Studen, "The dose accumulation and the impact of deformable image registration on dose reporting parameters in a moving patient undergoing proton radiotherapy," *Radiol Oncol*, vol. 56, no. 2, pp. 248–258, May 2022, doi: 10.2478/raon-2022-0016.

[33] O. M. Dona Lemus, M. Cao, B. Cai, M. Cummings, and D. Zheng, "Adaptive Radiotherapy: Next-Generation Radiotherapy," *Cancers (Basel)*, vol. 16, no. 6, p. 1206, Mar. 2024, doi: 10.3390/cancers16061206.

[34] W. Wang *et al.*, "Clinical Study of the Necessity of Replanning Before the 25th Fraction During the Course of Intensity-Modulated Radiotherapy for Patients With Nasopharyngeal Carcinoma,"

*International Journal of Radiation Oncology*Biology*Physics*, vol. 77, no. 2, pp. 617–621, Jun. 2010, doi: 10.1016/j.ijrobp.2009.08.036.

[35] R. Avgousti *et al.*, "Adaptive radiation therapy: When, how and what are the benefits that literature provides?," *Cancer/Radiothérapie*, vol. 26, no. 4, pp. 622–636, Jun. 2022, doi: 10.1016/j.canrad.2021.08.023.

[36] N. Andratschke *et al.*, "Reirradiation − still navigating uncharted waters?," *Clin Transl Radiat Oncol*, vol. 49, p. 100871, Nov. 2024, doi: 10.1016/j.ctro.2024.100871.

[37] H. J. Kang, Y.-K. Kwak, S. J. Lee, and M. Kim, "Re-Irradiation with Intensity-Modulated Radiation Therapy for the Treatment of Recurrent Cervical Cancer in the Pelvis: An Analysis of Outcomes and Toxicity," *Medicina (B Aires)*, vol. 59, no. 6, p. 1164, Jun. 2023, doi: 10.3390/medicina59061164.

[38] X. Ren *et al.*, "Image-guided interstitial brachytherapy for recurrent cervical cancer after radiotherapy: A single institution experience," *Front Oncol*, vol. 12, Jul. 2022, doi: 10.3389/fonc.2022.943703.

[39] W. Nobnop, I. Chitapanarux, H. Neamin, S. Wanwilairat, V. Lorvidhaya, and T. Sanghangthum, "Evaluation of deformable image registration (DIR) methods for dose accumulation in nasopharyngeal cancer patients during radiotherapy," *Radiol Oncol*, vol. 51, no. 4, pp. 438–446, Sep. 2017, doi: 10.1515/raon-2017-0033.

[40] M. Vozzo, J. Poder, J. Yuen, J. Bucci, and A. Haworth, "Use of deformable image registration techniques to estimate dose to organs at risk following prostate external beam radiation therapy and high-dose-rate brachytherapy," *J Contemp Brachytherapy*, vol. 13, no. 1, pp. 72–79, 2021, doi: 10.5114/jcb.2021.103589.

[41] Varian Systems, "Application Quick Tip Velocity Off-line Dose Review Quick Tip."

[42] S. Kuznetsova, P. Grendarova, S. Roy, R. Sinha, K. Thind, and N. Ploquin, "Structure guided deformable image registration for treatment planning CT and post stereotactic body radiation therapy (SBRT) Primovist ® (Gd-EOB-DTPA) enhanced MRI," *J Appl Clin Med Phys*, vol. 20, no. 12, pp. 109–118, Dec. 2019, doi: 10.1002/acm2.12773.

[43] I.-A. Jurkovic, N. Papanikolaou, S. Stathakis, N. Kirby, and P. Mavroidis, "Objective assessment of the quality and accuracy of deformable image registration," *J Med Phys*, vol. 45, no. 3, p. 156, 2020, doi: 10.4103/jmp.JMP_47_19.

[44] N. Kadoya *et al.*, "Evaluation of various deformable image registration algorithms for thoracic images," *J Radiat Res*, vol. 55, no. 1, pp. 175–182, Jan. 2014, doi: 10.1093/jrr/rrt093.

[45] N. Hardcastle *et al.*, "A multi-institution evaluation of deformable image registration algorithms for automatic organ delineation in adaptive head and neck radiotherapy," *Radiation Oncology*, vol. 7, no. 1, p. 90, Dec. 2012, doi: 10.1186/1748-717X-7-90.

[46] O. Yariv, K. Camphausen, and A. V. Krauze, "Small Bowel Dose Constraints in Radiation Therapy—Where Omics-Driven Biomarkers and Bioinformatics Can Take Us in the Future," *BioMedInformatics*, vol. 4, no. 1, pp. 158–172, Jan. 2024, doi: 10.3390/biomedinformatics4010011.

Appendix

A.

Patient 1

Bladder

Dose Plan		Dose Replan		Dose Replan Deformed		Dplannormal.	Dreplandefnormal.
Minimum		Minimum	13,63	Minimum	15,71		
Mean		Mean	34,55	Mean	41,45		
Maximum		Maximum	56,84	Maximum	59,06		
V35Gy<50%	52,40	V35Gy<50%	48,48	V35Gy<50%	67,18	1,05	1,34
V40Gy<35%	43,40	V40Gy<35%	39,22	V40Gy<35%	59,83	1,24	1,71
V50Gy<5%	10,30	V50Gy<5%	9,57	V50Gy<5%	27,53	2,06	5,51
						2,06	5,51

Small Bowel

Dose Plan		Dose Replan		Dose Replan Deformed		Dplannormal.	Dreplandefnormal.	Dplanmaxnormal.	Dreplanmaxnormal.
Minimum		Minimum	1,86	Minimum	2,25				
Mean		Mean	23,86	Mean	24,26				
Maximum		Maximum	50,12	Maximum	64,01				
V15Gy<120cc	964,80	V15Gy<120cc	1375,40	V15Gy<120cc	1264,80	8,04	10,54		
V30Gy<200cc	387,00	V30Gy<200cc	380,10	V30Gy<200cc	447,30	1,94	2,24		
V35Gy<150cc	269,40	V35Gy<150cc	248,40	V35Gy<150cc	306,00	1,80	2,04		
V45Gy<20cc	123,00	V45Gy<20cc	108,10	V45Gy<20cc	150,30	6,15	15,30		
V45Gy<195cc	123,00	V45Gy<195cc	108,10	V45Gy<195cc	150,30	0,63	0,77		
Dmax<50Gy	50,30	Dmax<50Gy	502,12	Dmax<50Gy	64,01			1,01	1,28
						8,04	15,30	1,01	1,28

Rectum

Dose Plan		Dose Replan		Dose Replan Deformed		Dplannormal.	Dreplandefnormal.
Minimum		Minimum	11,08	Minimum	14,61		
Mean		Mean	40,82	Mean	40,77		
Maximum		Maximum	56,51	Maximum	56,89		
V30Gy<200cc	53,80	V30Gy<200cc	49,10	V30Gy<200cc	52,80	0,27	0,26
V35Gy<150cc	44,80	V35Gy<150cc	40,80	V35Gy<150cc	43,70	0,30	0,29
V45Gy<20cc	21,20	V45Gy<20cc	25,40	V45Gy<20cc	22,10	1,06	1,11
V50Gy<50%	13,50	V50Gy<50%	17,68	V50Gy<50%	12,16	0,27	0,24
						1,06	1,11

Sigmoid

Dose Plan		Dose Replan		Dose Replan Deformed		Dplannormal.	Dreplandefnormal.
Minimum		Minimum	11,22	Minimum	9,80		
Mean		Mean	44,34	Mean	43,50		
Maximum		Maximum	57,32	Maximum	58,71		
V30Gy<200cc	156,70	V30Gy<200cc	163,90	V30Gy<200cc	166,00	0,78	0,83
V35Gy<150cc	146,20	V35Gy<150cc	158,00	V35Gy<150cc	159,60	0,97	1,06
V45Gy<20cc	104,80	V45Gy<20cc	131,60	V45Gy<20cc	121,60	5,24	6,08
V50Gy<50%	17,80	V50Gy<50%	23,40	V50Gy<50%	15,97	0,36	0,32
						5,24	6,08

Patient 2

Bladder

Dose Plan		Dose Replan		Dose Replan Deformed		Dplannormalizada	Dreplandefnormalizada
Minimum		Minimum	10,85	Minimum	9,47		
Mean		Mean	32,79	Mean	37,79		
Maximum		Maximum	55,96	Maximum	58,77		
V35Gy<50%	52,40	V35Gy<50%	47,08	V35Gy<50%	66,47		
V40Gy<35%	44,20	V40Gy<35%	37,47	V40Gy<35%	58,99	0,88	1,18
V50Gy<5%	5,30	V50Gy<5%	2,69	V50Gy<5%	5,53	0,15	0,16
						0,00	0,00
						0,88	1,18

Small Bowel

Dose Plan		Dose Replan		Dose Replan Deformed		Dplannormal.	Dreplandefnormal.	Dplanmaxnormal.	Dreplanmaxnormal.
Minimum		Minimum	1,50	Minimum	1,28				
Mean		Mean	20,55	Mean	23,07				
Maximum		Maximum	48,94	Maximum	49,71				
V15Gy<120cc	371,50	V15Gy<120cc	422,60	V15Gy<120cc	475,40	3,10	3,96		
V30Gy<200cc	259,90	V30Gy<200cc	189,80	V30Gy<200cc	221,00	1,30	1,11		
V35Gy<150cc	234,90	V35Gy<150cc	120,60	V35Gy<150cc	180,10	1,57	1,20		
V45Gy<20cc	146,50	V45Gy<20cc	40,30	V45Gy<20cc	97,80	7,33	9,01		
V45Gy<195cc	146,50	V45Gy<195cc	40,30	V45Gy<195cc	97,80	0,75	0,50		
Dmax<50Gy	51,30	Dmax<50Gy	48,94	Dmax<50Gy	49,71			1,03	0,99
						7,33	9,01	1,03	0,99

Rectum

Dose Plan		Dose Replan		Dose Replan Deformed		Dplannormal.	Dreplandefnormal.
Minimum		Minimum	2,71	Minimum	2,74		
Mean		Mean	33,70	Mean	41,44		
Maximum		Maximum	55,75	Maximum	59,19		
V30Gy<200cc	42,70	V30Gy<200cc	47,50	V30Gy<200cc	60,40	0,21	0,30
V35Gy<150cc	38,80	V35Gy<150cc	35,60	V35Gy<150cc	57,80	0,26	0,39
V45Gy<20cc	23,50	V45Gy<20cc	15,50	V45Gy<20cc	44,20	1,18	2,21
V50Gy<50%	18,90	V50Gy<50%	7,51	V50Gy<50%	30,66	0,38	0,61
						1,18	2,21

Sigmoid

Dose Plan		Dose Replan		Dose Replan Deformed		Dplannormal.	Dreplandefnormal.
Minimum		Minimum	10,85	Minimum	12,75		
Mean		Mean	40,10	Mean	40,36		
Maximum		Maximum	71,77	Maximum	72,33		
V30Gy<200cc	78,70	V30Gy<200cc	123,70	V30Gy<200cc	121,10	0,39	0,61
V35Gy<150cc	56,10	V35Gy<150cc	111,10	V35Gy<150cc	108,70	0,37	0,72
V45Gy<20cc	21,60	V45Gy<20cc	64,20	V45Gy<20cc	70,60	1,08	3,53
V50Gy<50%	0,78	V50Gy<50%	2,41	V50Gy<50%	2,59	0,02	0,05
						1,08	3,53

Patient 3

Bladder

Dose Plan		Dose Replan		Dose Replan Deformed		Dplannormalizada	Dreplandefnormalizada
Minimum		Minimum	9,20	Minimum	19,39		
Mean		Mean	37,56	Mean	43,17		
Maximum		Maximum	56,27	Maximum	59,31		
V35Gy<50%	67,70	V35Gy<50%	59,61	V35Gy<50%	75,01		
V40Gy<35%	53,90	V40Gy<35%	49,08	V40Gy<35%	65,09	1,08	1,30
V50Gy<5%	18,60	V50Gy<5%	23,48	V50Gy<5%	35,35	0,53	1,01
						0,00	0,00
						1,08	1,30

Small Bowel

Dose Plan		Dose Replan		Dose Replan Deformed		Dplannormal.	Dreplandefnormal.	Dplanmaxnormal.	Dreplanmaxnormal.
Minimum		Minimum	0,58	Minimum	1,71				
Mean		Mean	22,35	Mean	25,55				
Maximum		Maximum	50,25	Maximum	57,02				
V15Gy<120cc	782,60	V15Gy<120cc	1019,80	V15Gy<120cc	957,90	6,52	7,98		
V30Gy<200cc	453,20	V30Gy<200cc	339,30	V30Gy<200cc	563,70	2,27	2,82		
V35Gy<150cc	389,90	V35Gy<150cc	227,30	V35Gy<150cc	438,60	2,60	2,92		
V45Gy<20cc	232,90	V45Gy<20cc	104,30	V45Gy<20cc	233,50	11,65	21,93		
V45Gy<195cc	232,90	V45Gy<195cc	104,30	V45Gy<195cc	233,50	1,19	1,20		
Dmax<50Gy	51,00	Dmax<50Gy	50,25	Dmax<50Gy	57,02			1,02	1,14
						11,65	21,93	1,02	1,14

Rectum

Dose Plan		Dose Replan		Dose Replan Deformed		Dplannormal.	Dreplandefnormal.
Minimum		Minimum	12,89	Minimum	19,71		
Mean		Mean	45,96	Mean	40,19		
Maximum		Maximum	57,08	Maximum	55,29		
V30Gy<200cc	72,70	V30Gy<200cc	63,70	V30Gy<200cc	63,90	0,36	0,32
V35Gy<150cc	65,10	V35Gy<150cc	60,00	V35Gy<150cc	52,60	0,43	0,35
V45Gy<20cc	37,10	V45Gy<20cc	46,70	V45Gy<20cc	19,20	1,86	0,96
V50Gy<50%	26,90	V50Gy<50%	46,65	V50Gy<50%	9,16	0,54	0,18
						1,86	0,96

Sigmoid

Dose Plan		Dose Replan		Dose Replan Deformed		Dplannormal.	Dreplandefnormal.
Minimum		Minimum	13,00	Minimum	12,52		
Mean		Mean	39,58	Mean	40,24		
Maximum		Maximum	53,47	Maximum	52,68		
V30Gy<200cc	59,10	V30Gy<200cc	91,60	V30Gy<200cc	106,60	0,30	0,53
V35Gy<150cc	55,10	V35Gy<150cc	83,50	V35Gy<150cc	97,40	0,37	0,65
V45Gy<20cc	38,70	V45Gy<20cc	69,10	V45Gy<20cc	61,00	1,94	3,05
V50Gy<50%	18,60	V50Gy<50%	43,71	V50Gy<50%	10,70	0,37	0,21
						1,94	3,05

Patient 4

Bladder							
Dose Plan		Dose Replan		Dose Replan Deformed		Dplannormalizada	Dreplandefnormalizada
Minimum		Minimum	10,23	Minimum	10,48		
Mean		Mean	27,67	Mean	28,25		
Maximum		Maximum	50,06	Maximum	49,56		
V35Gy<50%	26,00	V35Gy<50%	29,00	V35Gy<50%	27,53		
V40Gy<35%	18,50	V40Gy<35%	21,82	V40Gy<35%	19,71	0,37	0,39
V50Gy<5%	0,00	V50Gy<5%	0,00	V50Gy<5%	0,00	0,00	0,00
						0,00	0,00
						0,37	0,39

Small Bowel									
Dose Plan		Dose Replan		Dose Replan Deformed		Dplannormal.	Dreplandefnormal.	Dplanmaxnormal.	Dreplanmaxnormal.
Minimum		Minimum	1,73	Minimum	1,85				
Mean		Mean	20,06	Mean	20,53				
Maximum		Maximum	50,24	Maximum	50,32				
V15Gy<120cc	186,90	V15Gy<120cc	287,60	V15Gy<120cc	296,30	1,56	2,47		
V30Gy<200cc	40,50	V30Gy<200cc	76,40	V30Gy<200cc	78,70	0,20	0,39		
V35Gy<150cc	26,60	V35Gy<150cc	56,10	V35Gy<150cc	56,40	0,18	0,38		
V45Gy<20cc	9,70	V45Gy<20cc	30,30	V45Gy<20cc	29,50	0,49	2,82		
V45Gy<195cc	9,70	V45Gy<195cc	30,30	V45Gy<195cc	29,50	0,05	0,15		
Dmax<50Gy	50,40	Dmax<50Gy	50,24	Dmax<50Gy	50,32			1,01	1,01
						1,56	2,82	1,01	1,01

Rectum							
Dose Plan		Dose Replan		Dose Replan Deformed		Dplannormal.	Dreplandefnormal.
Minimum		Minimum	16,02	Minimum	18,14		
Mean		Mean	36,69	Mean	38,35		
Maximum		Maximum	49,61	Maximum	49,72		
V30Gy<200cc	37,50	V30Gy<200cc	34,60	V30Gy<200cc	37,70	0,19	0,19
V35Gy<150cc	30,00	V35Gy<150cc	28,80	V35Gy<150cc	31,50	0,20	0,21
V45Gy<20cc	15,00	V45Gy<20cc	14,20	V45Gy<20cc	15,70	0,75	0,79
V50Gy<50%	0,00	V50Gy<50%	0,00	V50Gy<50%	0,00	0,00	0,00
						0,75	0,79

Sigmoid							
Dose Plan		Dose Replan		Dose Replan Deformed		Dplannormal.	Dreplandefnormal.
Minimum		Minimum	14,65	Minimum	15,40		
Mean		Mean	43,48	Mean	44,54		
Maximum		Maximum	49,48	Maximum	49,91		
V30Gy<200cc	28,50	V30Gy<200cc	31,40	V30Gy<200cc	32,60	0,14	0,16
V35Gy<150cc	25,70	V35Gy<150cc	30,80	V35Gy<150cc	31,60	0,17	0,21
V45Gy<20cc	14,70	V45Gy<20cc	30,20	V45Gy<20cc	30,40	0,74	1,52
V50Gy<50%	0,00	V50Gy<50%	0,00	V50Gy<50%	0,00	0,00	0,00
						0,74	1,52

Patient 5

Bladder							
Dose Plan		Dose Replan		Dose Replan Deformed		Dplannormalizada	Dreplandefnormalizada
Minimum		Minimum	11,15	Minimum	12,93		
Mean		Mean	32,30	Mean	35,84		
Maximum		Maximum	56,17	Maximum	58,63		
V35Gy<50%	43,00	V35Gy<50%	42,94	V35Gy<50%	55,89		
V40Gy<35%	34,10	V40Gy<35%	34,11	V40Gy<35%	44,45	0,68	0,89
V50Gy<5%	4,70	V50Gy<5%	4,74	V50Gy<5%	9,38	0,13	0,27
						0,00	0,00
						0,68	0,89

Small Bowel									
Dose Plan		Dose Replan		Dose Replan Deformed		Dplannormal.	Dreplandefnormal.	Dplanmaxnormal.	Dreplanmaxnormal.
Minimum		Minimum	1,75	Minimum	1,12				
Mean		Mean	26,83	Mean	26,90				
Maximum		Maximum	52,20	Maximum	49,95				
V15Gy<120cc	803,10	V15Gy<120cc	803,50	V15Gy<120cc	750,80	6,69	6,26		
V30Gy<200cc	339,00	V30Gy<200cc	339,60	V30Gy<200cc	377,90	1,70	1,89		
V35Gy<150cc	267,50	V35Gy<150cc	268,30	V35Gy<150cc	308,10	1,78	2,05		
V45Gy<20cc	138,50	V45Gy<20cc	140,70	V45Gy<20cc	123,40	6,93	15,41		
V45Gy<195cc	138,50	V45Gy<195cc	140,70	V45Gy<195cc	123,40	0,71	0,63		
Dmax<50Gy	52,30	Dmax<50Gy	52,20	Dmax<50Gy	49,95			1,05	1,00
						6,93	15,41	1,05	1,00

Rectum							
Dose Plan		Dose Replan		Dose Replan Deformed		Dplannormal.	Dreplandefnormal.
Minimum		Minimum	16,11	Minimum	12,03		
Mean		Mean	37,33	Mean	36,26		
Maximum		Maximum	57,12	Maximum	58,64		
V30Gy<200cc	58,80	V30Gy<200cc	59,10	V30Gy<200cc	56,80	0,29	0,28
V35Gy<150cc	47,90	V35Gy<150cc	48,20	V35Gy<150cc	46,50	0,32	0,31
V45Gy<20cc	27,60	V45Gy<20cc	27,80	V45Gy<20cc	26,60	1,38	1,33
V50Gy<50%	17,10	V50Gy<50%	17,17	V50Gy<50%	18,63	0,34	0,37
						1,38	1,33

Sigmoid							
Dose Plan		Dose Replan		Dose Replan Deformed		Dplannormal.	Dreplandefnormal.
Minimum		Minimum	14,50	Minimum	13,45		
Mean		Mean	37,84	Mean	37,00		
Maximum		Maximum	53,15	Maximum	48,97		
V30Gy<200cc	82,40	V30Gy<200cc	82,80	V30Gy<200cc	81,30	0,41	0,41
V35Gy<150cc	71,70	V35Gy<150cc	72,00	V35Gy<150cc	69,90	0,48	0,47
V45Gy<20cc	51,30	V45Gy<20cc	51,70	V45Gy<20cc	39,50	2,57	1,98
V50Gy<50%	0,13	V50Gy<50%	0,21	V50Gy<50%	0,00	0,00	0,00
						2,57	1,98

Patient 6

Bladder							
Dose Plan		Dose Replan		Dose Replan Deformed		Dplannormalizada	Dreplandefnormalizada
Minimum		Minimum	10,01	Minimum	9,91		
Mean		Mean	29,55	Mean	31,55		
Maximum		Maximum	55,33	Maximum	57,41		
V35Gy<50%	43,80	V35Gy<50%	35,15	V35Gy<50%	42,48		
V40Gy<35%	31,90	V40Gy<35%	26,46	V40Gy<35%	31,74	0,64	0,63
V50Gy<5%	1,60	V50Gy<5%	3,11	V50Gy<5%	5,20	0,05	0,15
						0,00	0,00
						0,64	0,63

Small Bowel									
Dose Plan		Dose Replan		Dose Replan Deformed		Dplannormal.	Dreplandefnormal.	Dplanmaxnormal.	Dreplanmaxnormal.
Minimum		Minimum	0,91	Minimum	1,55				
Mean		Mean	20,65	Mean	24,95				
Maximum		Maximum	51,05	Maximum	58,52				
V15Gy<120cc	264,80	V15Gy<120cc	621,30	V15Gy<120cc	735,40	2,21	6,13		
V30Gy<200cc	108,70	V30Gy<200cc	245,50	V30Gy<200cc	378,80	0,54	1,89		
V35Gy<150cc	69,00	V35Gy<150cc	195,20	V35Gy<150cc	299,70	0,46	2,00		
V45Gy<20cc	25,70	V45Gy<20cc	120,60	V45Gy<20cc	195,20	1,29	14,99		
V45Gy<195cc	25,70	V45Gy<195cc	120,60	V45Gy<195cc	195,20	0,13	1,00		
Dmax<50Gy	50,00	Dmax<50Gy	51,05	Dmax<50Gy	58,52			1,00	1,17
						2,21	14,99	1,00	1,17

Rectum							
Dose Plan		Dose Replan		Dose Replan Deformed		Dplannormal.	Dreplandefnormal.
Minimum		Minimum	19,31	Minimum	13,11		
Mean		Mean	40,72	Mean	39,02		
Maximum		Maximum	56,20	Maximum	56,32		
V30Gy<200cc	35,60	V30Gy<200cc	33,90	V30Gy<200cc	32,40	0,18	0,16
V35Gy<150cc	33,10	V35Gy<150cc	30,00	V35Gy<150cc	27,90	0,22	0,19
V45Gy<20cc	16,90	V45Gy<20cc	15,90	V45Gy<20cc	11,40	0,85	0,57
V50Gy<50%	12,20	V50Gy<50%	4,20	V50Gy<50%	4,90	0,24	0,10
						0,85	0,57

Sigmoid							
Dose Plan		Dose Replan		Dose Replan Deformed		Dplannormal.	Dreplandefnormal.
Minimum		Minimum	8,13	Minimum	10,89		
Mean		Mean	35,89	Mean	40,73		
Maximum		Maximum	48,34	Maximum	56,59		
V30Gy<200cc	30,30	V30Gy<200cc	32,80	V30Gy<200cc	34,70	0,15	0,17
V35Gy<150cc	28,40	V35Gy<150cc	30,40	V35Gy<150cc	34,40	0,19	0,23
V45Gy<20cc	18,70	V45Gy<20cc	16,20	V45Gy<20cc	31,20	0,94	1,56
V50Gy<50%	0,72	V50Gy<50%	0,00	V50Gy<50%	16,25	0,01	0,33
						0,94	1,56

Patient 7

Bladder							
Dose Plan		Dose Replan		Dose Replan Deformed		Dplannormalizada	Dreplandefnormalizada
Minimum		Minimum	12,89	Minimum	13,48		
Mean		Mean	33,77	Mean	36,40		
Maximum		Maximum	54,28	Maximum	58,05		
V35Gy<50%	48,90	V35Gy<50%	48,83	V35Gy<50%	57,96		
V40Gy<35%	39,10	V40Gy<35%	41,68	V40Gy<35%	48,59	0,78	0,97
V50Gy<5%	1,80	V50Gy<5%	3,04	V50Gy<5%	4,22	0,05	0,12
						0,00	0,00
						0,78	0,97

Small Bowel									
Dose Plan		Dose Replan		Dose Replan Deformed		Dplannormal.	Dreplandefnormal.	Dplanmaxnormal.	Dreplanmaxnormal.
Minimum		Minimum	1,33	Minimum	1,31				
Mean		Mean	28,47	Mean	30,09				
Maximum		Maximum	50,35	Maximum	56,96				
V15Gy<120cc	350,70	V15Gy<120cc	495,80	V15Gy<120cc	494,00	2,92	4,12		
V30Gy<200cc	215,50	V30Gy<200cc	267,30	V30Gy<200cc	310,10	1,08	1,55		
V35Gy<150cc	165,60	V35Gy<150cc	211,20	V35Gy<150cc	248,30	1,10	1,66		
V45Gy<20cc	55,10	V45Gy<20cc	91,10	V45Gy<20cc	100,70	2,76	12,42		
V45Gy<195cc	55,10	V45Gy<195cc	91,10	V45Gy<195cc	100,70	0,28	0,52		
Dmax<50Gy	51,20	Dmax<50Gy	50,35	Dmax<50Gy	56,96			1,02	1,14
						2,92	12,42	1,02	1,14

Rectum										Sigmoid									
Dose Plan		Dose Replan		Dose Replan Deformed		Dplannormal.	Dreplandefnormal.			Dose Plan		Dose Replan		Dose Replan Deformed		Dplannormal.	Dreplandefnormal.		
Minimum		Minimum	8,64	Minimum	10,98					Minimum		Minimum	14,46	Minimum	12,97				
Mean		Mean	36,98	Mean	31,27					Mean		Mean	38,17	Mean	39,87				
Maximum		Maximum	54,70	Maximum	52,77					Maximum		Maximum	54,16	Maximum	58,00				
V30Gy<200cc	43,10	V30Gy<200cc	43,10	V30Gy<200cc	31,10	0,22	0,16			V30Gy<200cc	52,70	V30Gy<200cc	41,40	V30Gy<200cc	43,50	0,26	0,22		
V35Gy<150cc	35,50	V35Gy<150cc	34,40	V35Gy<150cc	21,80	0,24	0,15			V35Gy<150cc	44,50	V35Gy<150cc	37,80	V35Gy<150cc	39,40	0,30	0,26		
V45Gy<20cc	15,20	V45Gy<20cc	15,20	V45Gy<20cc	4,70	0,76	0,24			V45Gy<20cc	18,10	V45Gy<20cc	25,20	V45Gy<20cc	25,60	0,91	1,28		
V50Gy<50%	0,94	V50Gy<50%	2,87	V50Gy<50%	1,27	0,02	0,03			V50Gy<50%	1,60	V50Gy<50%	2,22	V50Gy<50%	12,25	0,03	0,25		
						0,76	0,24									0,91	1,28		

Patient 8

Bladder										Small Bowel									
Dose Plan		Dose Replan		Dose Replan Deformed		Dplannormalizada	Dreplandefnormalizada			Dose Plan		Dose Replan		Dose Replan Deformed		Dplannormal.	Dreplandefnormal.	Dplanmaxnormal.	Dreplanmaxnormal.
Minimum		Minimum	10,67	Minimum	11,44					Minimum		Minimum	1,07	Minimum	1,03				
Mean		Mean	32,45	Mean	32,35					Mean		Mean	20,63	Mean	25,98				
Maximum		Maximum	56,49	Maximum	57,62					Maximum		Maximum	51,55	Maximum	58,09				
V35Gy<50%	43,40	V35Gy<50%	45,99	V35Gy<50%	44,35					V15Gy<120cc	175,30	V15Gy<120cc	472,20	V15Gy<120cc	594,60	1,46	4,96		
V40Gy<35%	35,30	V40Gy<35%	39,39	V40Gy<35%	37,06	0,71	0,74			V30Gy<200cc	62,20	V30Gy<200cc	215,00	V30Gy<200cc	337,80	0,31	1,69		
V50Gy<5%	3,00	V50Gy<5%	6,08	V50Gy<5%	5,49	0,09	0,16			V35Gy<150cc	39,10	V35Gy<150cc	175,80	V35Gy<150cc	277,80	0,26	1,85		
						0,00	0,00			V45Gy<20cc	11,70	V45Gy<20cc	104,30	V45Gy<20cc	162,40	0,59	13,89		
										V45Gy<195cc	11,70	V45Gy<195cc	104,30	V45Gy<195cc	162,40	0,06	0,83		
						0,71	0,74			Dmax<50Gy	48,60	Dmax<50Gy	51,55	Dmax<50Gy	58,09			0,97	1,16
																1,46	13,89	0,97	1,16

Rectum										Sigmoid									
Dose Plan		Dose Replan		Dose Replan Deformed		Dplannormal.	Dreplandefnormal.			Dose Plan		Dose Replan		Dose Replan Deformed		Dplannormal.	Dreplandefnormal.		
Minimum		Minimum	4,07	Minimum	5,74					Minimum		Minimum	16,27	Minimum	16,66				
Mean		Mean	31,99	Mean	34,91					Mean		Mean	37,64	Mean	41,41				
Maximum		Maximum	53,83	Maximum	56,11					Maximum		Maximum	49,94	Maximum	54,88				
V30Gy<200cc	26,10	V30Gy<200cc	27,20	V30Gy<200cc	31,20	0,13	0,16			V30Gy<200cc	27,50	V30Gy<200cc	15,20	V30Gy<200cc	18,40	0,14	0,09		
V35Gy<150cc	19,40	V35Gy<150cc	20,00	V35Gy<150cc	23,80	0,13	0,16			V35Gy<150cc	24,20	V35Gy<150cc	13,80	V35Gy<150cc	17,40	0,16	0,12		
V45Gy<20cc	7,20	V45Gy<20cc	7,20	V45Gy<20cc	10,30	0,36	0,52			V45Gy<20cc	14,90	V45Gy<20cc	11,10	V45Gy<20cc	14,70	0,75	0,74		
V50Gy<50%	3,00	V50Gy<50%	1,04	V50Gy<50%	3,65	0,06	0,07			V50Gy<50%	2,70	V50Gy<50%	0,00	V50Gy<50%	5,43	0,05	0,11		
						0,36	0,52									0,75	0,74		

Patient 9

Bladder										Small Bowel									
Dose Plan		Dose Replan		Dose Replan Deformed		Dplannormalizada	Dreplandefnormalizada			Dose Plan		Dose Replan		Dose Replan Deformed		Dplannormal.	Dreplandefnormal.	Dplanmaxnormal.	Dreplanmaxnormal.
Minimum		Minimum	12,59	Minimum	12,86					Minimum		Minimum	1,44	Minimum	1,37				
Mean		Mean	36,66	Mean	35,18					Mean		Mean	27,90	Mean	25,81				
Maximum		Maximum	55,40	Maximum	55,71					Maximum		Maximum	48,01	Maximum	48,36				
V35Gy<50%	61,60	V35Gy<50%	62,02	V35Gy<50%	56,09					V15Gy<120cc	613,10	V15Gy<120cc	480,90	V15Gy<120cc	430,50	5,11	3,59		
V40Gy<35%	53,20	V40Gy<35%	53,54	V40Gy<35%	47,07	1,06	0,94			V30Gy<200cc	237,40	V30Gy<200cc	195,50	V30Gy<200cc	152,70	1,19	0,76		
V50Gy<5%	6,90	V50Gy<5%	7,69	V50Gy<5%	3,14	0,20	0,09			V35Gy<150cc	166,50	V35Gy<150cc	138,90	V35Gy<150cc	110,20	1,11	0,73		
						0,00	0,00			V45Gy<20cc	70,70	V45Gy<20cc	58,00	V45Gy<20cc	50,10	3,54	5,51		
										V45Gy<195cc	70,70	V45Gy<195cc	58,00	V45Gy<195cc	50,10	0,36	0,26		
						1,06	0,94			Dmax<50Gy	48,20	Dmax<50Gy	48,01	Dmax<50Gy	48,36			0,96	0,97
																5,11	5,51	0,96	0,97

Rectum										Sigmoid									
Dose Plan		Dose Replan		Dose Replan Deformed		Dplannormal.	Dreplandefnormal.			Dose Plan		Dose Replan		Dose Replan Deformed		Dplannormal.	Dreplandefnormal.		
Minimum		Minimum	11,68	Minimum	7,95					Minimum		Minimum	2,38	Minimum	2,32				
Mean		Mean	38,73	Mean	39,15					Mean		Mean	38,26	Mean	36,48				
Maximum		Maximum	56,49	Maximum	57,88					Maximum		Maximum	55,36	Maximum	56,64				
V30Gy<200cc	46,60	V30Gy<200cc	49,00	V30Gy<200cc	46,20	0,23	0,23			V30Gy<200cc	217,70	V30Gy<200cc	210,40	V30Gy<200cc	190,80	1,09	0,95		
V35Gy<150cc	43,00	V35Gy<150cc	43,50	V35Gy<150cc	42,20	0,29	0,28			V35Gy<150cc	199,40	V35Gy<150cc	196,00	V35Gy<150cc	172,40	1,33	1,15		
V45Gy<20cc	29,90	V45Gy<20cc	29,80	V45Gy<20cc	32,60	1,50	1,63			V45Gy<20cc	153,10	V45Gy<20cc	153,60	V45Gy<20cc	132,10	7,66	6,61		
V50Gy<50%	21,30	V50Gy<50%	26,30	V50Gy<50%	31,52	0,43	0,63			V50Gy<50%	5,10	V50Gy<50%	3,21	V50Gy<50%	1,63	0,10	0,03		
						1,50	1,63									7,66	6,61		

Patient 10

Bladder										Small Bowel									
Dose Plan		Dose Replan		Dose Replan Deformed		Dplannormalizada	Dreplandefnormalizada			Dose Plan		Dose Replan		Dose Replan Deformed		Dplannormal.	Dreplandefnormal.	Dplanmaxnormal.	Dreplanmaxnormal.
Minimum		Minimum	13,13	Minimum	15,74					Minimum		Minimum	1,02	Minimum	0,00				
Mean		Mean	35,08	Mean	35,87					Mean		Mean	24,66	Mean	26,02				
Maximum		Maximum	56,48	Maximum	58,04					Maximum		Maximum	51,01	Maximum	58,53				
V35Gy<50%	66,60	V35Gy<50%	52,76	V35Gy<50%	51,68					V15Gy<120cc	537,70	V15Gy<120cc	791,40	V15Gy<120cc	747,10	4,48	6,23		
V40Gy<35%	57,60	V40Gy<35%	44,77	V40Gy<35%	43,58	1,15	0,87			V30Gy<200cc	268,10	V30Gy<200cc	350,00	V30Gy<200cc	422,80	1,34	2,11		
V50Gy<5%	11,00	V50Gy<5%	7,40	V50Gy<5%	11,73	0,31	0,34			V35Gy<150cc	218,90	V35Gy<150cc	290,60	V35Gy<150cc	368,40	1,46	2,46		
						0,00	0,00			V45Gy<20cc	123,00	V45Gy<20cc	175,20	V45Gy<20cc	247,90	6,15	18,42		
										V45Gy<195cc	123,00	V45Gy<195cc	175,20	V45Gy<195cc	247,90	0,63	1,27		
						1,15	0,87			Dmax<50Gy	51,20	Dmax<50Gy	51,01	Dmax<50Gy	58,53			1,02	1,17
																6,15	18,42	1,02	1,17

Rectum										Sigmoid									
Dose Plan		Dose Replan		Dose Replan Deformed		Dplannormal.	Dreplandefnormal.			Dose Plan		Dose Replan		Dose Replan Deformed		Dplannormal.	Dreplandefnormal.		
Minimum		Minimum	16,79	Minimum	12,14					Minimum		Minimum	13,42	Minimum	14,18				
Mean		Mean	38,49	Mean	43,16					Mean		Mean	31,66	Mean	35,11				
Maximum		Maximum	56,20	Maximum	58,32					Maximum		Maximum	47,78	Maximum	48,36				
V30Gy<200cc	34,00	V30Gy<200cc	43,40	V30Gy<200cc	48,20	0,17	0,24			V30Gy<200cc	45,10	V30Gy<200cc	37,30	V30Gy<200cc	47,40	0,23	0,24		
V35Gy<150cc	30,60	V35Gy<150cc	34,90	V35Gy<150cc	44,30	0,20	0,30			V35Gy<150cc	33,20	V35Gy<150cc	29,10	V35Gy<150cc	37,50	0,22	0,25		
V45Gy<20cc	19,10	V45Gy<20cc	18,50	V45Gy<20cc	29,10	0,96	1,46			V45Gy<20cc	15,90	V45Gy<20cc	13,40	V45Gy<20cc	17,30	0,80	0,87		
V50Gy<50%	27,00	V50Gy<50%	14,88	V50Gy<50%	34,81	0,54	0,70			V50Gy<50%	0,00	V50Gy<50%	0,00	V50Gy<50%	0,00	0,00	0,00		
						0,96	1,46									0,80	0,87		

Patient 11

Bladder							
Dose Plan		Dose Replan		Dose Replan Deformed		Dplannormalizada	Dreplandefnormalizada
Minimum		Minimum	9,76	Minimum	7,94		
Mean		Mean	26,26	Mean	28,83		
Maximum		Maximum	49,23	Maximum	49,24		
V35Gy<50%	37,60	V35Gy<50%	28,99	V35Gy<50%	34,30		
V40Gy<35%	30,50	V40Gy<35%	23,78	V40Gy<35%	27,33	0,61	0,55
V50Gy<5%	0,00	V50Gy<5%	0,00	V50Gy<5%	0,00	0,00	0,00
						0,00	0,00
						0,61	0,55

Small Bowel									
Dose Plan		Dose Replan		Dose Replan Deformed		Dplannormal.	Dreplandefnormal.	Dplanmaxnormal.	Dreplanmaxnormal.
Minimum		Minimum	1,29	Minimum	1,07				
Mean		Mean	16,00	Mean	14,93				
Maximum		Maximum	49,18	Maximum	49,00				
V15Gy<120cc	465,50	V15Gy<120cc	477,50	V15Gy<120cc	401,80	3,88	3,35		
V30Gy<200cc	82,80	V30Gy<200cc	61,80	V30Gy<200cc	55,70	0,41	0,28		
V35Gy<150cc	56,90	V35Gy<150cc	32,70	V35Gy<150cc	34,30	0,38	0,23		
V45Gy<20cc	27,10	V45Gy<20cc	6,60	V45Gy<20cc	9,50	1,36	1,72		
V45Gy<195cc	27,10	V45Gy<195cc	6,60	V45Gy<195cc	9,50	0,14	0,05		
Dmax<50Gy	49,30	Dmax<50Gy	49,18	Dmax<50Gy	49,00			0,99	0,98
						3,88	3,35	0,99	0,98

Rectum							
Dose Plan		Dose Replan		Dose Replan Deformed		Dplannormal.	Dreplandefnormal.
Minimum		Minimum	10,84	Minimum	4,41		
Mean		Mean	36,16	Mean	36,77		
Maximum		Maximum	48,99	Maximum	49,08		
V30Gy<200cc	43,90	V30Gy<200cc	40,60	V30Gy<200cc	40,30	0,22	0,20
V35Gy<150cc	35,70	V35Gy<150cc	36,20	V35Gy<150cc	36,90	0,24	0,25
V45Gy<20cc	20,40	V45Gy<20cc	24,20	V45Gy<20cc	26,50	1,02	1,33
V50Gy<50%	0,00	V50Gy<50%	0,00	V50Gy<50%	0,00	0,00	0,00
						1,02	1,33

Sigmoid							
Dose Plan		Dose Replan		Dose Replan Deformed		Dplannormal.	Dreplandefnormal.
Minimum		Minimum	12,04	Minimum	13,52		
Mean		Mean	27,08	Mean	28,55		
Maximum		Maximum	49,02	Maximum	49,50		
V30Gy<200cc	9,50	V30Gy<200cc	22,30	V30Gy<200cc	26,50	0,05	0,13
V35Gy<150cc	4,30	V35Gy<150cc	13,00	V35Gy<150cc	13,30	0,03	0,09
V45Gy<20cc	0,89	V45Gy<20cc	4,20	V45Gy<20cc	4,10	0,04	0,21
V50Gy<50%	0,00	V50Gy<50%	0,00	V50Gy<50%	0,00	0,00	0,00
						0,05	0,21

Patient 12

Bladder							
Dose Plan		Dose Replan		Dose Replan Deformed		Dplannormalizada	Dreplandefnormalizada
Minimum		Minimum	20,42	Minimum	31,61		
Mean		Mean	40,70	Mean	46,73		
Maximum		Maximum	56,92	Maximum	57,80		
V35Gy<50%	99,80	V35Gy<50%	69,05	V35Gy<50%	99,48		
V40Gy<35%	83,80	V40Gy<35%	57,34	V40Gy<35%	86,03	1,68	1,72
V50Gy<5%	27,50	V50Gy<5%	15,54	V50Gy<5%	24,87	0,79	0,71
						0,00	0,00
						1,68	1,72

Small Bowel									
Dose Plan		Dose Replan		Dose Replan Deformed		Dplannormal.	Dreplandefnormal.	Dplanmaxnormal.	Dreplanmaxnormal.
Minimum		Minimum	4,14	Minimum	4,86				
Mean		Mean	31,16	Mean	32,02				
Maximum		Maximum	50,71	Maximum	59,72				
V15Gy<120cc	888,00	V15Gy<120cc	839,90	V15Gy<120cc	831,70	7,40	6,93		
V30Gy<200cc	581,20	V30Gy<200cc	506,30	V30Gy<200cc	530,50	2,91	2,65		
V35Gy<150cc	501,70	V35Gy<150cc	440,40	V35Gy<150cc	464,50	3,34	3,10		
V45Gy<20cc	281,00	V45Gy<20cc	316,70	V45Gy<20cc	313,30	14,05	23,23		
V45Gy<195cc	281,00	V45Gy<195cc	316,70	V45Gy<195cc	313,30	1,44	1,61		
Dmax<50Gy	50,50	Dmax<50Gy	50,71	Dmax<50Gy	59,72			1,01	1,19
						14,05	23,23	1,01	1,19

Rectum							
Dose Plan		Dose Replan		Dose Replan Deformed		Dplannormal.	Dreplandefnormal.
Minimum		Minimum	22,83	Minimum	24,41		
Mean		Mean	46,42	Mean	47,57		
Maximum		Maximum	57,37	Maximum	57,42		
V30Gy<200cc	60,80	V30Gy<200cc	61,10	V30Gy<200cc	61,30	0,30	0,31
V35Gy<150cc	59,80	V35Gy<150cc	59,70	V35Gy<150cc	60,20	0,40	0,40
V45Gy<20cc	42,60	V45Gy<20cc	40,40	V45Gy<20cc	42,80	2,13	2,14
V50Gy<50%	35,30	V50Gy<50%	23,56	V50Gy<50%	33,89	0,71	0,68
						2,13	2,14

Sigmoid							
Dose Plan		Dose Replan		Dose Replan Deformed		Dplannormal.	Dreplandefnormal.
Minimum		Minimum	9,68	Minimum	12,64		
Mean		Mean	30,09	Mean	31,33		
Maximum		Maximum	53,96	Maximum	52,33		
V30Gy<200cc	23,80	V30Gy<200cc	91,20	V30Gy<200cc	96,60	0,12	0,48
V35Gy<150cc	19,70	V35Gy<150cc	64,90	V35Gy<150cc	70,40	0,13	0,47
V45Gy<20cc	11,00	V45Gy<20cc	31,30	V45Gy<20cc	31,00	0,55	1,55
V50Gy<50%	2,90	V50Gy<50%	3,36	V50Gy<50%	1,66	0,06	0,03
						0,55	1,55

Patient 13

Bladder							
Dose Plan		Dose Replan		Dose Replan Deformed		Dplannormalizada	Dreplandefnormalizada
Minimum		Minimum	14,29	Minimum	18,11		
Mean		Mean	36,22	Mean	42,28		
Maximum		Maximum	55,64	Maximum	58,80		
V35Gy<50%	66,20	V35Gy<50%	55,02	V35Gy<50%	69,37		
V40Gy<35%	58,10	V40Gy<35%	46,21	V40Gy<35%	22,94	1,16	0,46
V50Gy<5%	20,60	V50Gy<5%	13,65	V50Gy<5%	38,21	0,59	1,09
						0,00	0,00
						1,16	1,09

Small Bowel									
Dose Plan		Dose Replan		Dose Replan Deformed		Dplannormal.	Dreplandefnormal.	Dplanmaxnormal.	Dreplanmaxnormal.
Minimum		Minimum	2,41	Minimum	1,99				
Mean		Mean	27,71	Mean	29,68				
Maximum		Maximum	50,38	Maximum	58,97				
V15Gy<120cc	357,10	V15Gy<120cc	664,60	V15Gy<120cc	656,40	2,98	5,47		
V30Gy<200cc	116,90	V30Gy<200cc	351,40	V30Gy<200cc	383,80	0,58	1,92		
V35Gy<150cc	84,50	V35Gy<150cc	286,90	V35Gy<150cc	323,10	0,56	2,15		
V45Gy<20cc	49,50	V45Gy<20cc	163,80	V45Gy<20cc	237,30	2,48	16,16		
V45Gy<195cc	49,50	V45Gy<195cc	163,80	V45Gy<195cc	237,30	0,25	1,22		
Dmax<50Gy	50,70	Dmax<50Gy	50,38	Dmax<50Gy	58,97			1,01	1,18
						2,98	16,16	1,01	1,18

Rectum							
Dose Plan		Dose Replan		Dose Replan Deformed		Dplannormal.	Dreplandefnormal.
Minimum		Minimum	20,69	Minimum	25,64		
Mean		Mean	42,69	Mean	49,41		
Maximum		Maximum	56,02	Maximum	58,84		
V30Gy<200cc	59,40	V30Gy<200cc	47,80	V30Gy<200cc	50,30	0,30	0,25
V35Gy<150cc	55,70	V35Gy<150cc	41,40	V35Gy<150cc	47,80	0,37	0,32
V45Gy<20cc	43,10	V45Gy<20cc	23,30	V45Gy<20cc	38,80	2,16	1,94
V50Gy<50%	38,50	V50Gy<50%	18,87	V50Gy<50%	59,40	0,77	1,19
						2,16	1,94

Sigmoid							
Dose Plan		Dose Replan		Dose Replan Deformed		Dplannormal.	Dreplandefnormal.
Minimum		Minimum	24,62	Minimum	30,28		
Mean		Mean	47,77	Mean	50,69		
Maximum		Maximum	54,34	Maximum	58,33		
V30Gy<200cc	48,70	V30Gy<200cc	73,50	V30Gy<200cc	75,10	0,24	0,38
V35Gy<150cc	47,50	V35Gy<150cc	71,00	V35Gy<150cc	74,40	0,32	0,50
V45Gy<20cc	43,70	V45Gy<20cc	61,70	V45Gy<20cc	66,50	2,19	3,33
V50Gy<50%	50,00	V50Gy<50%	47,43	V50Gy<50%	50,30	1,00	1,01
						2,19	3,33

Patient 14

Bladder							
Dose Plan		Dose Replan		Dose Replan Deformed		Dplannormalizada	Dreplandefnormalizada
Minimum		Minimum	5,33	Minimum	11,81		
Mean		Mean	16,45	Mean	35,96		
Maximum		Maximum	24,81	Maximum	58,34		
V35Gy<50%	56,20	V35Gy<50%	0,00	V35Gy<50%	52,74		
V40Gy<35%	49,00	V40Gy<35%	0,00	V40Gy<35%	43,88	0,98	0,88
V50Gy<5%	29,80	V50Gy<5%	0,00	V50Gy<5%	21,49	0,85	0,61
						0,00	0,00
						0,98	0,88

Small Bowel									
Dose Plan		Dose Replan		Dose Replan Deformed		Dplannormal.	Dreplandefnormal.	Dplanmaxnormal.	Dreplanmaxnormal.
Minimum		Minimum	0,50	Minimum	1,17				
Mean		Mean	12,04	Mean	25,10				
Maximum		Maximum	22,10	Maximum	53,40				
V15Gy<120cc	355,80	V15Gy<120cc	154,30	V15Gy<120cc	338,10	2,97	2,82		
V30Gy<200cc	109,90	V30Gy<200cc	0,00	V30Gy<200cc	143,90	0,55	0,72		
V35Gy<150cc	71,40	V35Gy<150cc	0,00	V35Gy<150cc	108,70	0,48	0,72		
V45Gy<20cc	34,50	V45Gy<20cc	0,00	V45Gy<20cc	60,70	1,73	5,44		
V45Gy<195cc	34,50	V45Gy<195cc	0,00	V45Gy<195cc	60,70	0,18	0,31		
Dmax<50Gy	50,50	Dmax<50Gy	22,10	Dmax<50Gy	53,40			1,01	1,07
						2,97	5,44	1,01	1,07

Rectum

Dose Plan		Dose Replan		Dose Replan Deformed		Dplannormal.	Dreplandefnormal.
Minimum		Minimum	7,64	Minimum	10,86		
Mean		Mean	19,19	Mean	46,10		
Maximum		Maximum	24,69	Maximum	53,13		
V30Gy<200cc	39,50	V30Gy<200cc	0,00	V30Gy<200cc	57,60	0,20	0,29
V35Gy<150cc	36,40	V35Gy<150cc	0,00	V35Gy<150cc	53,80	0,24	0,36
V45Gy<20cc	27,00	V45Gy<20cc	0,00	V45Gy<20cc	40,20	1,35	2,01
V50Gy<50%	37,60	V50Gy<50%	0,00	V50Gy<50%	41,15	0,75	0,82
						1,35	2,01

Sigmoid

Dose Plan		Dose Replan		Dose Replan Deformed		Dplannormal.	Dreplandefnormal.
Minimum		Minimum	6,38	Minimum	19,99		
Mean		Mean	20,70	Mean	48,55		
Maximum		Maximum	26,13	Maximum	58,90		
V30Gy<200cc	101,90	V30Gy<200cc	0,00	V30Gy<200cc	66,00	0,51	0,33
V35Gy<150cc	95,50	V35Gy<150cc	0,00	V35Gy<150cc	64,50	0,64	0,43
V45Gy<20cc	81,70	V45Gy<20cc	0,00	V45Gy<20cc	62,60	4,09	3,13
V50Gy<50%	48,40	V50Gy<50%	0,00	V50Gy<50%	83,67	0,97	1,67
						4,09	3,13

Patient 15

Bladder

Dose Plan		Dose Replan		Dose Replan Deformed		Dplannormalizada	Dreplandefnormalizada
Minimum		Minimum	8,05	Minimum	9,21		
Mean		Mean	26,78	Mean	26,27		
Maximum		Maximum	49,21	Maximum	49,70		
V35Gy<50%	43,20	V35Gy<50%	31,56	V35Gy<50%	27,21		
V40Gy<35%	35,30	V40Gy<35%	25,41	V40Gy<35%	20,03	0,71	0,40
V50Gy<5%	0,00	V50Gy<5%	0,00	V50Gy<5%	0,00	0,00	0,00
						0,00	0,00
						0,71	0,40

Small Bowel

Dose Plan		Dose Replan		Dose Replan Deformed		Dplannormal.	Dreplandefnormal.	Dplanmaxnormal.	Dreplanmaxnormal.
Minimum		Minimum	0,67	Minimum	1,20				
Mean		Mean	25,07	Mean	25,91				
Maximum		Maximum	49,38	Maximum	49,70				
V15Gy<120cc	989,80	V15Gy<120cc	964,70	V15Gy<120cc	1009,00	8,25	8,41		
V30Gy<200cc	351,40	V30Gy<200cc	406,40	V30Gy<200cc	431,10	1,76	2,16		
V35Gy<150cc	255,30	V35Gy<150cc	290,50	V35Gy<150cc	326,90	1,70	2,18		
V45Gy<20cc	124,60	V45Gy<20cc	143,30	V45Gy<20cc	179,80	6,23	16,35		
V45Gy<195cc	124,60	V45Gy<195cc	143,30	V45Gy<195cc	179,80	0,64	0,92		
Dmax<50Gy	49,20	Dmax<50Gy	49,38	Dmax<50Gy	49,70			0,98	0,99
						8,25	16,35	0,98	0,99

Rectum

Dose Plan		Dose Replan		Dose Replan Deformed		Dplannormal.	Dreplandefnormal.
Minimum		Minimum	1,91	Minimum	1,73		
Mean		Mean	29,42	Mean	30,49		
Maximum		Maximum	48,79	Maximum	49,11		
V30Gy<200cc	27,40	V30Gy<200cc	27,00	V30Gy<200cc	31,80	0,14	0,16
V35Gy<150cc	21,80	V35Gy<150cc	21,30	V35Gy<150cc	25,40	0,15	0,17
V45Gy<20cc	9,20	V45Gy<20cc	9,90	V45Gy<20cc	12,50	0,46	0,63
V50Gy<50%	0,00	V50Gy<50%	0,00	V50Gy<50%	0,00	0,00	0,00
						0,46	0,63

Sigmoid

Dose Plan		Dose Replan		Dose Replan Deformed		Dplannormal.	Dreplandefnormal.
Minimum		Minimum	7,55	Minimum	13,20		
Mean		Mean	26,41	Mean	29,98		
Maximum		Maximum	49,15	Maximum	49,76		
V30Gy<200cc	29,50	V30Gy<200cc	20,70	V30Gy<200cc	24,30	0,15	0,12
V35Gy<150cc	23,70	V35Gy<150cc	17,20	V35Gy<150cc	19,60	0,16	0,13
V45Gy<20cc	15,20	V45Gy<20cc	10,90	V45Gy<20cc	12,20	0,76	0,61
V50Gy<50%	0,00	V50Gy<50%	0,00	V50Gy<50%	0,00	0,00	0,00
						0,76	0,61

Patient 16

Bladder

Dose Plan		Dose Replan		Dose Replan Deformed		Dplannormalizada	Dreplandefnormalizada
Minimum		Minimum	8,50	Minimum	9,32		
Mean		Mean	30,25	Mean	29,86		
Maximum		Maximum	56,05	Maximum	56,88		
V35Gy<50%	39,60	V35Gy<50%	40,03	V35Gy<50%	40,67	0,79	0,81
V40Gy<35%	31,00	V40Gy<35%	31,64	V40Gy<35%	32,45	0,89	0,93
V50Gy<5%	2,70	V50Gy<5%	2,84	V50Gy<5%	3,37	0,54	0,67
						0,89	0,93

Small Bowel

Dose Plan		Dose Replan		Dose Replan Deformed		Dplannormal.	Dreplandefnormal.	Dplanmaxnormal.	Dreplanmaxnormal.
Minimum		Minimum	1,53	Minimum	1,05				
Mean		Mean	20,74	Mean	23,93				
Maximum		Maximum	48,66	Maximum	49,09				
V15Gy<120cc	226,20	V15Gy<120cc	429,80	V15Gy<120cc	479,20	1,89	3,99		
V30Gy<200cc	93,70	V30Gy<200cc	151,80	V30Gy<200cc	243,60	0,47	1,22		
V35Gy<150cc	68,60	V35Gy<150cc	117,40	V35Gy<150cc	182,60	0,46	1,22		
V45Gy<20cc	33,00	V45Gy<20cc	60,40	V45Gy<20cc	91,20	1,65	9,13		
V45Gy<195cc	33,00	V45Gy<195cc	60,40	V45Gy<195cc	91,20	0,17	0,47		
Dmax<50Gy	49,20	Dmax<50Gy	48,66	Dmax<50Gy	49,09			0,98	0,98
						1,89	9,13	0,98	0,98

Rectum

Dose Plan		Dose Replan		Dose Replan Deformed		Dplannormal.	Dreplandefnormal.
Minimum		Minimum	5,83	Minimum	8,42		
Mean		Mean	34,28	Mean	39,98		
Maximum		Maximum	56,46	Maximum	58,47		
V30Gy<200cc	28,80	V30Gy<200cc	40,80	V30Gy<200cc	51,60	0,14	0,26
V35Gy<150cc	20,80	V35Gy<150cc	32,80	V35Gy<150cc	43,20	0,14	0,29
V45Gy<20cc	9,60	V45Gy<20cc	17,50	V45Gy<20cc	28,40	0,48	1,42
V50Gy<50%	9,30	V50Gy<50%	7,14	V50Gy<50%	25,62	0,19	0,51
						0,48	1,42

Sigmoid

Dose Plan		Dose Replan		Dose Replan Deformed		Dplannormal.	Dreplandefnormal.
Minimum		Minimum	11,48	Minimum	13,81		
Mean		Mean	32,97	Mean	38,91		
Maximum		Maximum	55,36	Maximum	57,90		
V30Gy<200cc	52,00	V30Gy<200cc	42,80	V30Gy<200cc	60,00	0,26	0,30
V35Gy<150cc	49,50	V35Gy<150cc	37,20	V35Gy<150cc	52,30	0,33	0,35
V45Gy<20cc	35,50	V45Gy<20cc	23,10	V45Gy<20cc	34,70	1,78	1,74
V50Gy<50%	5,20	V50Gy<50%	1,97	V50Gy<50%	9,22	0,10	0,18
						1,78	1,74

Patient 17

Bladder

Dose Plan		Dose Replan		Dose Replan Deformed		Dplannormalizada	Dreplandefnormalizada
Minimum		Minimum	5,21	Minimum	15,01		
Mean		Mean	15,33	Mean	47,09		
Maximum		Maximum	26,74	Maximum	59,09		
V35Gy<50%	72,80	V35Gy<50%	0,00	V35Gy<50%	87,46	1,46	1,75
V40Gy<35%	66,70	V40Gy<35%	0,00	V40Gy<35%	82,44	1,91	2,36
V50Gy<5%	16,80	V50Gy<5%	0,00	V50Gy<5%	35,91	3,36	7,18
						3,36	7,18

Small Bowel

Dose Plan		Dose Replan		Dose Replan Deformed		Dplannormal.	Dreplandefnormal.	Dplanmaxnormal.	Dreplanmaxnormal.
Minimum		Minimum	3,14	Minimum	8,03				
Mean		Mean	10,46	Mean	25,27				
Maximum		Maximum	25,46	Maximum	66,79				
V15Gy<120cc	1498,00	V15Gy<120cc	231,10	V15Gy<120cc	1666,00	12,48	13,88		
V30Gy<200cc	581,70	V30Gy<200cc	0,00	V30Gy<200cc	503,50	2,91	2,52		
V35Gy<150cc	425,50	V35Gy<150cc	0,00	V35Gy<150cc	319,90	2,84	2,13		
V45Gy<20cc	200,80	V45Gy<20cc	0,00	V45Gy<20cc	109,50	10,04	16,00		
V45Gy<195cc	200,80	V45Gy<195cc	0,00	V45Gy<195cc	109,50	1,03	0,56		
Dmax<50Gy	50,40	Dmax<50Gy	25,46	Dmax<50Gy	66,79			1,01	1,34
						12,48	16,00	1,01	1,34

Rectum

Dose Plan		Dose Replan		Dose Replan Deformed		Dplannormal.	Dreplandefnormal.
Minimum		Minimum	5,03	Minimum	17,16		
Mean		Mean	20,62	Mean	40,12		
Maximum		Maximum	26,89	Maximum	57,10		
V30Gy<200cc	55,20	V30Gy<200cc	0,00	V30Gy<200cc	61,90	0,28	0,31
V35Gy<150cc	44,00	V35Gy<150cc	0,00	V35Gy<150cc	50,20	0,29	0,33
V45Gy<20cc	25,30	V45Gy<20cc	0,00	V45Gy<20cc	30,10	1,27	1,51
V50Gy<50%	14,20	V50Gy<50%	0,00	V50Gy<50%	18,25	0,28	0,37
						1,27	1,51

Sigmoid

Dose Plan		Dose Replan		Dose Replan Deformed		Dplannormal.	Dreplandefnormal.
Minimum		Minimum	7,59	Minimum	14,29		
Mean		Mean	19,85	Mean	45,94		
Maximum		Maximum	31,67	Maximum	65,88		
V30Gy<200cc	87,30	V30Gy<200cc	0,50	V30Gy<200cc	166,60	0,44	0,83
V35Gy<150cc	85,60	V35Gy<150cc	0,00	V35Gy<150cc	159,70	0,57	1,06
V45Gy<20cc	72,80	V45Gy<20cc	0,00	V45Gy<20cc	116,50	3,64	5,83
V50Gy<50%	29,40	V50Gy<50%	0,00	V50Gy<50%	23,89	0,59	0,48
						3,64	5,83

B.

Patient 1

Bladder

Dose Plan 3#		Dose Replan 5#		Dose Replan Deformada 5#		Dplannormal.	Dreplandefnormal.
Mínimo	0.5	Mínimo	2.56	Mínimo	0.52		
Média	7.63	Média	11.32	Média	7.07		
Máximo	26.09	Máximo	27.32	Máximo	27.4		
V28.2Gy<=0.035cc	0,00	V38Gy<=0.035cc	0,00	V38Gy<=0.035cc	0,00	0,00	0,00
V16,2Gy<=15cc	14,50	V18,3Gy<=15cc	6,10	V18,3Gy<=15cc	3,00	0,97	0,20
						0,00	0,00
						0,97	0,20

Small Bowel

Dose Plan 3#		Dose Replan 5#		Dose Replan Deformada 5#		Dplannormal.	Dreplandefnormal.
Mínimo	0.32	Mínimo	0.12	Mínimo	0,00		
Média	0.68	Média	7.41	Média	0.24		
Máximo	2.21	Máximo	38.23	Máximo	20.76		
V25,2Gy<=0,035cc	0,00	V35Gy<=0,035cc	0,01	V35Gy<=0,035cc	0,00	0,00	0,00
V17,7Gy<=5cc	0,00	V19,5Gy<=5cc	42,40	V19,5Gy<=5cc	0,00	0,00	0,00
						0,00	0,00

Rectum

Dose Plan 3#		Dose Replan 5#		Dose Replan Deformada 5#		Dplannormal.	Dreplandefnormal.
Mínimo	23.53	Mínimo	0.86	Mínimo	0.27		
Média	31.18	Média	12.49	Média	6.25		
Máximo	35.03	Máximo	33.58	Máximo	31.12		
V28,2Gy<=0,035cc	0,00	V38Gy<=0,035cc	0,00	V38Gy<=0,035cc	0,00	0,00	0,00
V24Gy<=20cc	1,80	V25Gy<=20cc	1,40	V25Gy<=20cc	1,50	0,09	0,08
						0,09	0,08

Sigmoid

Dose Plan 3#		Dose Replan 5#		Dose Replan Deformada 5#		Dplannormal.	Dreplandefnormal.
Mínimo	0.38	Mínimo	4.2	Mínimo	0.18		
Média	5.28	Média	13.83	Média	1.88		
Máximo	16.12	Máximo	38.29	Máximo	21.64		
V28,2Gy<=0,035cc	0,00	V38Gy<=0,035cc	0,00	V38Gy<=0,035cc	0,00	0,00	0,00
V24Gy<=20cc	0,00	V25Gy<=20cc	7,30	V25Gy<=20cc	0,00	0,00	0,00
						0,00	0,00

Patient 2

Bladder

Dose Plan 1#		Dose Replan 3#		Dose Replan Deformada 3#		Dplannormal.	Dreplandefnormal.
Mínimo	9,27	Mínimo	0,20	Mínimo	9,28		
Média	27,14	Média	3,81	Média	22,80		
Máximo	44,96	Máximo	12,87	Máximo	44,83		
V18,4Gy<=0,035cc	0,40	V28.2Gy<=0,035cc	0,00	V28.2Gy<=0,035cc	0,04	11,43	1,14
V11,4Gy<=15cc	133,90	V16,2Gy<=15cc	0,00	V16,2Gy<=15cc	20,70	8,93	1,38
			0,00		0,00		0,00
						11,43	1,38

Small Bowel

Dose Plan 1#		Dose Replan 3#		Dose Replan Deformada 3#		Dplannormal.	Dreplandefnormal.
Mínimo	1,05	Mínimo	0,12	Mínimo	9,67		
Média	21,40	Média	1,32	Média	26,61		
Máximo	42,73	Máximo	10,67	Máximo	45,23		
V15,4Gy<=0,035cc	0,10	V25,2Gy<=0,035cc	0,00	V25,2Gy<=0,035cc	0,40	2,86	11,43
V11,9Gy<=5cc	6,40	V17,7Gy<=5cc	0,00	V17,7Gy<=5cc	13,40	1,28	2,68
						2,86	11,43

Rectum

Dose Plan 1#		Dose Replan 3#		Dose Replan Deformada 3#		Dplannormal.	Dreplandefnormal.
Mínimo	5,01	Mínimo	0,16	Mínimo	3,96		
Média	27,71	Média	2,14	Média	31,75		
Máximo	45,67	Máximo	14,66	Máximo	45,61		
V18,4Gy<=0,035cc	0,60	V28,2Gy<=0,035cc	0,00	V28,2Gy<=0,035cc	0,05	17,14	1,43
V14,3Gy<=20cc	49,90	V24Gy<=20cc	0,00	V24Gy<=20cc	53,30	2,50	2,67
						17,14	2,67

Sigmoid

Dose Plan 1#		Dose Replan 3#		Dose Replan Deformada 3#		Dplannormal.	Dreplandefnormal.
Mínimo	10,24	Mínimo	0,28	Mínimo	16,55		
Média	34,07	Média	1,16	Média	26,17		
Máximo	45,16	Máximo	10,39	Máximo	44,63		
V18,4Gy<=0,035cc	0,15	V28,2Gy<=0,035cc	0,00	V28,2Gy<=0,035cc	0,03	4,29	0,86
V14,3Gy<=20cc	69,30	V24Gy<=20cc	0,00	V24Gy<=20cc	8,60	3,47	0,43
						0,00	0,00
						0,00	0,00
						4,29	0,86

Patient 3

Bladder

Dose Plan 5#		Dose Replan 5#		Dose Replan Deformada 5#		Dplannormal.	Dreplandefnormal.
Mínimo	0,14	Mínimo	0,36	Mínimo	0,05		
Média	5,66	Média	6,02	Média	0,13		
Máximo	27,46	Máximo	29,52	Máximo	0,38		
V38Gy<=0,035cc	0,00	V38Gy<=0,035cc	0,00	V38Gy<=0,035cc	0,00	0,00	0,00
V18,3Gy<=15cc	10,20	V18,3Gy<=15cc	5,12	V18,3Gy<=15cc	0,00	0,68	0,00
						0,00	0,00
						0,68	0,00

Small Bowel

Dose Plan 5#		Dose Replan 5#		Dose Replan Deformada 5#		Dplannormal.	Dreplandefnormal.
Mínimo	0,11	Mínimo	0,04	Mínimo	0,29		
Média	0,22	Média	0,06	Média	0,56		
Máximo	0,39	Máximo	0,09	Máximo	1,07		
V35Gy<=0,035cc	0,00	V35Gy<=0,035cc	0,00	V35Gy<=0,035cc	0,00	0,00	0,00
V19,5Gy<=5cc	0,00	V19,5Gy<=5cc	0,00	V19,5Gy<=5cc	0,00	0,00	0,00
						0,00	0,00
						0,00	0,00
						0,00	0,00

Rectum

Dose Plan 5#		Dose Replan 5#		Dose Replan Deformada 5#		Dplannormal.	Dreplandefnormal.
Mínimo	0,15	Mínimo	0,04	Mínimo	0,35		
Média	4,20	Média	0,19	Média	6,35		
Máximo	26,87	Máximo	1,44	Máximo	29,02		
V38Gy<=0,035cc	0,00	V38Gy<=0,035cc	0,00	V38Gy<=0,035cc	0,00	0,00	0,00
V25Gy<=20cc	0,08	V25Gy<=20cc	0,56	V25Gy<=20cc	0,00	0,00	0,00
						0,00	0,00
						0,00	0,00

Sigmoid

Dose Plan 5#		Dose Replan 5#		Dose Replan Deformada 5#		Dplannormal.	Dreplandefnormal.
Mínimo	0,04	Mínimo	0,00	Mínimo	0,11		
Média	0,20	Média	0,04	Média	0,65		
Máximo	1,10	Máximo	0,12	Máximo	13,03		
V38Gy<=0,035cc	0,00	V38Gy<=0,035cc	0,00	V38Gy<=0,035cc	0,00	0,00	0,00
V25Gy<=20cc	0,00	V25Gy<=20cc	0,00	V25Gy<=20cc	0,00	0,00	0,00
						0,00	0,00
						0,00	0,00

Patient 4

Bladder

Dose Plan 5#		Dose Replan 1#		Dose Replan Deformada 1#		Dplannormal.	Dreplandefnormal.
Mínimo	-	Mínimo	0,07	Mínimo	0,11		
Média	-	Média	0,12	Média	0,17		
Máximo	-	Máximo	0,21	Máximo	0,28		
V38Gy<=0,035cc	-	V18,4Gy<=0,035cc	0,00	V18,4Gy<=0,035cc	0,00	#VALOR!	0,00
V18,3Gy<=15cc	-	V11,4Gy<=15cc	0,00	V11,4Gy<=15cc	0,00	#VALOR!	0,00
						0,00	0,00
						#VALOR!	0,00

Small Bowel

Dose Plan 5#		Dose Replan 1#		Dose Replan Deformada 1#		Dplannormal.	Dreplandefnormal.
Mínimo	0,23	Mínimo	0,03	Mínimo	0,10		
Média	3,13	Média	1,27	Média	1,68		
Máximo	16,08	Máximo	9,31	Máximo	11,44		
V35Gy<=0,035cc	0,00	V15,4Gy<=0,035cc	0,00	V15,4Gy<=0,035cc	0,00	0,00	0,00
V19,5Gy<=5cc	0,00	V11,9Gy<=5cc	0,00	V11,9Gy<=5cc	0,00	0,00	0,00
						0,00	0,00
						0,00	0,00
						0,00	0,00

Rectum

Dose Plan 5#		Dose Replan 1#		Dose Replan Deformada 1#		Dplannormal.	Dreplandefnormal.
Mínimo	-	Mínimo	0,06	Mínimo	0,08		
Média	-	Média	0,13	Média	0,18		
Máximo	-	Máximo	0,33	Máximo	0,46		
V38Gy<=0,035cc	-	V18,4Gy<=0,035cc	0,00	V18,4Gy<=0,035cc	0,00	#VALOR!	#REF!
V25Gy<=20cc	-	V14,3Gy<=20cc	0,00	V14,3Gy<=20cc	0,00	#VALOR!	#REF!
						0,00	0,00
						0,00	0,00
						#VALOR!	#REF!

Sigmoid

Dose Plan 5#		Dose Replan 1#		Dose Replan Deformada 1#		Dplannormal.	Dreplandefnormal.
Mínimo	0,23	Mínimo	-	Mínimo	-		
Média	4,59	Média	-	Média	-		
Máximo	11,16	Máximo	-	Máximo	-		
V38Gy<=0,035cc	0,00	V18,4Gy<=0,035cc	-	V18,4Gy<=0,035cc	-	0,00	#VALOR!
V25Gy<=20cc	0,00	V14,3Gy<=20cc	-	V14,3Gy<=20cc	-	0,00	#VALOR!
						0,00	0,00
						0,00	0,00
						0,00	#VALOR!

Patient 5

Bladder

Dose Plan 5#		Dose Replan 1#		Dose Replan Deformada 1#		Dplannormal.	Dreplandefnormal.
Mínimo	-	Mínimo	-	Mínimo	-		
Média	-	Média	-	Média	-		
Máximo	-	Máximo	-	Máximo	-		
V38Gy<=0,035cc	-	V18,4Gy<=0,035cc	-	V18,4Gy<=0,035cc	-	#VALOR!	#VALOR!
V18,3Gy<=15cc	-	V11,4Gy<=15cc	-	V11,4Gy<=15cc	-	#VALOR!	#VALOR!
					-	0,00	#VALOR!
						#VALOR!	#VALOR!

Small Bowel

Dose Plan 5#		Dose Replan 1#		Dose Replan Deformada 1#		Dplannormal.	Dreplandefnormal.
Mínimo	0,07	Mínimo	0,19	Mínimo	0,10		
Média	0,14	Média	2,34	Média	2,16		
Máximo	0,31	Máximo	15,65	Máximo	16,77		
V35Gy<=0,035cc	0,00	V15,4Gy<=0,035cc	0,00	V15,4Gy<=0,035cc	0,01	0,00	0,00
V19,5Gy<=5cc	0,00	V11,9Gy<=5cc	0,10	V11,9Gy<=5cc	2,20	0,00	0,44
						0,00	0,00
						0,00	0,00
						0,00	0,00
						0,00	0,44

Rectum

Dose Plan 5#		Dose Replan 1#		Dose Replan Deformada 1#		Dplannormal.	Dreplandefnormal.
Mínimo	-	Mínimo	0,42	Mínimo	2,71		
Média	-	Média	1,02	Média	6,20		
Máximo	-	Máximo	2,31	Máximo	14,10		
V38Gy<=0,035cc	-	V18,4Gy<=0,035cc	0,00	V18,4Gy<=0,035cc	0,00	#VALOR!	#REF!
V25Gy<=20cc	-	V14,3Gy<=20cc	0,00	V14,3Gy<=20cc	0,00	#VALOR!	#REF!
						0,00	0,00
						0,00	0,00
						#VALOR!	#REF!

Sigmoid

Dose Plan 5#		Dose Replan 1#		Dose Replan Deformada 1#		Dplannormal.	Dreplandefnormal.
Mínimo	0,21	Mínimo	0,31	Mínimo	0,16		
Média	4,05	Média	3,92	Média	2,33		
Máximo	10,21	Máximo	9,03	Máximo	6,47		
V38Gy<=0,035cc	0,00	V18,4Gy<=0,035cc	0,00	V18,4Gy<=0,035cc	0,00	0,00	0,00
V25Gy<=20cc	0,00	V14,3Gy<=20cc	0,00	V14,3Gy<=20cc	0,00	0,00	0,00
						0,00	0,00
						0,00	0,00
						0,00	0,00

Patient 6

Bladder

Dose Plan 5#		Dose Replan 5#		Dose Replan Deformada 5#		Dplannormal.	Dreplandefnormal.
Mínimo	0,09	Mínimo	0,05	Mínimo	0,08		
Média	0,16	Média	0,07	Média	0,12		
Máximo	0,24	Máximo	0,09	Máximo	0,16		
V38Gy<=0,035cc	0,00	V38Gy<=0,035cc	0,00	V38Gy<=0,035cc	0,00	0,00	0,00
V18,3Gy<=15cc	0,00	V18,3Gy<=15cc	0,00	V18,3Gy<=15cc	0,00	0,00	0,00
						0,00	0,00
						0,00	0,00
						0,00	0,00

Small Bowel

Dose Plan 5#		Dose Replan 5#		Dose Replan Deformada 5#		Dplannormal.	Dreplandefnormal.
Mínimo	-	Mínimo	0,29	Mínimo	0,33		
Média	-	Média	2,22	Média	3,60		
Máximo	-	Máximo	7,05	Máximo	12,52		
V35Gy<=0,035cc	-	V35Gy<=0,035cc	0,00	V35Gy<=0,035cc	0,00	#VALOR!	0,00
V19,5Gy<=5cc	-	V19,5Gy<=5cc	0,00	V19,5Gy<=5cc	0,00	#VALOR!	0,00
						0,00	0,00
						0,00	0,00
						0,00	0,00
						#VALOR!	0,00

Rectum

Dose Plan 5#		Dose Replan 5#		Dose Replan Deformada 5#		Dplannormal.	Dreplandefnormal.
Mínimo	0,01	Mínimo	0,03	Mínimo	0,00		
Média	0,25	Média	0,09	Média	0,13		
Máximo	0,64	Máximo	0,20	Máximo	0,27		
V38Gy<=0,035cc	0,00	V38Gy<=0,035cc	0,00	V38Gy<=0,035cc	0,00	0,00	0,00
V25Gy<=20cc	0,00	V25Gy<=20cc	0,00	V25Gy<=20cc	0,00	0,00	0,00
						0,00	0,00
						0,00	0,00
						0,00	0,00

Sigmoid

Dose Plan 5#		Dose Replan 5#		Dose Replan Deformada 5#		Dplannormal.	Dreplandefnormal.
Mínimo	-	Mínimo	-	Mínimo	-		
Média	-	Média	-	Média	-		
Máximo	-	Máximo	-	Máximo	-		
V38Gy<=0,035cc	-	V38Gy<=0,035cc	-	V38Gy<=0,035cc	-	#VALOR!	#VALOR!
V25Gy<=20cc	-	V25Gy<=20cc	-	V25Gy<=20cc	-	#VALOR!	#VALOR!
						0,00	0,00
						0,00	0,00
						#VALOR!	#VALOR!

Patient 7

Bladder

Dose Plan 3#		Dose Replan 5#		Dose Replan Deformada 5#		Dplannormal.	Dreplandefnormal.
Mínimo	-	Mínimo	-	Mínimo	-		
Média	-	Média	-	Média	-		
Máximo	-	Máximo	-	Máximo	-		
V28,2Gy<=0,035cc	-	V35Gy<50%	-	V35Gy<50%	-	#VALOR!	#VALOR!
V16,2Gy<=15cc	-	V40Gy<35%	-	V40Gy<35%	-	#VALOR!	#VALOR!
		V50Gy<5%	-	V50Gy<5%	-	0,00	#VALOR!
						#VALOR!	#VALOR!

Small Bowel

Dose Plan 3#		Dose Replan 5#		Dose Replan Deformada 5#		Dplannormal.	Dreplandefnormal.
Mínimo	0,05	Mínimo	0,30	Mínimo	0,02		
Média	1,13	Média	5,31	Média	0,58		
Máximo	5,57	Máximo	15,44	Máximo	5,88		
V25,2Gy<=0,035cc	0,00	V35Gy<=0,035cc	0,00	V35Gy<=0,035cc	0,00	0,00	0,00
V17,7Gy<=5cc	0,00	V19,5Gy<=5cc	0,00	V19,5Gy<=5cc	0,00	0,00	0,00
						0,00	0,00
						0,00	0,00
						0,00	0,00

Rectum										Sigmoid									
Dose Plan 3#		Dose Replan 5#		Dose Replan Deformada 5#		Dplannormal.	Dreplandefnormal.			Dose Plan 3#		Dose Replan 5#		Dose Replan Deformada 5#		Dplannormal.	Dreplandefnormal.		
Mínimo	-	Mínimo	2,91	Mínimo	0,46					Mínimo	0,06	Mínimo	0,41	Mínimo	0,02				
Média	-	Média	4,66	Média	1,78					Média	0,93	Média	3,07	Média	0,25				
Máximo	-	Máximo	6,76	Máximo	3,22					Máximo	5,35	Máximo	8,85	Máximo	3,78				
V28,2Gy<=0,035cc	-	V38Gy<=0,035cc	0,00	V38Gy<=0,035cc	0,00	#VALOR!	0,00			V28,2Gy<=0,035cc	0,00	V38Gy<=0,035cc	0,00	V38Gy<=0,035cc	0,00	0,00	0,00		
V24Gy<=20cc	-	V25Gy<=20cc	0,00	V25Gy<=20cc	0,00	#VALOR!	0,00			V24Gy<=20cc	0,00	V25Gy<=20cc	0,00	V25Gy<=20cc	0,00	0,00	0,00		
						0,00	0,00									0,00	0,00		
						0,00	0,00									0,00	0,00		
						#VALOR!	0,00									0,00	0,00		